Recent advances in designing and developing efficient sillenite-based materials for photocatalytic applications

Oussama Baaloudj, Nhu-Nang Vu, Aymen Amine Assadi, Le van Quyet, Phuong Nguyen-Tri

Recent advances in designing and developing efficient sillenite-based materials for photocatalytic applications.

Oussama Baaloudj[1,2,3], Nhu-Nang Vu[1,2], Aymen Amin Assadi[4,5], Le Van Quyet[6] and Phuong Nguyen-Tri[1,2]*

[1] *Department of Chemistry, Biochemistry and Physics, Université du Québec à Trois-Rivières (UQTR), 3351 Boulevard des Forges, Trois-Rivières, Québec, G8Z 4M3, Canada*

[2] *Laboratory of Advanced Materials for Energy and Environment, Université du Québec à Trois-Rivières (UQTR), 3351 Boulevard des Forges, Trois-Rivières, Québec G8Z 4M3, Canada*

[3] *Laboratory of Reaction Engineering, Faculty of Mechanical Engineering and Process Engineering, USTHB, BP 32, 16111 Algiers, Algeria*

[4] *College of Engineering, Imam Mohammad Ibn Saud Islamic University, IMSIU, Riyadh, 11432, Saudi Arabia*

[5] *Univ Rennes, ENSCR-équipe Chimie et Ingénierie des Procédés, URM 6226 CNRS, ENSCR-11, allée de Beaulieu, CS 508307-35708 Rennes, France*

[6] *Department of Materials Science and Engineering, 145 Anam-ro, Seongbuk-gu, Seoul 02841, Republic of Korea*

* Corresponding author: E-mail: phuong.nguyen-tri@uqtr.ca (P. Nguyen-Tri)

Abstract

Sillenite materials have been the subject of intense investigation for recent years due to their unique characteristics. They possess a distinct structure with space group I23, allowing them to exhibit distinctive features, such as an electronic structure ideal for certain applications such as photocatalysis. The present research delves into the structure, synthesis, and properties of sillenites, highlighting their suitability for photocatalysis. It explores also advanced engineering strategies for designing sillenite-based photocatalysts, including heterojunction formation, morphology modification, doping, and hybrid processes. Each strategy offers advantages and limitations that are critically discussed. The review then lists and discusses the photocatalytic performance of various sillenite-based systems recently developed for common applications, such as removing hazardous organic and inorganic contaminants, and even infrequent applications, such as microbial inactivation, H_2 generation, CO_2 reduction and N_2 fixation. Finally, valuable insights and suggestions are put forward for future research directions in the field of sillenite-based photocatalysis. This comprehensive overview would provide a valuable resource for the development of efficient photocatalytic systems to address environmental and energy challenges.

Keywords: Sillenite, Photocatalysis, Synthesis, Properties, Photocatalyst design, Enhanced photocatalytic applications.

1. Introduction

Water treatment and energy production are two critical concerns in ensuring a healthy and sustainable environment, and their demand has soared in recent years [1,2]. The United Nations estimates that a quarter of the worldwide people are suffering from a water shortage due to economic reasons, and by 2030, the water demand will have significantly increased [3,4]. Wastewater reuse and recycling are proposed as possible means of ensuring a reliable supply of fresh water; however, traditional wastewater treatment systems face substantial limitations due to their high energy consumption and operational costs [5,6]. It has been demonstrated that the energy consumed for the treatment process amounts to approximately 3% of the world's energy consumption and is expected to almost double in the coming years [7,8]. This makes energy supply another worldwide issue, along with the problem of water scarcity. The increase of carbon dioxide levels in the atmosphere, along with the depletion of fossil fuel supplies, generate also severe worries about the consequences for the global climate and future energy supply [9]. Finding alternative fuels with high energy density and carbon-free emissions such as hydrogen (H_2) and ammonia (NH_3) would be a potential solution. To meet those issues, nexus thinking is necessary [10,11]. This is an approach to natural resource management that emphasizes interconnection instead of an isolated system [12,13]. The water-energy nexus is always being applied from two perspectives: energy consumption by water systems and water usage by energy systems [14]. Numerous recent studies have demonstrated the viability of sustaining the water-energy nexus, in which certain water treatment procedures can generate different energy types that can be leveraged to reduce treatment expenses and the damage of fossil fuels [15]. Moreover, effective treatment can result in lower energy consumption and higher energy production, particularly when renewable energy sources are employed [13,16].

There has been an increase in interest in advanced treatment systems that allow simultaneous wastewater cleaning and the production of energy, especially when that energy is ecologically benign and sustainable [17]. It is critical to invest in renewable energy sources as well as treatment techniques that safeguard the environment and decrease the danger of pollution [18]. Water treatment techniques that use solar energy and fuel are appealing forms of sustainable treatment and energy production owing to their efficacy and long durability [19]. Photocatalysis one of the advanced processes has acquired a lot of attention as an environmentally friendly and green approach for water treatment and energy production [20]. That is because it uses solar energy and that has a significant impact by reducing energy consumption and concurrently reducing the effects of anthropogenic pollutants [21,22].

Photocatalysis has been extensively investigated in diverse fields and areas, including water splitting [23], solar energy conversion [24], water/air purification [25], CO_2 reduction [26], N_2 fixation [27] and H_2 production [28]. Photocatalysis using heterogeneous catalysts based on semiconductors has received a lot of interest in recent years, notably in water and energy applications because it is effective, simple to conduct, and used as a powder (suspension) that is simpler to separate from water [29,30]. Semiconductor materials qualified for heterogeneous photocatalysis should have essential qualities such as optical absorption, electronic structure, and the ability to create charge carriers when powered by a light source by converting light energy into chemical reactions [31–33]. Despite the development of highly various metal oxide semiconductors such as TiO_2 and ZnO, their practical applicability is limited by their low irradiation sensitivity, high photo-electron pair recombination rate, and large band gap [34–37]. To solve these challenges, novel, efficient, and multifunctional semiconductors are required.

One of the most crucial factors in the development of efficient photocatalysts is the core metal ion of the semiconductors [38]. It has been proved in previous works, that the metal ions of bismuth (Bi), titanium (Ti), tin (Sn), and zinc (Zn) have been classified as the best ions to generate efficient catalysts for numerous photocatalytic applications [39,40]. Bismuth ions have recently drawn a lot of researchers as the metal core of catalysts, due to a variety of unique characteristics, most notably their remarkably high chemical stability, high light absorption, low rate of pair recombination, and narrow band gap [41]. Bismuth sillenites with the chemical formula $Bi_x[A]O_y$ are current materials with high photocatalytic potential, in which $Bi_{12}[A]O_{20}$ has been most widely investigated [42]. Sillenites have lately intrigued researchers owing to their nonlinear optical characteristics and photocatalytic capabilities [41,43]. They are regarded as attractive materials for a variety of potentially promising applications, including photocatalysis and other photonic domains, due to their combination of strong nonlinear characteristics, the relative simplicity of manufacture, and inexpensive production cost [44,45]. It is true that bismuth ions are harmful and dangerous in their ionic form, particularly in the nitrate form; nevertheless, by using their ions to produce chemically stable catalysts, their risk can be reduced, as a previous paper demonstrated that synthesizing sillenites using bismuth ion reduces their risk [40]. This provides additional benefit to sillenite by improving waste management by lowering harmful ions while also providing valuable and useful components that may be used in a variety of practical applications.

Although bismuth sillenites have been synthesized and studied in many recent papers, the majority of those investigations focused exclusively on the characterizations and efficacy of those materials in photocatalytic applications, without a detailed discussion of their

interesting properties in comparison to other catalysts, which left a lack of understanding of this material class. The different properties or synthesis techniques of those intriguing materials have not been yet the subject of a systematic review. Additionally, there has only been a cursory investigation of the use of sillenite photocatalysts for water filtration, water splitting, CO_2 abatement, and N_2 fixation. Furthermore, there has never been a thorough analysis of the numerous approaches to enhancing sillenite-type photocatalysts. Only a short critical review has dealt with sillenite-type materials for some photocatalytic applications, and it has concentrated on the stoichiometry "$Bi_{12}MO_{20}$" [33]. For this purpose, this research paper aims to comprehensively and thoroughly review sillenite crystals as an interesting material type. Various procedures for the synthesis of sillenites, their advantages and conditions have been described. The structure, electronic properties as well as optical characteristics of sillenites have also been studied, along with a detailed discussion of the potential of those sillenite catalysts for photocatalytic applications. Furthermore, current advances in designing sillenite-based materials to enhance the efficiency of those materials based on the literature have been summarized and analyzed, to elucidate the advantages of various methods in the improvement of the proprieties and efficiency of those materials. In the end, this study has concluded with perspectives, in which general opinions have been proposed.

2. Fundamental of photocatalytic applications

Before demonstrating the intriguing properties of the sillenite-type materials as photocatalysts, it is important to describe their mechanism of action in photocatalysis applications. It is crucial to explain the reason for selecting the photocatalysis approach as well. Numerous approaches and technologies have been used to remove pollutants from drinking water and municipal wastewater treatment plans, but most of these approaches have disadvantages and limitations in terms of applications, time, design, by-products, scale, efficacy, and economics [46–49]. For example, membranes and adsorption can only concentrate the pollutants or move them from one phase to another without completely removing them [50]. For biological treatment, refractory and high-concentration contaminants have an effect on the activity of aquatic microorganisms and are time-consuming [51]. The chemical method and UV radiation do not adhere to the regulations for sewage disposal, and the classic treatment techniques create toxic degradation by-products that are harmful to human health and the environment [49,52]. This indicates that the most common treatment methods are not able to preserve up with the rising demand for clean water on a worldwide scale [48,49,53]. Advanced Oxidation processes (AOPs) are the most innovative and economical

water and wastewater treatment techniques for the removal of recalcitrant chemicals, as they can inexpensively eliminate a variety of contaminants at room temperature and atmospheric pressure [54,55]. The photocatalysis process among AOPs has acquired a lot of attention as an environmentally friendly, green, cost-effective and efficient method for treating and producing water and energy [56]. This interest was sparked not only because photocatalysis may be used to treat and purify water in a non-hazardous approach, but also because photocatalysis can be utilized to create energy by producing hydrogen or other fuels [57].

Indeed, photocatalysis has become a versatile and promising technology with extensive uses in a range of sectors [58,59]. Photocatalysts enable chemical reactions that can break down toxic pollutants and transform them into less harmful or useful chemicals, providing an eco-friendly method for ensuring the sustainability of the environment [58,59]. Due to its promise in multiple practical uses, photocatalysis has recently been applied and explored in a wide range of areas and domains. Photocatalysts have been studied in the area of water splitting for their potential to split water into hydrogen and oxygen, producing a clean and sustainable source of fuel [60]. The potential of photocatalysis to capture solar energy and transform it into useful power or chemical fuels has also attracted interest, advancing the development of renewable energy systems [61,62]. Photocatalysts may decompose organic pollutants, purify water, and enhance indoor air quality [20]. Photocatalysis has also shown to be successful in water and air treatment operations. Another use of photocatalysis that has promise is the desalination of seawater, which might help to address the problem of water shortage and give a long-term method of acquiring freshwater [63]. In addition, photocatalysis has been investigated for nitrogen fixation, which aims to transform atmospheric nitrogen into forms that are more useful to plants [64]. This process is important in agriculture and the manufacture of fertilizers [64]. A crucial strategy in the battle against climate change is the conversion of carbon dioxide into useful goods using photocatalysts [65]. This can help to capture and employ this greenhouse gas. In addition, photocatalytic hydrogen synthesis offers a sustainable substitute for conventional techniques and a possible source of clean energy [66].

2.1. General photocatalytic mechanism

To understand the utility of the photocatalytic process in diverse fields and areas, it is important to explain the mechanism of this process for every field. Basically, the principle of photocatalysis is the same for each field; however, the mechanism of the reaction is different from one application to another. This general photocatalytic process typically consists of three basic steps:

1) Formation of electron-hole pairs (e^-/h^+) upon absorption of photons with energy greater than the bandgap of catalysts. Electrons are excited from the valance band (V_B) to the conduction band (C_B) while leaving holes in the VB [40,67,68]. The following equation summarizes the first step:

$$\text{Catalyst} + h\upsilon \rightarrow \text{Catalyst}^* + e^- + h^+ \quad (1)$$

2) Separation and transportation of charge carriers to the active sites on the surface of a photocatalyst [69].

3) Surface chemical reactions at the surface of the photocatalyst, where the electron/hole pairs or active species generated from them react with the target, depending on the field of photocatalytic application [70,71]. As there are different reaction mechanisms for different applications, the photocatalytic reaction mechanism for major fields will be discussed.

2.2. Photocatalytic mechanism for water treatment

In wastewater, there are various types of pollutants, such as inorganic and organic pollutants as well as microorganisms and their removal mechanism using photocatalysis is changed from one pollutant to another.

For organic compounds degradation, AOPs function by employing a physicochemical process to active reaction species including hydroxyl radicals ($^{\bullet}OH$), oxygen radicals ($O_2^{\bullet-}$), singlet oxygen (O), ozone (O_3), hydrogen peroxide (H_2O_2), and others at ambient pressure and temperature, which subsequently decomposes organic pollutants into carbon dioxide and water [5,72–75]. **Table 1** elucidates the relative oxidation potential of the main oxidizing species used in water treatment techniques [54].

Table 1. Relative oxidation potential of the main oxidizing species used in water treatment techniques.

Oxidizing species	Relative oxidation power compared to OH radicals
$^{\bullet}OH$ radicals	1
Ozone	0.74
Hydrogen peroxide	0.63
Perhydroxyl radical	0.61
Permanganate	0.61
Chlorine dioxide	0.56
Chlorine	0.49
Oxygen radicals	0.43

According to the table, $^{\bullet}OH$ radicals have the greatest oxidation capability than other oxidants, which are frequently generated with H_2O_2 and $O_2^{\bullet-}$ in photocatalysis. The mechanism of organic pollutant degradation in photocatalysis is directly linked to reaction pathways that

are controlled by the reactive oxygen species (ROS) $^{\bullet}OH$, H_2O_2 and $O_2^{\bullet-}$ [20,54]. In photocatalysis, $O_2^{\bullet-}$ is produced through the reduction of O_2 by e^- while the oxidation of H_2O by h^+ generates $^{\bullet}OH$ [76–78]. H_2O_2 is formed by the reaction between oxygen radicals $O_2^{\bullet-}$ and protons H^+. Those reactions are summarized in the following equations:

$$O_2 + e^- \rightarrow O_2^{\bullet-} \quad (2)$$

$$H_2O + h^+ \rightarrow {}^{\bullet}OH + H^+ \quad (3)$$

$$e^- + 2H^+ + O_2^{\bullet-} \rightarrow H_2O_2 \quad (4)$$

$$H_2O_2 + e^- \rightarrow OH^- + {}^{\bullet}OH \quad (5)$$

Due to the high reactivity, ROS can rapidly oxidize organic pollutants, resulting in their degradation to CO_2, H_2O, and less hazardous small particles (by-products) [79]. Various research has demonstrated the effectiveness of photocatalysis for water disinfection by inactivating a variety of microorganisms, including bacteria, viruses, fungus, and protozoa [80]. The mechanism of inactivation of photocatalytic microorganisms is similar to that of organic photodegradation with the involvement of ROS, because almost all pathogenic microbes include organic molecules, such as proteins, carbohydrates, lipids, sugars, amino acids, and DNA [81]. However, photoinactivation involves a little more complicated mechanisms. Alike photodegradation, the photo-generated electron-hole pairs in the photocatalyst surface undergo redox reactions with molecules, such as H_2O and O_2, to produce ROS [5,72–75]. The ROS could apply different inactivation actions for the microorganisms, such as oxidative stress, an imbalance in membrane permeability, protein inhibition, changes in cell structure, metabolic alterations, and DNA/RNA damage, which result in cell death and lysis [82–86].

For the reduction of inorganic ions by photocatalysis, it is directly linked to reaction pathways that are controlled by photoelectrons (e^-) [32,87]. The photoelectrons are produced by the electric field that results in the leveling of Fermi levels when the catalyst is being activated by light energy greater than its band gap [88–90]. These photoelectrons move to the semiconductor active sites, where they participate in reduction reactions with adsorbed inorganic ions [91]. The reduction of the adsorbed inorganic ions occurs if the inorganic ions' reduction potential is a higher positive charge than of the catalyst's conduction band [92]. The mechanism of three photocatalytic processes over photocatalysts can be summarized in **Figure 1**.

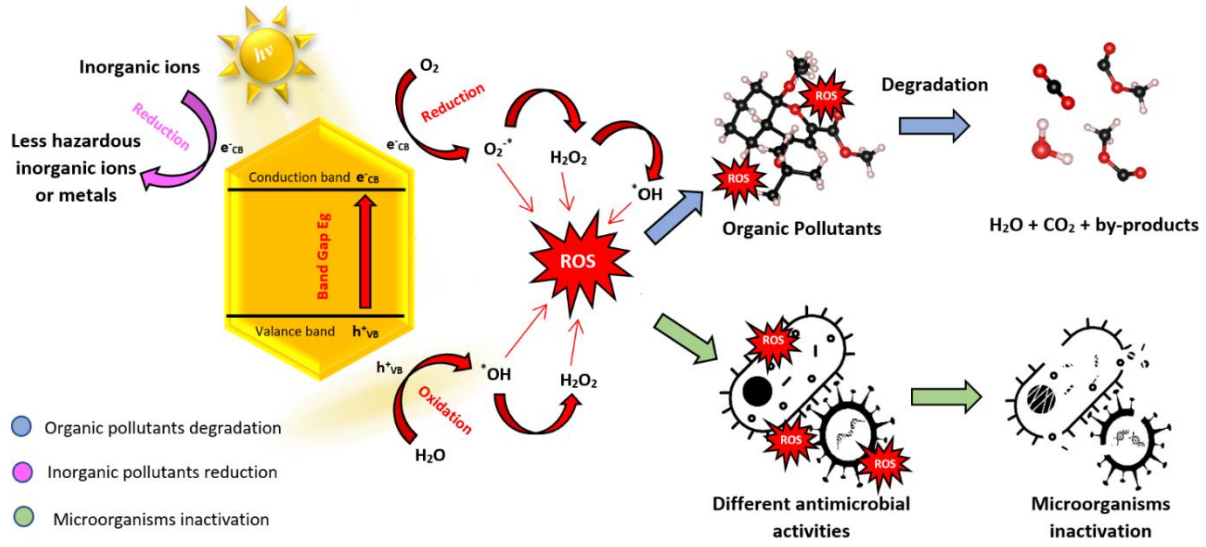

Figure 1. Photocatalytic mechanisms of organic pollutant degradation, inorganic pollutant reduction, and microorganism inactivation.

2.3. Photocatalytic mechanism for water splitting, CO_2 reduction and nitrogen fixation

The mechanisms of water splitting, CO_2 reduction, and nitrogen fixation share a common characteristic, they heavily depend on the potential energy of reactions. These reactions require a certain amount of energy input to overcome the energy barrier and undergo a chemical transformation, where the potential energy of the reactants is converted into the energy required for the reaction to occur. Therefore, explaining the potential energy of reactions is crucial for understanding the photocatalytic mechanisms for those applications.

Water splitting, to generate both H_2 and O_2, is an upward chemical reaction with an increase in Gibbs free energy [93]. The water-splitting mechanism is divided into two reactions which are the hydrogen evolution reaction (HER) and the oxygen evolution reaction (OER) [94]. In HER, electrons reduce protons to generate H_2, while in OER, holes oxidize water to produce O_2 [93]. The following equations list these reactions as well as the accompanying reduction potentials (versus normal hydrogen electrode (NHE) at pH 7.0).

$$2\,H_2O + 4\,h^+ \rightarrow O_2 + 4\,H^+ \qquad E^0 = +0.82\ V \quad (6)$$

$$2\,H^+ + 2\,e^- \rightarrow H_2 \qquad E^0 = +0.059\ V \quad (7)$$

HER occurs within two stages on the catalyst's active surface. The first stage is the Volmer reaction, in which an electron transfer to the catalyst surface area is paired with proton adsorption on an empty active site of the catalyst to produce a hydrogen atom, where the water molecule is the source of the protons [93,94]. The second stage is the creation of H_2 and it can

occur via two distinct chemical paths, the Heyrovsky and Tafel mechanisms [94]. In the Heyrovsky mechanism, a second electron is transferred to the adsorbed hydrogen atom with another proton transferred from the water to evolve H_2. In the Tafel mechanism, two adsorbed hydrogen atoms formed in the first stage combine to form H_2. Generally, water splitting occurs when the CB minimum edge of the catalyst is located at a potential that is more negative than the H^+/H_2 reduction potential, and the VB maximum edge is located at a potential that is more positive than the H_2O/O_2 oxidation potential [95–98].

CO_2 reduction is more complicated than water splitting because CO_2 has a high C=O double-bond energy, making it very stable. As a result, its reduction is extremely difficult; nonetheless, several studies have demonstrated the efficacy of the photocatalysis method in CO_2 reduction [99]. CO_2 reduction happens primarily on the surface of the catalyst with the participation of photo-generated electrons and protons with an appropriate reduction potential level [9,65]. Those react electrons and protons with CO_2 reduction within different pathways, which are formaldehyde, carbene and glyoxal pathways [9,100]. Different reduction products and intermediates are formed during the CO_2 reduction based on the potential of the reaction, equations 8 to 13 list the theoretical reactions related to CRR in the presence of photocatalyst, as well as the accompanying reduction potentials (versus normal hydrogen electrode (NHE) at pH 7.0) [9,100–102].

$$CO_2 + e^- \rightarrow CO_2^{\bullet -} \qquad E^0 = -1.9\ V \qquad (8)$$

$$CO_2 + 2H^+ + 2e^- \rightarrow HCOOH \qquad E^0 = -0.61\ V \qquad (9)$$

$$CO_2 + 2H^+ + 2e^- \rightarrow CO + H_2O \qquad E^0 = -0.53\ V \qquad (10)$$

$$CO_2 + 4H^+ + 4e^- \rightarrow HCHO + H_2O \qquad E^0 = -0.48\ V \qquad (11)$$

$$CO_2 + 6H^+ + 6e^- \rightarrow CH_3OH + H_2O \qquad E^0 = -0.38\ V \qquad (12)$$

$$CO_2 + 8H^+ + 8e^- \rightarrow CH_4 + 2H_2O \qquad E^0 = -0.24\ V \qquad (13)$$

The most crucial reaction in the CO_2 reduction process that scientists and researchers prefer is the direct single-electron step in equation 8, which includes the formation of the anion radical CO_2. However, due to the closed-shell electronic arrangement of CO_2 and the substantially negative redox potential of up to -1.9 V, this reduction process is exceedingly challenging [99]. To our knowledge, up to today, almost no photocatalyst has demonstrated adequate capability to drive such a single-electron CO_2 reduction reaction. On the other hand, the multi-electron/proton reduction reactions in equations 9 to 13 are alternate options because of the substantially lower reduction potential required for CO_2 reduction [101]. There is relatively little support for the multiple-electron reduction of CO_2, even though most research

advocated single-electron reduction [100]. The single electron reduction of CO_2 in equation 8 can be enabled by the energy barrier which might be lowered by the stable configuration of CO_2 molecules being altered by chemisorption on the photocatalyst surface [101,103]. Water presence also provides various challenges that compete with CO_2 reduction. Firstly, water oxidation can produce highly oxidizing hydroxyl radicals $^{\bullet}OH$, as already seen in previous mechanisms, which can oxidize various stages of CO_2 reduction, disrupting the process [100]. For this, the oxidation of water in the VB is better has to be selective to the reaction shown in equation 6, as it generates protons that participate in the CO_2 conversion. CO_2 reduction is also highly contested because the potential of HER for H_2 generation in CB (as elucidated in equation 7) is greater than that of CCR and needs only fewer photo-generated electrons [99,101]. To overcome the challenges of direct single-electron reactions, it is critical to develop a high-efficiency photocatalyst for CO_2 reduction, where considering a variety of parameters and factors such as easily generated and migrated electrons and protons, more negative photo-generated electron potentials, easy adsorption of reactants on the active sites of a catalyst, and depleted photo-induced holes on the VB of the catalyst [101,103].

Photocatalytic nitrogen fixation or ammonia generation is the conversion of inert nitrogen (N_2) into ammonia (NH_3) in the presence of a photocatalyst [104]. Living organisms in water can then convert NH_3 into amino acids, amines, and urea, making nitrogen less dangerous [105]. The photocatalytic process of nitrogen fixation which can be called N_2 reduction reaction (NNR) can occur within two main pathways, which are distal and alternating mechanisms. The distal pathway proposes that (e^-/H^+) couples sequentially connect to one nitrogen atom of N_2 to produce nitride intermediates, freeing the initial NH_3 and leaving a single nitrogen that eventually changes into another NH_3 [104,106]. The alternating pathway, on the other hand, proposes that (e^-/H^+) couples occur alternately on the two nitrogen atoms to form N_2 [104,106]. Photocatalytic nitrogen fixation, like CO_2 reduction, is heavily reliant on the relative positions of the reactant's reduction potential, with the C_B position of the photocatalyst must be more negative than the reduction potential of the N_2 redox reaction, and the V_B level must be more positive than the oxidation potential of water [66]. Photocatalytic nitrogen fixation also largely depends on the chemisorption ability of photocatalysts towards N_2 molecules, because N_2 molecules are even more persistent and inert than CO_2 molecules, which makes them difficult to adsorb [66]. Equations 14 to 19 list the theoretical reactions related to N_2 photoreduction by a semiconductor, as well as the accompanying reduction potentials (NHE at pH 0.0) [66,104–108].

$$N_2 + e^- \rightarrow N_2^- \qquad E^0 = -4.16\ V \quad (14)$$

$N_2 + H^+ + e^- \rightarrow N_2H$ E^0= -3.20 V (15)

$N_2 + 2H^+ + 2e^- \rightarrow N_2H_2$ E^0= -1.10 V (16)

$N_2 + 4H^+ + 4e^- \rightarrow N_2H_4$ E^0= -0.36 V (17)

$N_2 + 6H^+ + 6e^- \rightarrow 2\,NH_3$ E^0= +0.55 V (18)

$N_2 + 8H^+ + 6e^- \rightarrow 2\,NH_4^+$ E^0= +0.27 V (19)

As can be seen from those reactions, nitrogen fixation appears to be a difficult process because of the great stability of N_2 molecules. Especially for direct N_2 reduction (equation 14), which requires a redox potential of -4.16 V, which is unattainable for most photocatalysts [104,105]. The presence of H+, on the other hand, greatly decreases the reduction potential, allowing photocatalysis to convert N_2 into its derivatives. This suggests an alternate strategy for N_2 fixation. Some effective strategies, such as selecting a suitable defect-rich photocatalyst with a high number of anion vacancies, supporting cocatalysts, and ion doping, must be developed to improve N_2 adsorption and activation at reactive sites for promoting nitrogen fixation and suppressing hydrogen generation (HER), as they are competitive in the valance band [104,105]. **Figure 2** summarizes the mechanism of water splitting (HER and OER), carbon dioxide reduction (CRR), and nitrogen fixation (NRR), as well as the potential reduction products with their redox potential energy.

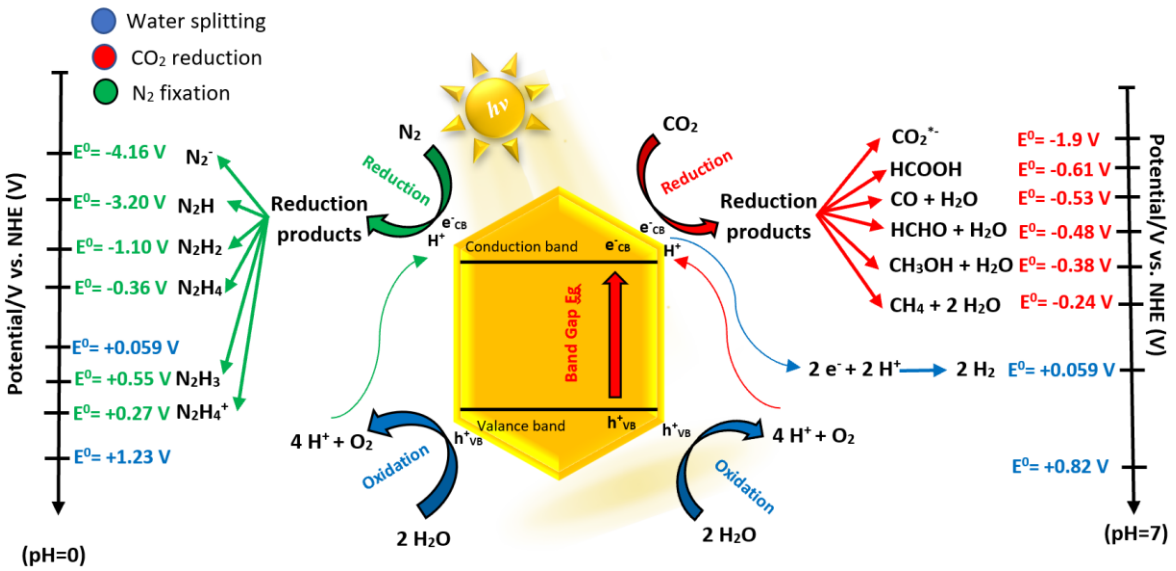

Figure 2. Photocatalytic mechanisms of water splitting, CO_2 reduction and N_2 fixation.

3. Sillenite-type materials

Sillenite is a form of crystal that belongs to a class of complex oxides with a distinct crystal structure made up of bismuth, oxygen, and other metals [109,110]. The first discovery of sillenite-type oxides was announced in 1937 by Swedish scientist Lars Gunnar Sillén, after

whom sillenite is called [111]. Sillén was primarily exploring bismuth and oxygen compounds, and by accident developed a body-centered cubic phase by burning Bi_2O_3 with Al_2O_3 for 5 minutes at 900 °C, which is a sillenite phase [111]. Schumb and Rittner developed a similar phase in 1943 by firing Bi_2O_3 and SiO_2 for 20 minutes at 875 °C [112,113]. After that, in 1945, Aurivillius et al. published the synthesis of several compounds that are isomorphic to $Bi_{12}SiO_{20}$ but include other cations [114]. Subsequently, several more compositions containing over 60 sillenite-type crystals have been studied and reported [115,116].

Sillenite crystals were characterized by the standard formula $Bi_{12}MO_{20}$, where M is the tetravalent ion of an element from the Periodic Table's II-VIII groups [117,118]. Nevertheless, other stoichiometries and altered sillenites are also discovered, such as $Bi_{25}GaO_{39}$, $Bi_{25}InO_{39}$, $Bi_{25}FeO_{39}$, $Bi_{25}TlO_{39}$, $Bi_{24}B_2O_{39}$, $Bi_{38}CoO_{58}$, $Bi_{38}ZnO_{58}$, and $Bi_{25}AlO_{39}$ [119,120]. For this, a research paper has been conducted based on crystallographic facts and the mechanisms of isomorphic substitution to construct the following standard formula for stoichiometric sillenites [121].

$$Bi_{12}(Bi_{\frac{4}{5}-nx}M_{n+5x})O_{19.2+nx} \quad (20)$$

This standard formula elucidates the potential range of homogeneity and how it relates to the charge of the tetrahedral M^{n+} ions, where the stoichiometric n can be any one of 2, 3, 4, or 5 and x is the upper limit for the M^{n+} incorporation which depends in the n value [121]. Where x is 1/15 for n=2, 1/10 for n=3, 1/5 for n=4, and 4/5 for n=5. Another study has simplified and generalized the formula for sillenite as follows [122].

$$Bi_xM_yO_z \quad (21)$$

Where M is one or more of the elements from the Periodic Table's II-VIII groups; x,y and z are the stoichiometric models. The stoichiometric models of sillenite crystals vary on the precise chemical composition of the crystal, with x ranging from 0.3 to 70, y from 0.05 to 8, and z from 1 to 100 [122].

The meta-stable form of bismuth oxide, γ-Bi_2O_3, is the parent structure of Sillenites. their structure is the body-centered cubic structure having the space group I_{23} and this structure is shared with many other synthetic materials, notably bismuth germanate and bismuth titanate [123–125]. The majority of sillenite materials are tiny and prismatic, and they feature a special crystal structure that is distinguished by an incredibly high number of symmetry planes. Although sillenite crystals are usually yellow, gray, or brown in appearance, their color did not have a significant effect on the penetration of light within the solution and the opacity will not decrease a lot. The transition-metal ion Bi^{3+} ions in the sillenite structure have several

advantages such as easy separation of photo-generated electron-hole pairs due to the presence of d10 configuration [30,43], creation of an internal polar electric field because of the 6s2 orbital pair of electrons [38,126], and the capacity to decrease the band-gap due to O 2p and Bi 6s orbital hybridization [38,43]. Other than the advantages of the Bi^{3+} ions in the sillenite structure, sillenite-type crystals are the most intriguing class due to their distinctive structures, pronounced photo-refractive effect, photochromic, piezo-electric, dielectric, and electro-optic capabilities, high birefringence, rapid response, lengthy optical storage duration in the dark, recyclable nature, high surface area and narrow band gap [41,127–133]. Sillenite crystals can also exhibit other properties, such as magneto-optical characteristics, by modifying their compositions [134].

Although having drawbacks like expensive costs and limited availability, sillenite crystal is extremely promising in a wide range of applications due to its advantageous features and unique properties [41,129]. The sillenite crystals have recently demonstrated great potential for a variety of applications where their properties can be taken advantage of, including electrooptics, electro-optic modulators, acoustics, piezotechnics, photovoltaic cells, fiber optic sensors, optical switches and waveguides, real-time and multi-wavelength holography, optical information processing and storage and some issues in metrological [135–139]. Moreover, they are utilized as dielectrics in the field of electronics and are thought to be promising materials for laser technology [121,140]. They also have an efficient energy transmission owing to the crystal structure's abundance of oxygen [140]. Ongoing research into their properties and applications is expected to lead to new and exciting discoveries in other fields. Sillenite crystals are very resistant to corrosion and radiation and have robust chemical inertness, crystal structure, and optical characteristics, making them perfect for photocatalytic applications that call for a stable and effective material [137]. During an irradiation test in 1994, the potential for sillenite to function as a photocatalyst was unintentionally uncovered [43,141]. Since then, numerous theoretical and experimental studies have been started in the mid-2000s to ascertain the ideal conditions for those materials [119,137,142], and they are now being used in extensive research studies of the photocatalytic applications to investigate the photocatalytic properties of sillenites [40,67,143,144], as they elucidated very promising efficiency in various environmental applications, including the production of hydrogen fuel and the removal of heavy metals and organic pollutants in water [33].

Numerous studies have shown that sillenites are effective at degrading organic pollutants such as dyes, pesticides, and pharmaceuticals in both aqueous and gaseous environments [144]. For example, Wu et al. discovered that the bismuth silicate $Bi_{12}SiO_{20}$ was

a highly efficient photocatalyst for the aqueous degradation of rhodamine B when exposed to visible light [145]. Previous research has studied the photocatalytic properties of sillenite-type crystals, finding that these types of materials have a wide range of potential applications due to their high photocatalytic activity, high surface area, and ability to absorb light. Additionally, coating with metals as co-catalysts or coupling with other materials can substantially improve their performance and thermal stability [33]. Oliveira et al. conducted a study on the challenges of sillenite crystals for photocatalysis. The authors noted that the synthesis of these crystals is still a difficult process, which can limit the ability to produce them in large quantities. These challenges must be addressed in order to effectively utilize sillenite crystals for photocatalysis and other applications [127]. If this material were to be developed further, it might open the door for new developments in the photocatalysis field.

3.1. Synthesis of sillenite materials

The synthesis of sillenite crystals has long been a concern in the field of material research, as it is a complicated process that requires the precise mixing of a variety of procedures and materials [146]. There are several synthesis techniques for synthesizing sillenite crystals, and each process might result in crystals with varied physical and chemical characteristics [147]. Physical and chemical procedures are the two basic types of synthesis methods for sillenite crystals [148,149]. Physical methods rely on mechanical or physical processes to synthesize catalysts, which generally involve high temperatures, pressures, or energy inputs. However, they may introduce impurities from the mechanical processes involved and result in less control over these properties. In contrast, chemical methods involve chemical reactions between metal precursors and supporting materials, which involve lower temperatures and pressures, resulting in purer catalysts with fewer impurities, and offering better constrained control over these properties [150]. To summarize, sillenite synthesis methods vary in terms of precursor materials, purity, mechanisms, control over characteristics, synthesis and reaction conditions, the temperature used to produce the crystals during the synthesis process, and particle size and shape. They do, however, have similar characteristics in their broad application, nanoparticle production, optimization, energy efficiency, precursor mixing, crystallization, catalytic activity, and synthesis condition optimization [151]. The synthesis of sillenite materials has been studied extensively in recent years, as this material type has shown interesting characteristics for a variety of applications, such as photocatalysis [33]. Several techniques for synthesizing sillenite materials have been reported in the literature; **Figure 3** depicts the different sillenite material forms and their available synthesis methods.

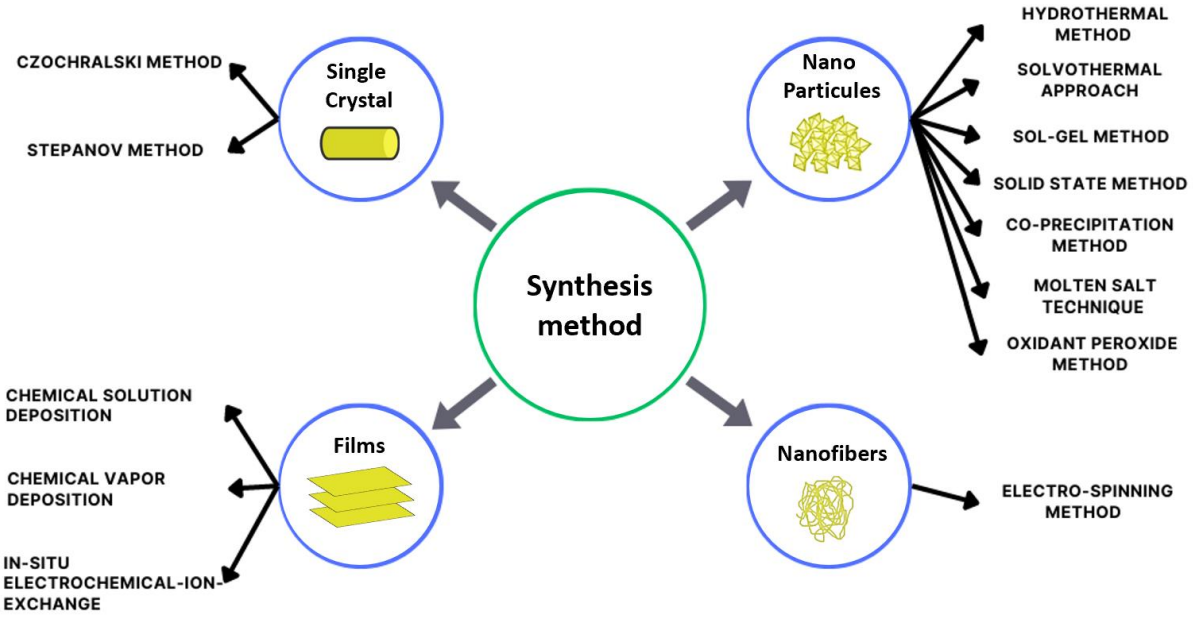

Figure 3. Different forms of sillenite materials and their synthesis methods.

Sillenite crystals can be synthesized using several methods, including the czochralski method, hydrothermal method, co-precipitation, sol-gel method, molten salt method, solid-state method and other methods, with each approach effectively producing sillenite crystals with a wide range of properties and uses [123]. These synthesis techniques can be tweaked to regulate the sillenite catalyst's size, shape, and surface characteristics, which can have a major influence on activities. The synthesis technique used is determined by the specific needs and desired qualities of the sillenite catalyst, the type of reactants, and the specific purpose of its application [151]. Although there are several techniques for synthesizing sillenite catalysts, there are obstacles and concerns connected with the approaches, such as the high cost of the energy necessary to produce high temperatures and pressures, and the complicated crystal formation mechanism. In this regard, different techniques for synthesizing sillenite crystals have been addressed in the following section, along with their advantages and disadvantages, using successful sillenite crystal synthesis experiments and findings as examples.

3.1.1. Czochralski method

The Czochralski method, which has been used widely to produce sillenite crystals, is a commonly used approach for the synthesis and crystal growth of single-crystal materials [152]. The process is based on the solidification from the melt principle, in which a seed crystal is dipped into a high-purity mixture of the component materials inside a cylindrical container or crucible composed of a molten mixture-resistant material such as platinum [153,154]. The crucible containing the melt is then turned, where the temperature of the melting is between

600 and 900 °C [155]. After that, the crystal is extracted from the revolving melt using a pulling mechanism, which is used to slowly generate the crystal from the melt while rotating the crucible and the seed crystal in opposite directions [156]. The melt gradually forms the boule around the seed crystal; once the crystal has grown to the required size, it is taken from the crucible and cleaned [157]. Then, the obtained crystal is sliced and cut into wafers of the desired thickness using a diamond paste and polishing pad [153,154]. The process of Czochralski synthesis was summarized and illustrated in **Figure S1** in the supporting information. The temperature, pulling speed, oxygen partial pressure, and rotation speed of the crucible and seed crystal are significant parameters during the crystal formation process [158,159]. Temperature is very critical in this process because it affects both the solvent-crystal contact and the growth rate [159]. The pulling rate influences the oxygen concentration and the defect structure of the crystal, whereas the oxygen partial pressure influences the size and form of the crystal [158]. The atmosphere of synthesis has also to be controlled to prevent contaminants from contaminating the crystal [160]. There have been several investigations of effective sillenites crystal synthesis using the Czochralski method.

Isik and Gasanly's team recently published a series of research papers on sillenite crystals synthesized by the Czochralski method, providing a comprehensive understanding of the process parameters involved in sillenite crystal synthesis using such a method [129,161]. They performed a case study in which they employed the Czochralski technique to produce several sillenite crystals, such as $Bi_{12}GeO_{20}$, $Bi_{12}TiO_{20,}$ and $Bi_{12}SiO_{20}$ [162–164]. According to their findings, the Czochralski process proved successful in generating sillenite crystals with high optical and electrical characteristics [165,166]. They also discovered that crystals created using the Czochralski process were highly crystalline [167]. Additionally, they concluded that the Czochralski procedure was both cost-effective and efficient in the production of sillenite crystals, making it a viable option for synthesizing these crystals [168,169]. Many more studies have demonstrated the effectiveness of the Czochralski process in synthesizing sillenites such as $Bi_{12}SiO_{20}$[155,158], $Bi_{12}GeO_{20}$[159,160], $Bi_{24}B_2O_{39}$ [157] and $Nd_{0.06}Bi_{11.94}SiO_{20}$[156].

The Czochralski method is a highly precise and efficient approach for synthesizing sillenite crystals of various sizes and shapes with excellent crystal quality and purity; however, the significant propensity of the solidification front to facet produced by kinetic phenomena related to development in distinct lattice orientations has a significant impact on the optical quality of such material [164,167]. Moreover, the developing crystal in the Czochralski method is not restricted by a crucible and can acquire a polyhedral exterior morphology generated by the intersection of thin facets in contact with the melt's free surface [160]. The Czochralski

approach has also the drawback of being difficult to monitor and control to ensure uniform crystal development since parameters must be carefully checked and modified during the synthesis process to ensure the appropriate sillenite crystal is formed [155]. For that, the application of Czochralski-synthesized sillenite crystals is limited to practical applications such as LED displays, electronic and optoelectronic devices, and sensor devices [166].

3.1.2. Hydrothermal method

The hydrothermal synthesis process has been widely investigated for its ability to produce sillenite crystals [123]. This approach involves producing crystals by using high pressure and low temperatures over 100°C with aqueous solutions in a closed system such as Teflon-lined stainless steel [170,171]. **Figure S2** in the supporting information illustrates the general hydrothermal synthesis method. Because of the cleaner environment and lower temperature, sillenite crystals formed via the hydrothermal process exhibit various distinct and favorable properties when compared to other synthesis methods [123]. Crystals with uniform crystal patterns and homogenous compositions can be generated by applying high pressure and little heat to the source materials [140]; It is also possible to generate crystals with high degrees of stability and constant physical characteristics, such as electrical conductivity and optical clarity [170]. This method can also be used to adjust the size and crystal shape of the catalysts [172]. In comparison to the previous technique Czochralski, the hydrothermal approach does not require high temperatures, whereas the Czochralski method requires a sintering process at high temperatures ranging from 600 to 900 °C, which consumes energy [173]. Apart from low process temperature and energy saving, additional advantages of hydrothermal synthesis method include excellent dispersion, small particle size, etc [140,174].

Sillenite crystals synthesized using the hydrothermal approach are becoming increasingly popular in the fields of optics, electronics, and photocatalysis applications because of their appealing properties and their synthesis simplicity [123,175]. Wang et al. investigated the hydrothermal synthesis of different sillenite crystals having the formula $Bi_{12}(Bi_xM_y)O_{20}$, where M is one of the elements Cd, B, Si, P, V, Mn, Fe, Ga, Ge. The authors demonstrated in this study that the hydrothermal approach may create bulk crystals with the greatest size of 5 mm and desirable forms [123]. Such forms are more practical and easier to utilize than the prior shape of sillenite synthesized using the Czochralsk process, especially in photocatalytic applications. The authors investigated also how initial composition, temperature, and alkalinity affect the crystal phase, size, and morphology of sillenites in hydrothermal conditions. It was discovered that alkalinity was critical in the crystal formation processes, and that particular sillenites required different pH levels [123].

Zhang et al. investigated the synthesis of sillenite crystals using the hydrothermal method and discovered that it was effective in creating high-quality crystals with high yields [176]. The authors discovered that maintaining the system's temperature and pressure was crucial and that contaminants in the aqueous solution might negatively affect crystal development. According to the literature, this process may be a cost-effective way to produce massive quantities of high-quality sillenite crystals [174]. Vavilapalli et al. used a hydrothermal approach to successfully synthesize sillenite $Bi_{12}FeO_{20}$ crystals, which were reddish brown crystals with an average size of 1 mm [177]. Y Sun et al. explored the possible uses of sillenite crystals synthesized using hydrothermal synthesis. The crystals were discovered to have a high degree of crystallinity, outstanding electrical characteristics, high thermal stability, strong chemical stability, a high dielectric constant, and high capacitors and other electronic devices. This research shows that these crystals have a wide variety of uses [173]. Shi et al. successfully synthesized a series of sillenite-type $Bi_{12}PbO_{20}$ materials using the hydrothermal method, and they discovered that this sillenite is efficient in the electrochemical degradation of antibiotics and pesticides, implying its potential environmental application capabilities [178].

There is also a similar synthesis process to the solvothermal approach, which uses a liquid solvent such as alcohol or glycol instead of aqueous solutions [179]. However, this approach has only been reported for synthesizing the sillenite $Bi_{36}Fe_2O_{57}$ to date [180]. The hydrothermal synthesis has also been aided by microwave making one of the potential strategies is the microwave hydrothermal method, which allows for extremely rapid heating to the crystallization temperature, and faster crystallization kinetics by one to two orders of magnitude compared to the regular hydrothermal process, short response time, and energy savings [181,182]. Zhang et al. used this process to synthesize $Bi_{12}SiO_{20}$ in order to improve the properties of this sillenite [182]. Zhu et al. also reported the effective microwave hydrothermal synthesis of sillenite-type bismuth ferric nano-crystals in another investigation, and they found the same characteristics as previous research [181].

3.1.3. Sol-gel method

The sol-gel combustion synthesis process is a flexible and frequently used method for preparing a wide range of minerals, including crystalline oxide compounds such as sillenites [183]. This method involves hydrolysis and condensation of metal alkoxides in a solution to produce a gel with the help of a gelling agent, which is then heat-treated and ignited to generate the final product by forming metal-oxygen bonds, which grow to form the crystalline sillenite oxide substance [184]. The process of sol-gel synthesis was succinctly summarized and visually depicted in **Figure S3** in the supporting information. According to certain research,

the sol-gel approach is closely associated with the combustion process [185]. There are certain distinctions to be discussed; the sol-gel process involves drying a reactive aqueous solution at a temperature lower than the solvent's boiling point, leading to water evaporation and the creation of a gel-like substance; the combination of the gel in the same temperature which then forms the solid [43]. Whereas, in the combustion method, the reactive solution is heated to roughly between 300 and 500 °C, resulting in the production and breakdown of the gel, combustion, and formation of the solid product all occurring in a single step [186]. The sol-gel process provides for fine control of the final material composition, shape, and pore structure, which may be adjusted to attain a large surface area. Both techniques' success is determined by synthesis parameters such as material type, compound concentrations, pH, calcination temperature, and others [186].

Several papers have studied the synthesis of different sillenites using the sol-gel method, such as $Bi_{12}TiO_{20}$ [143,187], $Bi_{12}SiO_{20}$ [188], $Bi_{12}ZnO_{20}$ [67], $Bi_{12}MnO_{20}$ [43], $Bi_{12}CoO_{20}$ [40], $(Bi_{13}Co_{11})Co_2O_{40}–Co_3O_4$ [186], $Bi_{12}NiO_{19}$ [144] and $Bi_{24}Fe_2O_{39}$[189]. These papers demonstrate the successful use of the sol-gel in forming sillenites that can be used in various applications, such as photocatalysis, where in their method they used different solvents such as acetic acid and different gelling agents such as Polyvinylpyrrolidone (PVP). A research paper was conducted on the synthesis of the sillenite $Bi_{0.9}Dy_{0.1}FeO_3$ to compare the prior hydrothermal method with the sol-gel approach. This study demonstrated that there is a difference in the calcination temperatures of those methods [184].

The Pechini, or liquid mix, procedure is another approach linked to the sol-gel method. Pechini's approach involves complexing cations in an aqueous-organic media with low-cost precursors, resulting in a molecularly homogenous ion distribution. The pechini method has also demonstrated the potential to generate catalysts with high performance, especially in photocatalysis applications [190]. Wu et al. investigated the Pechini technique for preparing pure $Bi_{12}SiO_{20}$ and assessed its strong photocatalytic activity [145], and Qiao et al. examined the structural properties and photocatalytic properties of $Bi_{25}VO_{40}$ sillenite nanoparticles [38].

3.1.4. Solid State method

The solid-state method is too facile compared to other methods, where the sillenite catalyst is created directly by pulverizing bismuth oxide and metal oxide precursors together, grinding, and heating them to high temperatures in the air or under an oxygen atmosphere [116,191]. The illustration of the process of synthesis can be found in **Figure S4** in the supporting information. Since ceramics and crystals of various shapes may be manufactured at a reasonable cost, solid-state reaction synthesis is one of the most widely used commercial

techniques among the numerous synthesis methods [192,193]. This method has been used to generate various sillenite crystals such as $Bi_{12}SiO_{20}$ [29], $Bi_{12}GeO_{20}$ [29], $Bi_{12}TiO_{20}$ [29], $Bi_{25}FeO_{40}$ [191], $Bi_{25}GaO_{39}$ [138], $Bi_{12}(B_{0.5}P_{0.5})O_{20}$ [194]. However, certain investigations have detected the appearance of secondary phases during the synthesis of specific catalysts, such as in the case of the sillenite phase $Bi_{12}TiO_{20}$, where they discovered the intermediate compounds $Bi_4Ti_3O_{12}$ and $Bi_2Ti_2O_7$ [192]. As a result, as compared to sol-gel and hydrothermal methods, the solid-state approach is less effective for synthesizing pure sillenite crystals.

A research paper has reported a unique form of solid-state reaction technique, high-energy ball milling, which is a relatively recent method for producing technologically valuable materials at high temperatures [195]. In that study, the process of ball milling in stainless steel jars in a planetary mill was effectively employed to synthesize the sillenites $Bi_{12}SiO_{20}$, $Bi_{12}GeO_{20}$ and $Bi_{12}TiO_{20}$ [195]. The authors have also justified in this study that high-impact energy imparted to minuscule quantities of powder briefly caught between two colliding balls causes a local transient of high temperature and pressure, which drives the reaction at the trapped particles' surface forming the sillenite phase [195]. However, even with this method, the issue of intermediate chemicals persists.

3.1.5. Chemical solution and vapor deposition

Chemical solution deposition (CSD) is a process that uses a chemical precursor solution to build a film, and it is a general term for several techniques such as sol-gel, metallo-organic breakdown, and chemical bath deposition [196]. CSD is based on layer synthesis from liquid-phase precursors that are converted into the final functional film material [196]. **Figure S5** in the supporting information provides an illustration of the CSD process of synthesis. The CSD approach can provide cost-effective access to big-area coatings, which are necessary to manage enormous quantities of energy in novel applications, such as photocatalysis [197]. Numerous works have discussed the use of the CSD method to create sillenite films, such as for $Bi_{12}TiO_{20}$ [132,197], $Bi_{12}GeO_{20}$ [198] and $Bi_{24}AlO_{39}$ [126]. These investigations demonstrated that sillenite films generated by the CSD approach exhibited a strong photocatalytic activity. Furthermore, those films had strong anti-inactivation stability and cling effectively to the silicate substrate after repeated application. Yao et al. investigated the synthesis of sillenite catalysts with the general formula $Bi_{12}MO_{20}$ where (M is Al, Ti, Pb, Fe and Ni), and demonstrated that such sillenite compounds were effective for the decomposition of methyl orange [141]. The main advantage of this approach is that it produces films; nevertheless, it has several disadvantages, such as a low surface area, since the particles inside the sillenite films cover each other, reducing the active surface area.

Chemical vapor deposition (CVD) is a similar approach to the CSD method, in which a gaseous precursor is passed over a substrate at high temperatures, resulting in the deposition of a solid coating on the substrate [199]. This approach has been used only in one study to create $Bi_{12}SiO_{20}$ films; however, it has not been employed since that time, owing to the difficulties in this procedure, a lack of benefits, and the availability of more relevant techniques [200]. Moreover, this method can create intermediary products such as in this study where it was found the sillenite phase $Bi_{24}Fe_2O_{39}$ as an intermediate in the synthesis of $BiFeO_3$ [199].

3.1.6. Co-precipitation method

In the co-precipitation process, two or more metal precursors are mixed in a solution, and then a precipitating agent is added to cause the metals to co-precipitate. The resultant solid is then washed several times and calcined to create the sillenite [68]. The co-precipitation process of synthesis is depicted in **Figure S6** in the supporting information. The Co-precipitation method has been utilized to synthesize a wide range of materials for various applications; However, in the case of sillenite, there is a lack of research that covers the synthesis of those crystals using this approach. $Bi_{12}ZnO_{20}$ [68], $Bi_{12}TiO_{20}$ [201], $Bi_{12}MnO_{20}$ [202] and $Bi_{25}FeO_{40}$ [203] have been synthesized and used for photocatalysis applications, and they have elucidated promising results. As a result, more research into the utilization of co-precipitation for sillenites synthesis is needed to see the benefits of this method rather than its ease of usage.

3.1.7. Other methods

While previous synthesis methods such as hydrothermal, sol-gel, solid-state synthesis, and chemical solution deposition have been extensively studied and employed, there exists a wide range of other methods for synthesizing sillenites; however, those methods are not widely used.

The molten salt technique is one of the less frequently used methods for synthesizing sillenite crystals, in which the reactants are melted in an eutectic salt mixture at high temperatures, often above 700°C [204,205]. The process of synthesis is explained in **Figure S7** in the supporting information. The molten salt acts as a reaction medium and creates a high-temperature environment that allows sillenite crystals to form. This approach has been used in previous studies to prepare the sillenite crystals $Bi_{12}SiO_{20}$ and $Bi_{25}FeO_{40}$ [204,205]. This technique allows for the synthesis of sillenites at lower temperatures and with faster diffusion speeds of reacting constituents due to the incorporation of salt media such as KCl-K_2CO_3 or KCl-KBr [204,206]. Although this method successfully synthesized these two sillenites, it remains a critical drawback. The presence of the salt medium can generate impurities rather

than the target phase. Moreover, because of their high temperatures and corrosiveness, the usage of molten salts can be hazardous. Therefore, it is not recommended for synthesizing sillenite materials, which are hard materials that require special conditions.

The Stepanov method is similar to the Czochralski technique, it is used to generate single crystals of multi-component oxide compounds with various structures from the melt by application of the capillary shaper method [207]. Heating platinum crucibles in the air are used in the technique and profiled multi-component single crystals are formed by optimizing the crystallographic directions of pulling from various-profile dies [208]. This method has been used to synthesize the sillenites only in one study, that deals with the synthesis of $Bi_{12}SiO_{20}$ and $Bi_{12}GeO_{20}$ [207]. This approach has not been employed to synthesize more sillenites after this work due to the availability of a simpler and more effective method, as well as the fact that it lacks advantages and has several physical issues in crystal formation [208].

The oxidant peroxide method (OPM) has been applied to make highly reactive ceramic materials with a wide range of particle sizes, morphologies, and compositions; however, for sillenites, this process has only been used to synthesize the sillenite $Bi_{12}TiO_{20}$ [128,209]. The OPM technique begins with the creation of a metal solution, which is then followed by the addition of a reducing agent such as hydrazine or ammonia, and then by the addition of a peroxide complex solution containing hydrogen peroxide as an oxidizing agent [128]. The reaction mixture is then cooled down in an ice-water bath to promote the creation of nanoparticles by precipitation, which is then rinsed with deionized water and ethanol before being dried, filtered, and calcinated [128]. The OPM synthesis process is visually presented in **Figure S8**. Although the OPM provides several advantages, such as a homogeneous distribution of elements, simplicity, inexpensive cost, and low-temperature processing, it also has numerous disadvantages [209]. They include low nanoparticle yield, difficulty reproducing consistently, environmental concerns due to the use of harsh chemicals such as hydrogen peroxide, limited control over particle size and shape, and high energy consumption, which can limit its practical applications. Alternative methods that offer better control over particle properties and are more environmentally friendly are already available, such as sol-gel and hydrothermal.

There is also a study by Hou et al. that discussed the synthesis of sillenite nanofibers $Bi_{12}TiO_{20}$, $Bi_{12}SiO_{20}$ and $Bi_{12}GeO_{20}$ with a facile electro-spinning method [30]. The electro-spinning method procedure involves the preparation of precursor solutions, the precursor solutions are then put into a plastic syringe to measure the feeding rate, and this syringe is outfitted with a stainless steel needle and an aluminum foil collector as the grounded counter

electrode [210]. A high voltage is applied to the metallic needle clamped by an electrode [30]. The composite nanofibers are formed during electro-spinning [30]. Then the as-collected electro-spun fibers are dried. Subsequently, the composite fibers are calcined [210]. **Figure S9** in the supporting information displays the electro-spinning synthesis method. This study provided the electro-spinning method as a facile, versatile strategy to prepare sillenite nanofibers; however, further studies are required to elucidate the advantages and drawbacks of this method.

Two recent research papers by Tingting Xue et al. reported a simple synthesis method based on in situ electrochemical-ion exchange approach, which generated effective sillenite films that can be used for various applications [211,212]. This method needs a plate as a substrate such as a Bi plate, and with an electrolyte solution with the agents NaBr, Na_2SiO_3, deionized water and ethylene glycolate, a precursor film is created by electrochemical technique in a pH of 10 adjusted by HNO_3. In this electrochemical step, the substrate was used as the anode and the Ti sheet as a cathode both after surface treatment. Then the sillenite was deposited by ion-exchange method on the precursor film by placing the substrate that contains the precursor form in a water bath with a specific temperature containing the sillenite, NaOH and Na_2SiO_3. After the sillenite was deposited in the substrate, the plate was washed with deionized water and ethanol to remove all other impurities and then dried. A Schematic representation of the in-situ electrochemical-ion-exchange method is illustrated in **Figure S10**.

3.2. Structure and properties of sillenite-type materials

As indicated in previous sections, sillenite crystals have specific structural, optical, electronic, and electrochemical properties that make them appropriate for a wide range of applications. The crystal structure of these materials provides unique features, such as huge surface area, unusual optical properties, and high photocatalytic efficiency. Moreover, the crystal structure of these materials produces a specific electronic structure, which assists charge separation and reduces electron-hole recombination, resulting in better photocatalytic performance. As a result, it is important to investigate each of the characteristics and attributes of sillenite materials, as well as their possible uses in different sectors. Consequently, this section will provide a complete understanding of the characteristics and behavior of sillenite-type materials as photocatalysts.

3.2.1. Crystal structure

Sillenites have a three-dimensional framework of corner-sharing BiO_6 octahedral with metal atoms occupying tetrahedral or octahedral that are stacked along the c-axis of the crystal lattice [120,213,214]. Sillenites, in general, have a pseudo-body-centered cubic unit cell, and

the average structure belongs to the non-centrosymmetric space group I23 (no. 197), which is isomorphic and structural to the γ-Bi_2O_3 polymorph of Bi_2O_3 [116,213]. In comparison to other crystal forms, the unit cell of sillenite is quite large [133,215]. No compounds with the sillenite structure have yet been discovered without bismuth oxide [123].

As previously stated in earlier sections, sillenites $Bi_xM_yO_z$ (where M are the elements of Periodic System groups I-VIII) can form numerous phases with sillenite-type structures. These phases can be either stable or metastable depending on the ionic charge of an M atom [121]. To understand the structure of sillenite materials, it is necessary to describe the cases for each ionic charge of the added metal M in the sillenite structure:

- M^{2+} sillenites with the chemical formula $Bi_{38}(M^{2+})O_{58}$ as elucidated in **Figure 4 (a)**: In the unit cells of these compounds, which include cations with oxidation degree +2, two-thirds of normal $[MO_4]$-tetrahedra are substituted by $[BiO_3]$-groups, resulting in the development of an O(3) vacancy [178], where O(3) is tetrahedra's oxygen atoms [133]. The presence of vacancies in the structure of materials plays a major role in various applications that depend on the potential energy of reactions. Rotation of Bi^{3+} ions in tetrahedral orientations is possible, as is the placement of extra oxygen atoms in the unit cell in the $Bi_{38}(M^{2+})O_{58}$ structure [181].
- M^{3+} sillenites with the chemical formula $Bi_{25}(M^{3+})O_{39}$ as shown in **Figure 4 (b)**: The unit cells of sillenites with various cations are distinguished by variable Bi-O distances in the $[BiO_5]$-polyhedra, which correlate to varied M-O distances in the $[MO_4]$-tetrahedron [213]. In this structure, $[BiO_5]$-groups replace one-half of the usual $[MO_4]$-tetrahedra, resulting in the formation of an O(3) vacancy [178]. This structural model is free of defects, and the electrical neutrality of the unit cell is preserved owing to the oxidation of bismuth atoms in the 2a location to the state Bi^{5+} [215]. Rotation of Bi^{3+} ions in tetrahedral orientations is also conceivable in this structure, as is the introduction of additional oxygen atoms into the unit cell [216].
- M^{4+} sillenites with the chemical formula $Bi_{12}(M^{4+})O_{20}$ as elucidated in **Figure 4 (c)**: Such sillenites are known as ideal sillenites and are the most well-known members of the sillenite family [123,133]. M^{4+} cations form dimers in the unit cell of ideal compounds with the sillenite structure because they are positioned in two tetrahedral voids of the framework consisting of edge-sharing $[BiO_5]$-polyhedra [217]. The M^{4+} cations are positioned in position 2a and have a 1.00 occupancy [177,218]. This structure can be defined by a bismuth atom accompanied by eight oxygen atoms whose exchange corners with other polyhedra BiO_8 and tetravalent ions that form tetrahedra MO_4 that are found both in the cube core and on the cube's corners [219–221]. Oxygen vacancies are also present within this sillenite structure type, which was formed

by their oxygen termination characteristic and the strain variations between interlayers and inner layers [66].

- M^{5+} sillenites with the chemical formula $Bi_{12}(Bi, M^{5+})O_{20}$ as shown in **Figure 4 (d)**: In the unit cells of these compounds, Bi and O atoms are mutually displaced, the location of the bismuth lone pair is changed, and new coordination [BiO_x] polyhedra are formed in the distorted anion sub-lattice as a result of the compensatory addition of an additional O anion located in large voids of the framework in position 8c or 6b to balance the excessive charge of the tetrahedral M^{5+} cation [116].

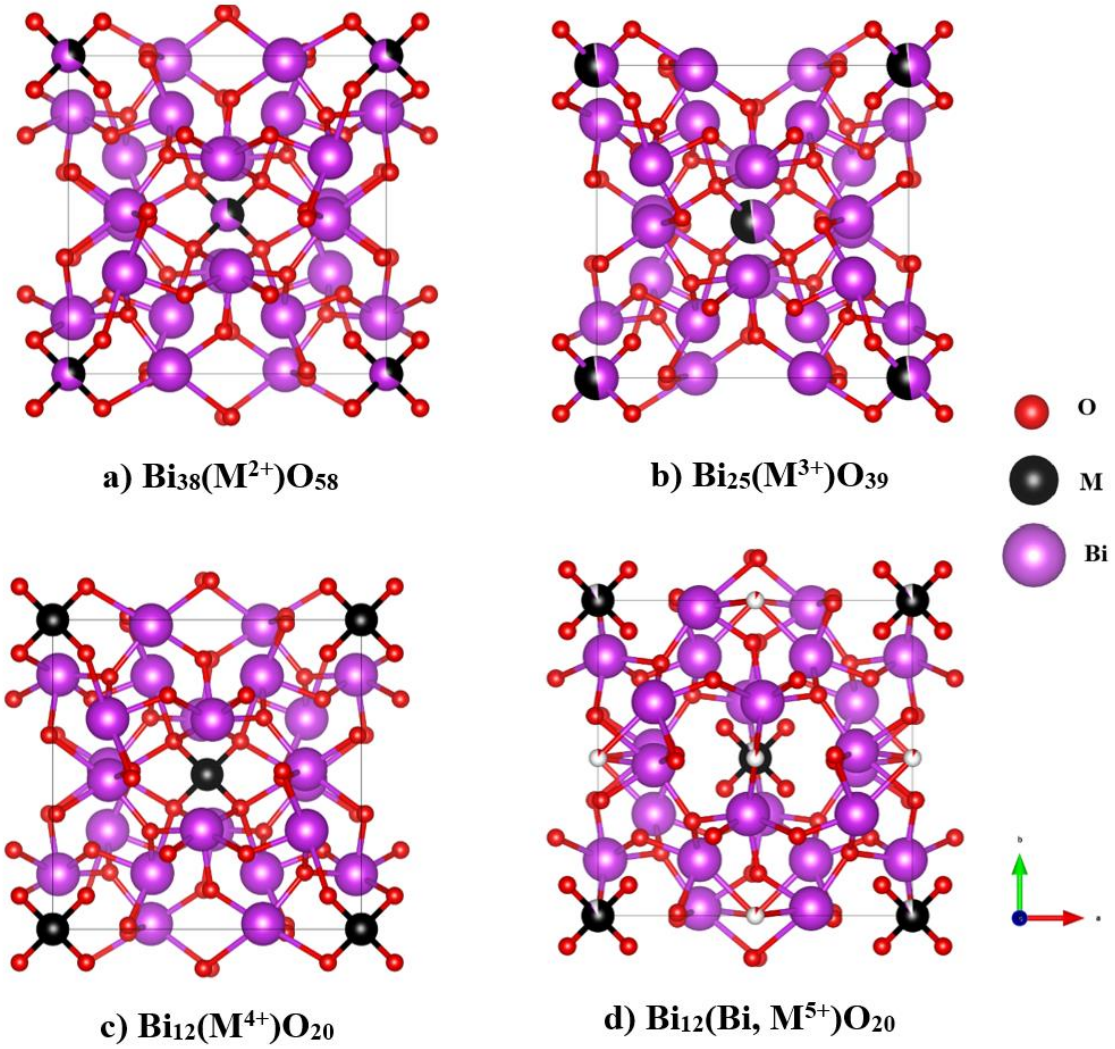

Figure 4. Crystal structure sillenites with different M ionic charges viewed along the (001) plane for (a) M^{2+}, (b) M^{3+}, (c) M^{4+} and (d) M^{5+}.

3.2.2. Optical properties

Sillenite materials have intriguing optical features due to the existence of a variety of energy levels in the crystal lattice. Light in the visible and UV ranges may excite these energy levels, resulting in several intriguing phenomena, such as photocatalysis and photoconductivity.

Previous research on the UV-Vis diffuse reflectance spectrums of sillenite crystals containing main group elements and transition metals (B, Co, Ni, Zn, Si, Ti, Ga, Ge, P, V, Mn, Fe, Cd) found that almost all sillenites spectra have steep absorption edges between 400-600 nm, corresponding to an indirect band gap energy of 1.66-2.9 eV [29,40,67,141,143,144]. This indicates that sillenites have significant absorptions from the visible region[123]. The change in optical absorption, band gap, and emission characteristics of such sillenites is connected to differences in crystal size, structure, and combination (M atom), as seen in the crystal structure section [123].

In order to demonstrate the correlations between optical properties, crystal structures, and element components, Burkov et al. conducted a rigorous investigation on the densities of states in sillenites [119]. They discovered that the electron transitions of the "building units" [BiO_5]-polyhedra and [MO_4]-complexes affect the optical characteristics of sillenites. Additionally, the contribution of electron transitions accompanied by charge transfer of optically active [MO_4]-complexes (with point symmetry T) to total optical rotation is opposed to the contribution of Bi^{3+} 6s2-sp transitions in [BiO_5]-polyhedra (with the point symmetry C1). This research also elucidated that sillenite crystals are gyrotropic due to the symmetry of their unit cells. The optical rotation changes due to compositional differences in the sillenite crystal to the location of [MO_4]-complexes on the energy scale, which is accompanied by charge transfer and is reliant on an atom's electronegativity. The authors found that electronic transitions localized at [BiO_5] structural fragments contribute to optical rotation. It was hypothesized that the electronic transition of [MO_4] compounds also contributes to optical spin scattering.

Chromophores, the components of molecules responsible for their color, also play an important role in the sillenites' optical properties [222]. Bismuth sillenites are composed of two chromophores that follow the previously stated symmetries [223]. The first chromophore is an asymmetric [BiO_5]-polyhedron with the symmetry C1 [119]. Because its electronic states are nondegenerate, the C1 symmetry permits any electronic transition in electric, magnetic-dipole, and electric-quadrupole approximations, as well as higher-order multipole approximations [119]. The situation is considerably different for the second one, which is viewed as an isolated molecule of the [MO_4]- complexes with symmetry T [223]. The wave functions of such a molecule's states are converted by either one-dimensional irreducible representations of A or three-dimensional irreducible representations of T [224]. In the sillenite unit cell, these two types of chromophores interact weakly with one another, where the concrete electron transitions of the chromophores and can be arbitrary [119].

3.2.3. Electronic properties

The electronic structure of sillenite materials could well be characterized in terms of energy bands in solid-state physics, with VB and CB being two major energy bands [43]. The highest energy band is the conduction band, which is separated from CB by an energy gap known as the band gap [177]. For an electron in VB to cross a band gap and pass into CB to become a mobile charge carrier, it must first absorb enough energy as photons more than its band gap [30]. The thickness of the band gap, as stated in the optical properties, is a critical feature in determining a material's electrical behavior because it affects how quickly electrons may move from VB into the conduction band and contribute to electrical conductivity [127]. In the case of sillenites, a narrow band gap has already been demonstrated. It is also significant in the electronic structure to demonstrate the contributions of element orbitals in the material to the conduction and valence bands [30].

Noh et al. investigated the electronic structure of sillenite materials and discovered that VB (below the Fermi level) in sillenites is mostly formed of O 2p and Bi 6s orbitals, whereas CB (above the Fermi level) is primarily composed of Bi 6p orbitals [29]. They discovered, however, that transition-metal ions M contribute to electronic structures where they may also participate in both conduction and valance bands, resulting in a variation in electronic structures between sillenite crystals when the transition-metal ions M are changed. M ions can contribute to both CB and VB depending on which element is present in the structure, where they can contribute slightly to VB via their 3p and 4p orbitals or substantially to CB via their 3d orbitals [29]. The band within the gap in all sillenite crystals is mostly composed of Bi-M 6s orbitals hybridized with the 2p orbitals of its O neighbors [225]. Charge transfers across the band gap edge are mostly contributions from the O-2p to Bi 6p orbitals [127]. **Figure 5** summarises and depicts the general electrical structure of sillenite crystals. The CB and VB positions can be obtained from experimental techniques such as Mott–Schottky measurements by determining the flat band potential level [40]. As in a previous study on the sillenite $Bi_{12}CoO_{20}$, the CB of this sillenite was located at − 1.84 V, while its VB edge was positioned at 0.72 V [40]. Those band positions are suitable for various types of photocatalysis applications as demonstrated by this work.

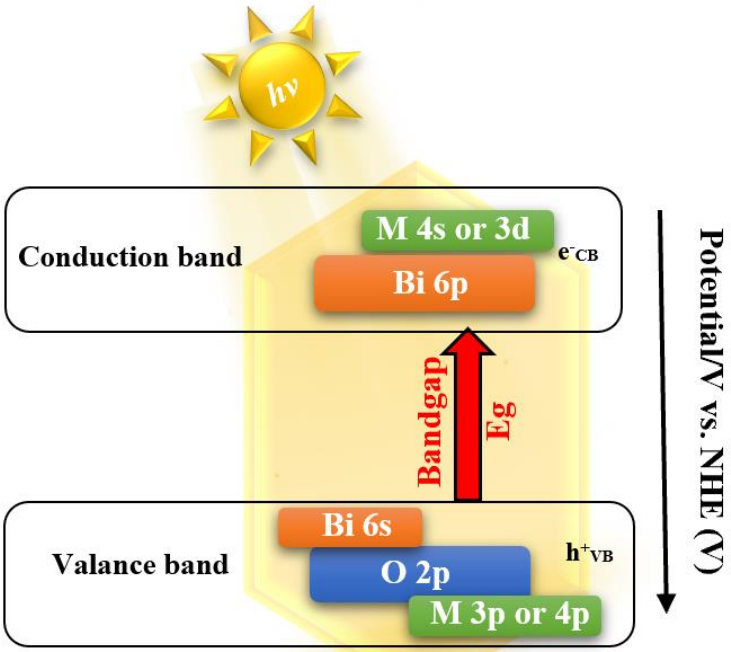

Figure 5. The basic electronic band structure of the sillenite crystals.

3.2.4. Other properties

Apart from the aforementioned properties, sillenites also possess intriguing additional properties, including photo-refractive, electrochemical, magnetic, and dielectric properties, making them suitable for a variety of applications, such as energy storage, photovoltaic, and electrochromic.

Certain sillenite-type crystals when exposed to light, including $Bi_{12}TiO_{20}$, $Bi_{12}GeO_{20}$, and $Bi_{12}SiO_{20}$, display photo-refractivity, which is the capacity to modify its refractive index [226]. This property has been exploited in a range of optical and photonic devices, such as holographic storage, optical signal processing, and interferometric applications [137]. Photo-refractive sillenite materials are also useful in the case of photocatalytic applications [143]. The propagation and diffraction of both transmitted and diffracted beams in sillenite crystals are affected by the concurrent appearance of the electro-optic effect, the secondary electro-optic effect, which is a combination of inverse piezoelectric and photoelastic effects, and the natural optical activity [227]. According to a study by Tian et al., intrinsic or extrinsic crystal defects also have a major role in influencing size and velocity and photo-refractive stability in crystals [228]. Understanding the diffraction phenomena in sillenite crystals is difficult because of the theoretical complexity of light diffraction phenomena in optically active photo-refractive

crystals of the sillenite class, where the diffraction is affected by the crystal configuration and state of polarisation, which includes the orientation of the intrinsic or extrinsic faces of the crystal, the crystal cut, the grating vector orientation, and other factors [229].

Certain sillenite-type crystals, such as $Bi_{12}CoO_{20}$ and $Bi_{12}FeO_{20}$ have shown temperature dependence of magnetic susceptibility, indicating the presence of paramagnetic compounds in these sillenites [115]. The magnetic susceptibility of sillenites crystals may be greatly increased by replacing the Bi content with magnetic cations M such as Co and Fe, where the disorder of such cations through M–O–M linkages positively affects the magnetic characteristics of the material [115]. It has been established that paramagnetic defects in sillenites have a direct correlation with optical transitions, resulting in magneto-optical characteristics [215].

Sillenites, as semiconductors, have been demonstrated to have a variety of fascinating electrochemical characteristics, including strong ionic conductivity, mixed conductivity, and electro-catalytic activity, attracting special research attention to their use in electrochemical cells [40,116]. The distinct crystal structure and electrical characteristics of sillenites, as discussed in earlier sections, allow for efficient charge separation and transport, making them intriguing materials for electrochemical applications such as energy conversion and storage [40,116].

Sillenite materials are also known for their low dielectric loss and temperature-stable permittivity [186]. These properties make them useful as catalysts for reactions that involve the transfer of electrons and also suitable dielectric materials in low-temperature co-fired ceramic technology [116]. Valant et al. investigated the dielectric characteristics of sillenite crystals $Bi_{12}MO_{20-\delta}$ (M = Ti, Si, Pb, Ge, Mn) in a research paper. They demonstrated reduced dielectric losses in the sillenites $Bi_{12}GeO_{20}$, $Bi_{12}SiO_{20}$, $Bi_{12}TiO_{20}$, and $Bi_{12}PbO_{19}$. Nevertheless, they discovered that sillenite $Bi_{12}MnO_{20-\delta}$ with an unstable valence state is not suitable for low-loss dielectric applications because partial oxidation of Mn^{4+} causes enhanced conductivity, which has a negative impact on dielectric loss [214].

3.3. Potentials of sillenite-type materials as photocatalyst

Based on earlier sections on the mechanism of photocatalysis, sillenite-type materials, their synthesis, and their properties, it is now possible to provide a comprehensive overview of the potential of sillenite crystals in the field of photocatalysis. As discussed in the previous sections, sillenite-type oxides have gained significant attention due to their unique crystal structure and remarkable properties and those materials have emerged as promising candidates for various applications. One of the most exciting application fields is photocatalysis, where

these materials can be used for water treatment, hydrogen production and energy generation, as already detailed in section 2. Therefore, it is important to delve into the potential of sillenite-type materials as photocatalysts based on their properties. Sillenites are useful for photocatalytic applications due to a variety of their characteristics. The key properties that are crucial for photocatalytic properties are explained below.

Starting with crystal structure and morphology, these properties are responsible for determining the surface area of the catalyst, which is essential for photocatalytic applications, as it determines the number of reactive sites available for catalysis. According to the literature, sillenites as nanoparticles have a high surface area based on the synthesis method used for their preparation, as indicated in the synthesis section. The surface area of sillenites can range from a few square meters per gram to several hundred square meters per gram, with specific values depending on the specific materials, conditions and method of synthesis.

The layered structures of bismuth sillenite, according to the structure part, can enhance an internal electric field that effectively separates photogenerated electrons and holes and direct their movement from the cluster to the surface for catalytic reactions. At the same time, bismuth sillenites possess oxygen vacancies in their structure, which play an important and major role in enhancing photocatalytic efficiency, particularly for nitrogen activation, by providing Lewis base and unsaturated sites.

Optical characteristics, such as band gap, are also essential to assessing sillenites' efficacy as photocatalysts. For photocatalytic applications, this feature is essential because it identifies the light energy absorbed by the material and converts it into chemical energy, which powers the photocatalytic reaction. It is already demonstrated in the optical properties section that sillenites may absorb light over the visible spectrum and even into the ultraviolet and that is due to their band gap, which was found to be between 1.66 eV and 2.9 eV. A narrow bandgap enhances light absorption efficiency and range, increasing the possibility of sunlight harvesting. The narrow band gap also provides another important feature in photocatalysis, which is high charge separation efficiency by promoting the relaxation of excited electrons. Sillenites have a specific electronic structure that allows for effective charge separation, which means that the electrons and holes formed during the photocatalytic process may be readily separated, limiting the possibility of recombination.

The high thermal and chemical stability, as well as the durability of sillenite crystals, are also essential for photocatalytic applications, where those properties make the crystals resistant to decomposing under harsh reaction conditions. As previously mentioned, sillenites have other properties, such as magnetic, dielectric, and photo-refractive properties. The

magnetic properties of the catalyst can give an advantage in separating it from the solutions using a magnet when used as a suspension, and the external magnetic field generated by this feature can also enhance the photocatalytic reaction. The dielectric and photo-refractive characteristics of sillenite crystals might improve photocatalytic activity in particular applications.

As demonstrated in the section on photocatalysis mechanisms, the electronic structure has a significant role in every photocatalytic application. The locations of the conduction and valance bands can decide whether this catalyst is acceptable for a photocatalytic application. Generally, for photocatalytic water treatment, the CB must be higher than the reduction potential of water ($O_2/O_2^{\bullet-}$, -0.33 V versus NHE), while the VB potential lower than the water oxidation potential ($H_2O/^{\bullet}OH$, +1.0 V versus NHE) [230,231]. For water splitting and hydrogen regeneration, CB must be higher than the reduction potential of water (H^+/H_2, 0 to +0.059 V versus NHE), while VB is lower than the water oxidation potential (H_2O/O_2, +1.23 V versus NHE) [95–98]. CO_2 reduction has multiple potentials for the CB due to the existence of various reduction pathways. However, the VB in CO_2 reduction shares the same conditions as water splitting, as elaborated in the CO_2 reduction mechanism [9,100–102]. The available literature supports the potential of sillenite crystals for photocatalytic applications due to their suitable and favorable electronic structure, and several studies have demonstrated that through theoretical studies using density functional theory (DFT) [29,127] or experimental studies using Mott-Schottky electrochemical technique [40].

Sillenite crystals are also tunable materials, which may have their physical, chemical, or electrical characteristics altered by applying an external stimulus [146]. Because of the unique structure of sillenites, it is possible to readily inject dual metals or dope foreign metals, which are impurities purposefully introduced to the material to change their characteristics. Doping may drastically alter the host material's characteristics and generate new electronic states that can be exploited to adjust the material's properties. The structure of sillenites allows also to modify through modifying the composition of this type of material by introducing different transition materials such as in the sillenite $Bi_{12}(B^{3+}{}_{1/2}P^{5+}{}_{1/2})O_{20}$ [116]. This can play a role in controlling the shape and size, electronic characteristics, and optical performance of the material. This opens the door to the next section, which discusses current advances in designing sillenite-based materials.

4. Current advances in designing sillenite-based materials for photocatalytic applications

Although sillenites have shown great properties as well as high efficiency in various photocatalytic applications, such as reducing or oxidizing a variety of inorganic pollutants, and degrading several organic contaminants in wastewater, they may encounter difficulties when used in a variety of real-life conditions and industrial applications, such as real wastewater, which can include considerable quantities of pollutants, making removal using them in photocatalysis alone extremely challenging [57,61]. In fact, some sillenites have several limitations and issues, including low removal efficiency, limited utility of visible light, rapid charge recombination, and poor mobility of charge carriers [33]. To overcome these weaknesses and drawbacks, various recent studies attempted to enhance the efficiency and performance of those sillenite catalysts by using various methods such as hybrid/composite systems, ion doping, hetero-junction and morphology modification [33,232]. The following section discusses the recent advances in the design of sillenite-based materials for photocatalytic applications. These advances have offered significant potential for increasing the efficiency and efficacy of sillenite catalysts, notably in hydrogen generation, water splitting and water treatment.

4.1. Modification of transitional metal M in sillenite crystals

As previously discussed in the crystal and electronic structure of sillenites, the transition metal M present in sillenite materials has an important influence in defining the majority of their characteristics, which are critical to photocatalytic applications. The electronic structure and band gap of sillenites are heavily influenced by the transition metal used, which also determines their stability as well as their capacity to absorb and utilize light for photocatalytic activities. Hu et al. in a study on structure-composition-property connections of stoichiometric and non-stoichiometric "$Bi_{12}MO_{20}$" sillenites, found that various transition metal substitutions in sillenites have a significant impact on their photocatalytic activity by affecting their optical and electrical properties [116]. They discovered in this study that the higher the M-site ion, the larger the unit cell, where the unit cell size of a catalyst plays an important role in defining its efficacy in photocatalysis applications because it affects the properties of the catalyst, such as its surface area, crystal structure, and electronic properties. They hypothesized that the unit cell parameters in terms of ionic radius for sillenites with different transition metals could be separated into two linear trends, indicating two different phase generation methods, as elucidated in **Figure 6** [116]. The first is for sillenites with M^{n+} ions with n values ranging from 2 to 4, while the second is for sillenites with M^{+5} ions, which have the same slope but a higher intercept on the Y axis. Other sillenites were found to be between these two linear lines, which

they ascribed to sillenites with mixed valent M ions, such as M^{3+}/M^{5+} as the sillenite $Bi_{12}(B^{3+}{}_{1/2}P^{5+}{}_{1/2})O_{20}$ [116].

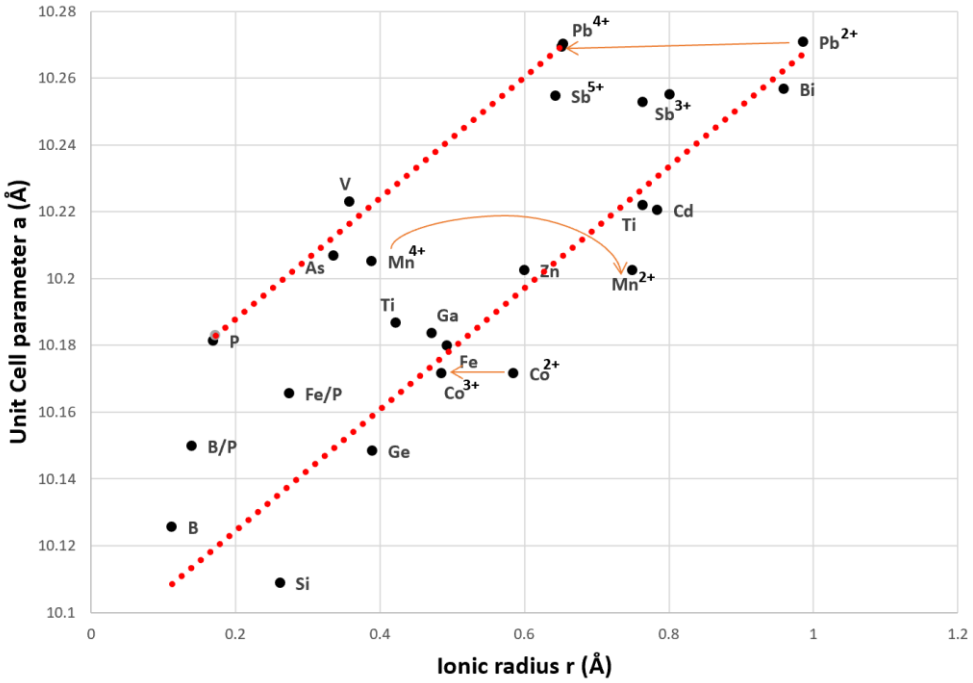

Figure 6. Unit cell parameter (a) in terms of ionic radius (r) for sillenites with several transition metals M. Reproduced under terms of the CC-BY license [116]. Copyright 2016, Yu Hu et al, published by White Rose eTheses Online.

Current research has concentrated on altering the metals in these structures to improve their photocatalytic characteristics. For example, researchers investigated the possibility of modifying bismuth sillenite $Bi_{12}MO_{20}$ with metals such as Ge, Si, and Ti to increase stability and performance [29,30,127]. These investigations elucidated that metal modification had a major effect on the photocatalytic efficiency and performance of sillenite-type materials. Nevertheless, depending on the specific application and conditions, the best metal choice and modification procedure may differ [29,30,127]. Therefore, carefully selecting transition metals in sillenite photocatalysts is crucial for enhancing photocatalytic activity and stability.

4.2. Morphological engineering

Morphology engineering, which includes changing the surface of a material to change its characteristics, has also had a significant influence on the performance of sillenite-based materials. Morphological engineering's purpose is to design and fabricate materials with specified characteristics and functionalities that are customized to certain photocatalytic applications. As previously demonstrated in the section on sillenite synthesis, the shape of the catalyst can alter its surface area, pore size distribution, and active sites, all of which are

important parameters in determining its performance. The shape of these crystals varies between methods and is also affected by the synthesis conditions [233].

Numerous sillenite crystals generated by hydrothermal techniques have been reported in various forms and sizes. The most common shape is a perfectly uniform tetrahedron/pyramidal with sharp edges and smooth surfaces; each plane in a single tetrahedron is recognized as an equilateral triangle [234,235], as illustrated in SEM photos in **Figure 7. (a)**. This method yielded particles with great crystallinity and purity, as well as thermal stability up to 1000 °C [235]. The particles synthesized by this method also showed an efficient photocatalytic activity from the reduction of Cr (VI) and the degradation of ampicillin-cloxacillin, which is attributable to the properties achieved by this method, such as the wide surface area due to the fine nature of the powder [234].

Sillenites synthesized by this approach can also take on nanowire shapes with uniform diameters as elucidated in **Figure 7. (b)** or spherical shapes with low crystallinity and dispersion, as seen in **Figure 7 (c)**. Sillenite nanowires synthesized by the hydrothermal method exhibited high photocatalytic properties for the removal of methyl orange, owing to a significantly greater specific surface area (25 m^2g^{-1}), which provides more active sites for the photocatalytic process while also increasing the efficiency of electron-hole separation due to high crystallinity [236]. Sillenite with spherical shapes synthesized by hydrothermal method exhibited an extended adsorption range of up to 1000 nm, and an excellent photothermal degradation for phenol, despite their low crystallinity, low surface area (0.190 m^2g^{-1}) and dispersion [237].

The differences in morphology are often attributable to alkaline concentration or pH value controls, hydrothermal temperature, reaction duration in synthesis methods, as well as the starting synthesis materials and their molar ratio [238]. Under certain conditions, unique morphologies can be generated using hydrothermal synthesis. In the presence of a high KOH concentration, sillenites, for example, might take on a spearhead-like shape, as seen in **Figure 7 (d)** [177]. Spearhead-like sillenite displayed an interesting microstructure and morphology with high photoactivity for Methylene blue degradation under natural sunlight [177]. Moreover, sillenite synthesized by the hydrothermal method may form cube-like columnar formations after 2 hours of calcination at 500 °C in a nitrogen environment, as illustrated in **Figure 7 (e)** [239]. The cube-like crystalline demonstrates tight size, dimensional control and a high photocurrent density which are effective in both photovoltaic and photocatalytic applications [239]. Wang et al. revealed an intriguing morphology for a sillenite crystal that is camellia-like, as illustrated in **Figure 7 (f)**; this unique morphology was generated in the presence of sodium

sulfosalicylate during the synthesis [240]. The rare camellia-like sillenite demonstrated high specific surface areas (98.37 m^2g^{-1}) and good photodegradation and water photolysis to produce H_2 [240].

Unlike the hydrothermal method by which different morphologies can be obtained, other methods have shown only one shape for each method. The particle obtained by the sol-gel process is mostly semi-spherical in form, as elucidated in **Figure 7 (g)**. According to one study, the amount of oxygen vacancies in sillenite produced by the sol-gel process is lower than that produced by the hydrothermal approach. Despite this, the photoactivity of materials produced by both approaches for rhodamine B and ciprofloxacin degradation were found to be almost similar [184]. Sillenite crystals prepared by solid-state reaction processes, almost have uneven shapes with big particles mixed in with smaller pieces, as seen in **Figure 7 (h)**. This morphology is not recommended for various types of applications, as the agglomeration in the big particles decreases the surface area of the crystals as catalysts. A study was conducted to compare the morphology of the sillenite $Bi_{24}Ga_2O_{39}$ synthesized by two different techniques, including hydrothermal and solid-state reaction methods [241]. It was found that the hydrothermal method exhibited uniformly distributed tetrahedral/pyramid-shaped microcrystals, the same as in **Figure 7 (a)**, whereas the solid-state reaction approach produced particles that vary in shape and are not evenly distributed. This also emphasizes the benefit of the hydrothermal procedure over the solid-state approach. For the co-precipitation method, obtained particles are bigger and randomly shaped, as shown in **Figure 7 (i)**. This method also requires higher calcination temperatures to achieve complete crystallinity, which results in a reduction in the BET surface area. Despite these disadvantages, this method still produces sillenites that can be used for photocatalysis applications, as already demonstrated in previous work about the removal of the organic pollutants Cefuroxime [68].

It can be generally concluded from **Figure 7** that diverse shapes and sizes of sillenite nanocrystals can be generated by different synthesis methods. Rather than the synthesis method, the synthesis conditions and materials utilized also have an impact on the shape of the catalyst. The shape of the synthesized materials was impacted by the alkaline concentration or pH value controls, hydrothermal temperature, reaction, and calcination time, and starting synthesis materials and their molar ratio. Consequently, morphological engineering techniques can be utilized to modify the shape, size, and surface area of the catalyst to improve its properties, giving a potent tool for enhancing sillenite performance.

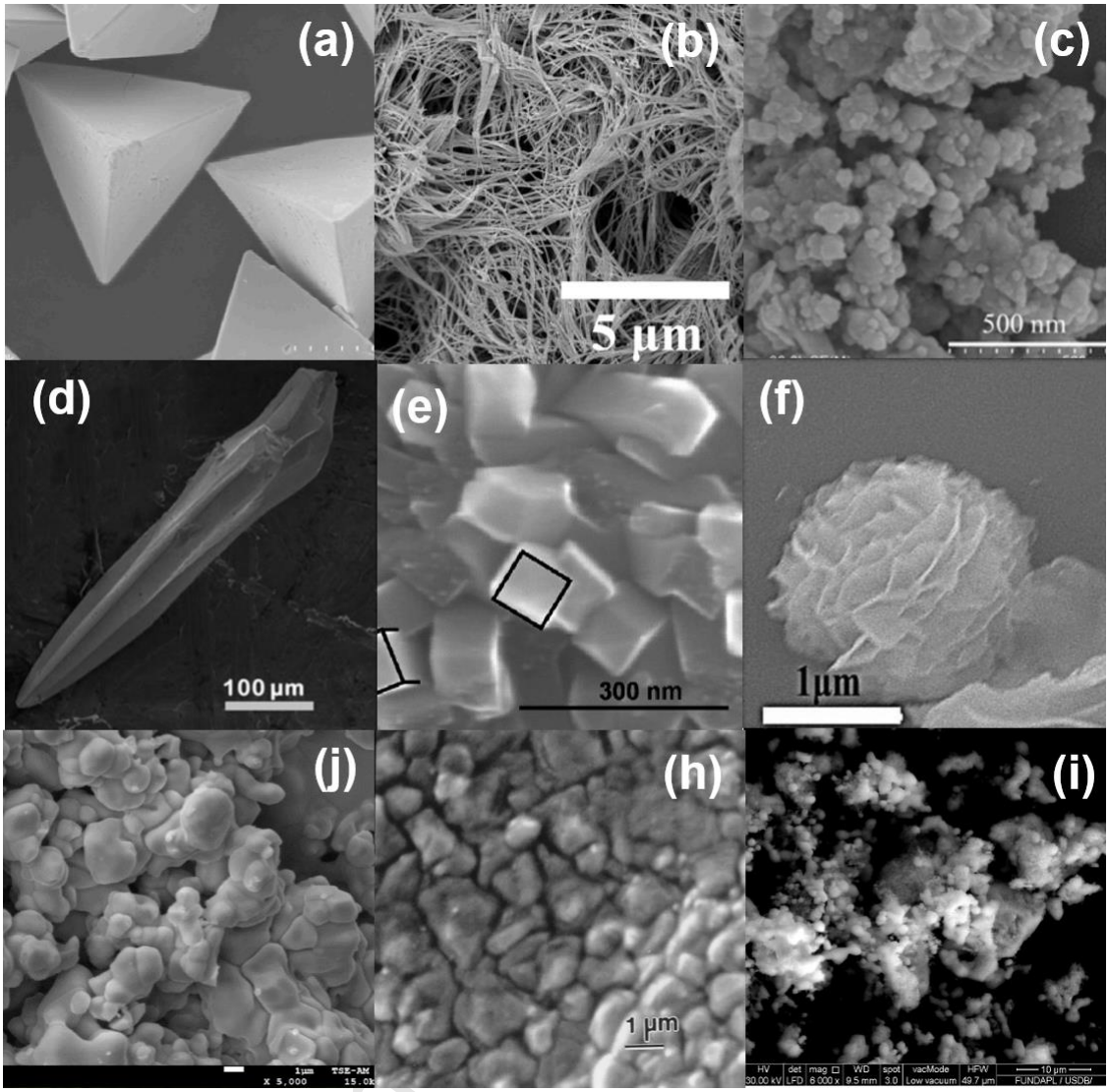

Figure 7. SEM images for different sillenites: (a-f) synthesized by the hydrothermal method: (a) $Bi_{25}FeO_{39}$ [235], (b) $Bi_{12}TiO_{20}$ [236], (c) $Bi_{12}CoO_{20}$ [237], (d) $Bi_{12}FeO_{20}$ [177], (e) $Bi_{12}TiO_{20}$ [239], (f) camellia-like $Bi_{12}ZnO_{20}$ [240], (j) $Bi_{12}TiO_{20}$ synthesized by sol-gel [143], (h) $Bi_{12}(B_{0.5}P_{0.5})O_{20}$ synthesized by solid-state [194], (i) $Bi_{12}ZnO_{20}$ synthesized by co-precipitation [68]. Reproduced with permission.

4.3. Doping

Doping is the technique of adding trace amounts of impurities, such as metals, into a material to change its characteristics and increase its activity. In sillenite-based materials, doping with metals has been widely investigated. For example, in recent research, Kowalczyk et al.[154] and Gao et al.[242] examined doping sillenite $Bi_{12}SiO_{20}$ with Eu^{3+} and doping sillenite $Bi_{25}FeO_{40}$ with heavy Co^{3+} and Fe^{3+}, respectively. Doping sillenite with Eu^{3+}, Co^{3+}, and Fe^{3+} has been proven to improve its transparency, luminescence, thermal stability, crystal magnetism, and magneto-optical characteristics [154,242]. A research paper indicated that

doping the sillenite $Bi_{12}ZnO_{20}$ with an ion, like Ag, can boost photosensitization or electronic life, resulting in a smaller recombination rate for the photo-generation of electron-hole pairs [67]. Another study looked at the optical characteristics of $Bi_{12}TiO_{20}$ doped with Cr and $Bi_{12}SiO_{20}$ doped with Fe, and it was discovered that it improved its magnetic and optical properties [243]. In fact, doping sillenites with metals is not a new subject; several studies have been conducted in this area due to the numerous benefits. Among these are Fe- and Cr-doped $Bi_{12}SiO_{20}$ [244], vanadium-doped $Bi_{12}TiO_{20}$ [245], $Bi_{12}TiO_{20}$ doped with CeO_2 and PbO [246], $Bi_{12}SiO_{20}$ and $Bi_{12}TiO_{20}$ doped with Cr, Fe, Mn, Cu, Al, P, Ag, Co and Al [247–249].

As demonstrated in these works, doping sillenites can lead to significant improvements in their optical, photoelectric, photo-refractive, and photochromic performance. By changing the number of charge carriers in a sillenite, doping can increase its electrical conductivity, making it more efficient at conducting electricity [250,251]. Additionally, doping can improve the mobility of charge carriers, allowing them to move more quickly and swiftly through the sillenite. Furthermore, doping can modify the optical properties of the sillenite, allowing it to absorb or emit light more efficiently and within a large range [245]. Moreover, doping can produce new energy levels within the sillenite, allowing for the creation of a conduction band and valence band for specific photocatalytic properties, as previously demonstrated that photocatalytic applications heavily depend on the electronic structure of the catalyst. Doping sillenites are impacted by essential features of the contributing metals such as their capacity to take various valences, symmetry of the occupied site, concentration, solubility, and magnitude and spectrum dependence of their absorption cross-section [250,252].

4.4. Hetero-junctions engineering

Hetero-junctions are interfaces between two different semiconductors, or between a semiconductor and a metal with different electronic properties sharing electrons/holes between each other [253,254]. One of the promising strategies for increasing the effectiveness of the sillenite photocatalytic system is hetero-junction, which involves combining sillenite with narrow-band-gap semiconductors or cocatalysts [234,255,256]. This strategy has been shown to be effective in controlling the light absorption range to lower the band gap energy and further improve the photocatalytic process's efficiency [257,258]. Three key factors of matching band placements, intimate and close interfacial contacts, are typically necessary to build an effective hetero-junction [259]. The interfacial contacts between the sillenite and the additional co-catalyst in hetero-junction are crucial and especially significant, as they can have a great impact on the migration and separation of photo-generated charges as well as further influence the material's activity [260].

A variety of hetero-junctions, including p-n hetero-junction [261,262], type I hetero-junction [234,255], type II hetero-junction [131,259,263–267], Z-type hetero-junction [255,260], S-type hetero-junction [268], and Schottky junction [269], have been employed in recent research to study sillenites-based hetero-junction photocatalyst. In every single one of those experiments, hetero-junction was shown to have a much higher photocatalytic activity than the matching solo sillenites. **Figure 8** elucidates a schematic explanation of the differences between different types of hetero-junctions based on the literature [265–270].

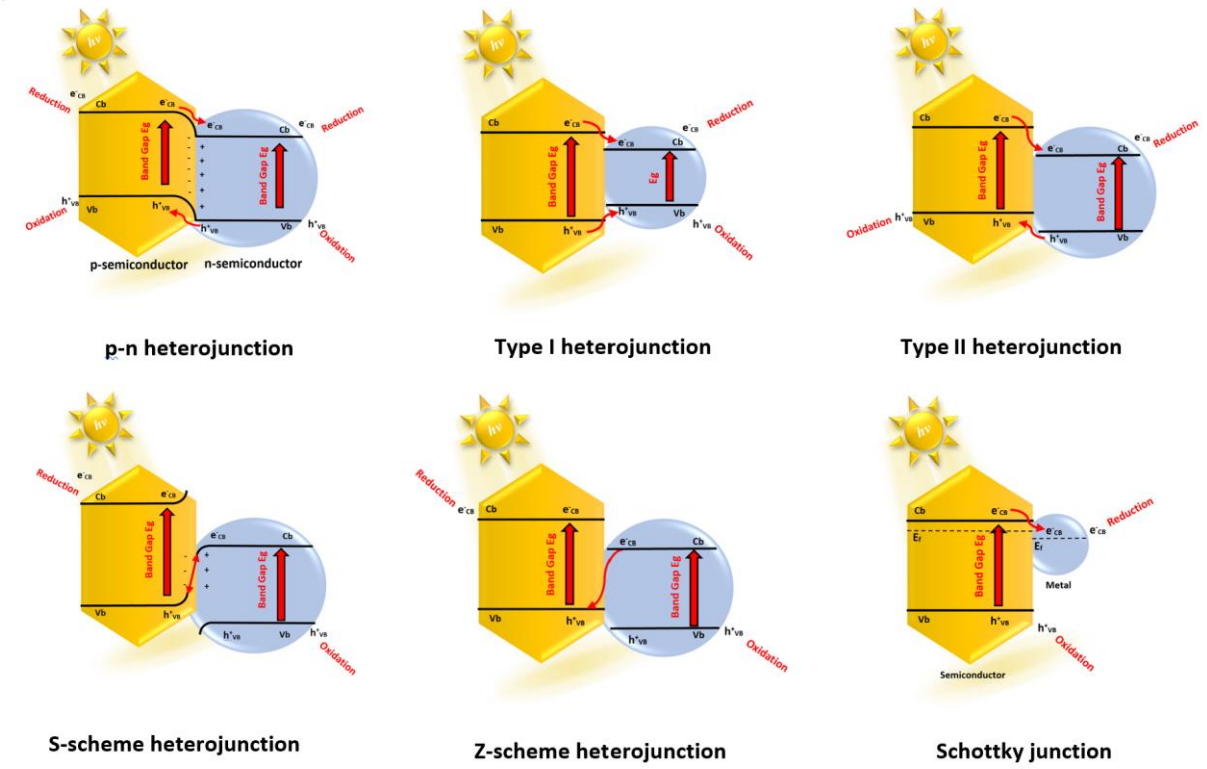

Figure 8. Schematic representation of the band structure and possible charge migration path in several sillenite-based hetero-junction types.

The p-n hetero-junction is created when a p-type semiconductor and an n-type semiconductor are combined, where the p-type material has an excess of holes which means positive charge carriers and the n-type material has an excess of electrons which means negative charge carriers [262,263]. Because of the different Fermi levels, the different charge carriers cause a potential difference across the contact surface of the materials, causing charges to redistribute at the interface [261]. This results in an internal electric field that is directed from the n-type to the p-type as a result of electron migration to balance Fermi levels [261]. The spatial separation of photo-induced carriers may be accelerated by the internal electric field, and that improves the photocatalytic activity [260,262]. p-n hetero-junctions can be employed in sillenites-based photocatalysts to increase charge separation and thus

photocatalytic activity, as in the following combinations $Bi_{12}GeO_{20}/Bi_2S_3$ [271], $Bi_4Ti_3O_{12}/Bi_2O_3/Bi_{12}TiO_{20}$ [260] and n-$Bi_{12}TiO_{20}$/p-BiOI [262].

In type I hetero-junctions, the VB and CB of the two materials align leading to a common electron/hole concentration at their interface, where the greater band gap semiconductor shares both electron/hole with the smaller band gap semiconductor [272]. This kind of hetero-junction often exhibits strong photocatalytic activity due to the effective charge separation. Sillenite-based photocatalysts frequently display type I hetero-junction behavior due to the alignment of their band structures with the additional semiconductor, as seen in the following combinations: $Bi_{24}Ga_2O_{39}/TiO_2$ [234] and $Ag_2O/Bi_{12}GeO_{20}$ [255].

Type II hetero-junction is the most commonly used type of hetero-junction in materials based on sillenite. This sort of hetero-junction occurs when the CBM and VBM of the two materials are not aligned, resulting in a potential energy difference at the interface where the higher conduction band shares an electron with the lower and the lower valance band shares a hole with the higher [265–267]. This kind of hetero-junction also has the potential to improve the separation of electron-hole pairs, leading to more effective photocatalysis [131,263,264]. Sillenite-based photocatalysts can display type II hetero-junction activity when combined with the right substances, the same as in the following combinations $Bi_{25}Fe_2O_{39}/SrTiO_3$ [265], $Bi_{12}SiO_{20}/Bi_2SiO_5$ [267], $Bi_{12}ZnO_{20}/Bi_2WO_6$ [266], $Bi_{25}FeO_{40}/Bi_2WO_6$ [259], Ag-$Bi_{12}GeO_{20}/Bi_2WO_6$ [263], $Bi_{12}TiO_{20}/Bi_2WO_6$ [131] and $BiVO_4/Bi_{25}VO_{40}$ [264].

The Z-scheme hetero-junction happens when two materials with differing band gap energies come together, but where one material's conduction band is higher than the other material's valance band [255]. As an electron migrates from the conduction band of the first material to the lower valance band of the second material, this results in a step-like potential energy (direct) that can aid in charge separation [260,261]. In sillenites-based photocatalysts, a Z-scheme hetero-junction has been found in the following combinations $Ag_2O/Bi_{12}GeO_{20}$ [255], $Bi_4Ti_3O_{12}/Bi_2O_3/Bi_{12}TiO_{20}$ [260], $Bi_{12}SiO_{20}/Bi_2S_3$ [261], and $CdS/Bi_{20}TiO_{32}/Bi_4Ti_3O_{12}$ [273].

The S-scheme hetero-junction is such a novel hetero-junction type, and it was put out in 2019 and is based on previous type-II and Z-scheme hetero-junctions [268]. This kind of hetero-junction is typically made up of two semiconductors with crossed band structures, where one semiconductor has a more negative conduction band position and the other has a more positive valance band position [268]. This causes an attraction between holes and electrons at the interface to create an internal electric field that is directed from CB of one semiconductor to VB of the other. The main distinction between S-scheme and Z-scheme hetero-junction

relates to the electron transport across semiconductors with different Fermi energies [268,270]. In S-scheme, the electron transport results in the creation of an internal electric field that enforces charge separations. According to studies on hetero-junction types, S-scheme hetero-junctions have a greater photocatalytic efficiency than conventional Z-scheme hetero-junction [270]. Unfortunately, just one work about $Bi_{12}TiO_{20}$-TiO_2 studied this form of hetero-junction in sillenites-based photocatalysts [268].

The Schottky junction type is established between a metal and a semiconductor, creating electron flow between them [269]. The usage of this kind of junction can aid in charge separation and hence support photocatalytic activity [269]. Unfortunately, Schottky junctions in sillenites-based photocatalysts have only been examined in one research. In this study, the metal Bi was added to the sillenite $Bi_{12}TiO_{20}$, and this addition effect not only increased the generation of more active species by generating electrons but also increased the separation of electrons, resulting in enhanced photocatalytic activity [269].

Not only can metal-based catalysts create hetero-junction or hetero-structure with sillenite-based materials, but even materials such as graphene [274] and graphitic carbon nitride (g-C_3N_4) [275] can create it. Graphene is an advantageous candidate for inclusion in heterojunctions sillenite-based materials because of its high surface area, chemical stability, high electron mobility, outstanding electrical conductivity, and non-toxicity [276]. Coupling graphene with sillenites in photocatalysis applications can provide several benefits, including increased photocatalytic activity by increasing surface area, improved electron conduction and transmission capability to limit recombination of photo-generated electrons and holes, and increased selectivity where graphene-based catalysts exhibit high selectivity in the production of hydrogen from water [277,278]. Only a few papers have addressed combining the graphene and sillenite type materials, such as graphene oxide/$Bi_{25}FeO_{40}$ [277–279], graphene oxide/ $Bi_{12}ZnO_{20}$ [280], and graphene oxide/$Bi_{12}MnO_{20}$ [276].

Graphitic carbon nitride has received a lot of attention in recent years as a popular and promising photocatalyst material because this material exhibits several promising properties and characteristics including strong photoconductivity, high discharge and charge current rates, good chemical stability, high absorption coefficient, low band gap of about 2.7 eV, and non-toxicity [281]. g-C_3N_4 has hybridization of carbon and nitrogen atoms in the sp2 arrangement as bonding, which creates π–conjugated graphitic planes and thus facilitates the charge separation in the system [282]. g-C_3N_4 has been recognized as a promising candidate for creating heterojunctions with semiconductors due to its previous characteristics as well as its abundance of active reaction sites and two-dimensional planar structure with the π–conjugated

system [283]. The stability of g-C_3N_4 can improve the overall stability of the hetero-system, which is especially important for long-term use. When combining g-C_3N_4 with sillenites, the band gap in g-C_3N_4 offers another significant benefit. The difference in energy levels between the two materials creates a hetero-junction between them, which significantly encourages charge transfer as well as the migration and separation of the carriers, improving photocatalytic performance. The literature generally states that the hetero-junction formed between sillenites and g-C_3N_4 is a sort of Z-scheme hetero-junction. Due to the advantages of g-C_3N_4 in hetero-junction, there are a large number of studies reported its combination with sillenite-type semiconductors, including g-C_3N_4/$Bi_{25}FeO_{40}$ [284,285], g-C_3N_4/$Bi_{12}GeO_{20}$ [281], g-C_3N_4/$Bi_{12}TiO_{20}$ [283,286–288] and g-C_3N_4/$Bi_{12}SiO_{20}$ [289].

4.5. Hybrid and modified sillenite-based photocatalytic systems

Previous research works have elucidated in the literature that combining processes by combining different types of materials reduces their drawbacks and enhances the performance of the combined system when compared to the performance of the separate processes [53,72]. It also provides fuel savings and energy recuperation [290,291]. Hybrid systems may also handle various issues with various methods and pathways, hence enhancing performance [292,293]. Moreover, combining the effects of several processes and systems can cause synergistic effects between them. These combinations increase efficiency by reducing the cost of using sillenites alone or by accelerating the reaction times of the materials [2,294]. The characteristics of sillenites can be improved and can provide even more benefits by mixing them with other types of materials [295,296].

When a sillenite photocatalytic system is combined with processes such as biological treatment, membrane, or absorption, the photocatalytic mechanism of the sillenite system does not change, but the total process efficiency improves. Taking an example, combining the adsorption process by adding a suitable adsorbent, such as and polymers with sillenite-based photocatalytic systems can create a hybrid process more efficient than both separately [295]. Polymers offer several characteristics that set them apart from sillenite materials, including high adsorption capacity, stability, affordability, biodegradability, and non-toxicity [297–299]. Accordingly, adding them to sillenite catalysts in photocatalysis applications can offer several benefits, including stability [295,300]. That is because polymers can act as stabilizing agents, protect from oxidation and corrosion, and increase surface area because polymers can enhance the catalyst's dispersion [188,300]. This has been proven in recent studies that combined sillenite-type minerals with polymers, such as polyaniline/$Bi_{12}TiO_{20}$ [295], polyethylene glycol 4000/$Bi_{25}FeO_{40}$ [300], Polyimide/$Bi_{12}SiO_{20}$ [188]. Some polymers have a highest occupied

molecular orbital (HOMO) as well as a lowest unoccupied molecular orbital (LUMO) making them have different energy band levels, which creates a gap in the materials [301]. Therefore, these types of polymers can form a hetero-junction with the sillenite by exchanging electrons/holes through π–π* transitions from the VB and CB of the sillenite with HOMO and the LUMO of the polymer [20]. **Figure 9** illustrates the mechanism of a hybrid process (combining sillenite $Bi_{12}TiO_{20}$ and the polymer polyaniline) for the removal of an organic pollutant which is Cefixime.

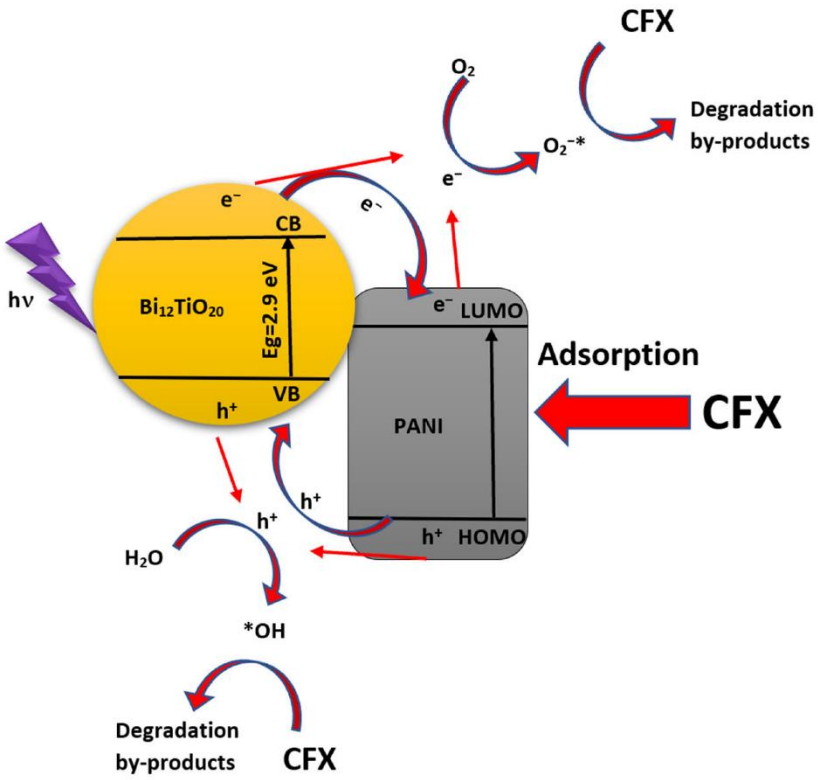

Figure 9. Mechanism of the hybrid system $Bi_{12}TiO_{20}$/PANI for the removal of Cefixime. Reproduced under terms of the CC-BY license [295]. Copyright 2023, Baaloudj et al, published by MDPI.

When a sillenite photocatalytic system is coupled with techniques such as ultrasonic radiation, microwaves, thermal treatment, or electrochemical treatment, the combination alters the photocatalytic mechanisms and thereby enhances the photocatalytic process's performance. Starting with ultrasound-assisted sillenite-based photocatalytic systems, a study by Wang et al. investigated the reduction of Cr(VI) using $Bi_{25}VO_{40}$ assisted by ultrasound, they discovered that this combination improved the separation of photo-generated holes and electrons while facilitating photocatalyst renewal [302], and this through enhancing uniform particle size distribution, increased surface area, enhanced crystallinity, and reduction of aggregation [303]. Thermal-assisted photocatalytic systems have also been demonstrated to be efficient novel

treatment systems, Wang et al. demonstrated that thermal treatment during the process affects the sillenite photocatalytic system by increasing the lattice dipole and promoting charge separation, adjusting the band structure, increasing the oxidation potential of photo-generated holes, and creating a synergetic effect with photocatalysis that increases the internal electric field and produces effective degradation [237]. The photoelectrochemical process, in which an externally supplied voltage is employed as an additional energy input to assist photocatalysis, has also been proven to be an effective photocatalytic-assisted system for various types of applications [304]. A research paper by Ropero-Vega et al. found that sillenite semiconductors are suitable for photoelectrochemical applications [305]. However, there has been still no work reported in practical applications.

Many techniques can be employed, besides coupling procedures, to enhance the photocatalytic activity, such as adding strong oxidants and reactive species such as hydrogen peroxide (H_2O_2) and sulfate radical ($^{\bullet}SO_4^-$), where their presence in water can induce the formation of more radicals [306]. Naghmash et al. elucidated that the chemical decomposition of H_2O_2 in the presence of $Bi_{12}SiO_{20}$ as the catalyst enabled the generation of reactive species such as $^{\bullet}OH$, which were subsequently employed as ROS in photocatalysis applications, such as water treatment. As a result, adding H_2O_2 to the $Bi_{12}SiO_{20}$ catalyst can improve its performance in photocatalysis applications [307]. Bu et al. added H_2O_2 to improve the efficiency of $Bi_{25}FeO_{40}$ sillenite crystals for the degradation of methyl orange [308]. The efficiency was enhanced from 27% for 3h to 87%, which revealed the advantage of adding H_2O_2 as an oxidized agent [308]. The sulfate radical ($^{\bullet}SO_4^-$) is also another active species that can improve the photocatalytic performance of sillenites, where $^{\bullet}SO_4^-$ and $^{\bullet}OH$ were found as the principal reactive species involved in the degradation of pollutants in water [309]. $^{\bullet}SO_4^-$ is formed when peroxydisulfate (PDS) or peroxymonosulfate (PMS) is activated, which may be accomplished by energy transfer such as UV and heat, hence PDS and PMS can be utilized as oxidants to efficiently boost the photocatalytic activity of catalysts. PDS and PMS can also generate the less reactive peroxydisulfate radical, which is $^{\bullet}S_2O_8^-$ [309].

The enhancement of sillenite catalyst by adding sulfate radical was reported in two previous papers [310,311], where those works focused on and investigated the photocatalytic efficiency of the sillenites $Bi_{25}FeO_{40}$ and $Co/Bi_{25}FeO_{40}$ in the presence of peroxymonosulfate. These studies elucidated that the presence of the sulfate radical can boost the photocatalytic activity of these sillenite materials because the sulfate radical can react with organic compounds, such as dyes and pesticides [312]. Because of its high oxidative potential, the sulfate radical is particularly powerful in degrading these pollutants, allowing it to break down

the chemical bonds in the pollutants and transform them into smaller, less hazardous molecules [310,311]. Moreover, the sulfate radical can improve the charge separation and transfer processes that occur during photocatalysis, resulting in increased catalyst efficiency. This is due to the sulfate radical's ability to behave as an electron acceptor, assisting in the passage of electrons from the sillenite material to the contaminants being targeted [310,311].

Despite the literature containing studies that tried to enhance the activity of sillenite-based systems, there is still a lack of exploration of other strategies, leaving a gap in the knowledge of these interesting materials. For example, combining sillenite systems with fluorine-doped tin oxide (FTO) glass by electrodeposition for photoelectrocatalysis could be a potential and great approach for creating hybrid systems with sillenites, as it will not only give sillenite materials more efficiency and conductivity but will also give them the advantage of acting as a fixed catalyst in the photocatalytic field. As a result, additional research is needed to investigate new combinations to produce unique and efficient processes with improved qualities and activities.

5. State of the art on the photocatalytic applications of sillenite-based systems

As seen in the preceding sections, sillenite-based materials have piqued the interest of researchers in recent years due to their unusual electrical and optical characteristics, and they have been studied in various research in various photocatalytic applications. Furthermore, various enhancement techniques have been established to improve the efficiency of these sillenite-based materials, and the theory behind them has been explained in previous parts as well. It is critical to discuss and show recent advancements in this field and the potential of these enhanced sillenite-based to demonstrate the efficiency of sillenite-based materials as well as different enhancement techniques used to improve photocatalytic activity. Through a comprehensive literature review and summarizing results from recent studies, this section will demonstrate the efficiency of sillenite-based materials and highlight the importance of enhancement techniques for their successful application in various photocatalytic processes, and their efficiency will be compared.

5.1. Degradation of organic pollutants

Most of the works in the literature have tested the sillenite-based photocatalysts for organic pollutants degradation, especially for Rhodamine B and Tetracycline. Almost all works showed high efficiency for different sillenite-based systems in the degradation of organic compounds. **Table 2** lists linked and recent works that used efficient sillenite-based systems to remove organic pollutants.

Table 2. Sillenite-based systems for organic pollutants degradation.

Sillenites-based systems	Pollutants	Pollutant concentration	Light Source	Reaction parameters	Degradation efficiency	Ref.
$Bi_{12}SiO_{20}$	Rhodamine B	10 mg L^{-1}	Xenon lamp, 300 W, λ ≥ 420 nm	Catalyst dose: 0.03 g/ 30 mL Irradiation time: 150 min	80%	[145]
$Bi_{12}SiO_{20}$ /Bi_2SiO_5	Rhodamine B	10 mg L^{-1}	Xenon lamp, 300 W, λ ≥ 420 nm	Catalyst dose: 0.03 g/ 30 mL Molar ratios of Bi/Si: 4 Irradiation time: 150 min	86.0%	[182]
Ag-$Bi_{12}SiO_{20}$ /Bi_2SiO_5	Rhodamine B	10 mg L^{-1}	Xenon lamp, 300 W, λ ≥ 420 nm	Catalyst dose: 0.03 g/ 30 mL Irradiation time: 150 min	90%	[256]
$Bi_{12}SiO_{20}$ /g-C3N4	Rhodamine B	10 mg L^{-1}	Xe arc lamp, 150 W, 31.2 W/m^2	Catalyst dose: 0.1 g L^{-1} gCN weight ratios: 5% Irradiation time: 74 h	99.5%	[289]
$Bi_{12}TiO_{20}$	Cefixime	10 mg L^{-1}	UVA lamp, 24 W, 20 mW cm^{-2}	Catalyst dose: 1.5 g L^{-1} pH of the solution: 6 Irradiation time: 4 h	94.93%	[143]
Polyaniline/ $Bi_{12}TiO_{20}$	Cefixime	30 mg L^{-1}	UVA lamp, 24 W, 20 mW cm^{-2}	Catalyst dose: 2 g L^{-1} (25% PANI/75% BTO) pH of the solution: 6 Irradiation time: 2 h	100%	[295]
$Bi_{12}TiO_{20}$ /g-C_3N_4	Rhodamine B	5 mg L^{-1}	Xe lamp, 500 W, 0.15 mW cm^{-2}, λ ≥ 420 nm	Catalyst dose: 0.015 g/10 mL BTO/gCN weight ratios: 0.5 Irradiation time: 2 h	90%	[288]
$Bi_{12}TiO_{20}$ /g-C_3N_4	Rhodamine B	10 mg L^{-1}	Xenon lamp, 500 W 0.15 mW cm^{-2}, λ ≥ 420 nm	Catalyst dose: 0.03 g/30 mL g-CN weight: 60 wt% Irradiation time: 5 h	96.9%	[286]
$Bi_{12}TiO_{20}$ /g-C_3N_4	Rhodamine B	10 mg L^{-1}	Xenon lamp, 500 W 0.15 mW cm^{-2}, λ ≥ 420 nm	Catalyst dose: 0.2 g/80 mL BTO/g-C_3N_4 MS mass ratios: 20 pH of the solution: 7 Irradiation time: 50 min	97%	[287]
$Bi_{12}TiO_{20}$ /$Bi_4Ti_3O_{12}$	Rhodamine B	10 mg L^{-1}	Xe lamp, 350 W	Catalyst dose: 1 g L^{-1}	100%	[313]

$Bi_{12}TiO_{20}$ /$Bi_4Ti_3O_{12}$ /Bi_2O_3	17β-estradiol	3 mg L^{-1}	Xenon lamp, 500 W	Molar ratio of Bi/Ti: 12/6 Irradiation time: 130 min	100%	[260]
Bi deposited $Bi_{12}TiO_{20}$	Tetracycline	10 mg L^{-1}	Iodine–Tungsten lamp, 300 W	Catalyst dose: 0.3 g L^{-1}, Molar ratio of Bi/Ti: 6/1 pH of the solution: 5.8 Irradiation time: 100 min	64%	[269]
$Bi_{25}VO_{40}$	Methylene blue	10 mg L^{-1}	Xe lamp, 500 W, λ ≥ 420 nm	Catalyst dose: 10 mg/100 mL Molar ratio of deposited Bi: 0.3 Irradiation time: 90 min	90%	[38]
$Bi_{25}VO_{40}$	Tetracycline	30 mg L^{-1}	Xenon lamp, 300 W, λ ≥ 420 nm	Catalyst dose: 0.05 g/300 mL pH of the solution: 7 Irradiation time: 4 h	60.4%	[264]
$Bi_{25}VO_{40}$ /$BiVO_4$	Tetracycline	30 mg L^{-1}	Xenon lamp, 300 W, λ ≥ 420 nm	Catalyst dose: 0.1 g/100 mL Irradiation time: 2 h	76.1%	[264]
$Bi_{12}ZnO_{20}$	Cefixime	10 mg L^{-1}	UVA lamp, 24 W, 20 mW cm^{-2}	Catalyst dose: 0.1 g/100 mL Irradiation time: 1 h	94.34%	[67]
$Bi_{12}ZnO_{20}$	Cefuroxime	15 mg L^{-1}	UVA lamp, 24 W, 20 mW cm^{-2}	Catalyst dose: 1 g L^{-1} pH of the solution: 6 Irradiation time: 4 h	80%	[68]
$Bi_{12}ZnO_{20}$ / graphene	Methylene blue and Methyl orange	10 mg L^{-1}	Xenon lamp, 300 W, λ ≥ 400 nm	Catalyst dose: 0.1 g/100 ml Go weight ratios: 3% Irradiation time: 2 h	96.04 and 94.52%	[280]
$Bi_{24}Ge_2O_{39}$	Methylene blue, Norfloxacin and Bisphenol	5, 10 and 5 mg L^{-1}	Sunlight	Irradiation time: 100, 100 and 210 min	92%, 82% and 84%	[241]
$Bi_{12}GeO_{20}$ /Ag_2O	Tetracycline	10 mg L^{-1}	Xenon lamp, 250 W, λ ≥ 420 nm	Catalyst dose: 50 mg/100 mL Irradiation time: 120 min	65%	[255]
$Bi_{12}FeO_{20}$	Methylene blue	3.5 mg L^{-1}	Natural sunlight	Catalyst dose: 0.25 g L^{-1} Irradiation time: 3h and 30 min	74.23%	[177]
$Bi_{24}Fe_2O_{39}$	Methyl orange	10 mg L^{-1}	Xe lamp, 500 W, λ ≥ 420 nm	Catalyst dose: 0.05 g/ 50 mL Irradiation time: 1 h	91%	[189]

$Bi_{25}Fe_2O_{39}$ /$SrTiO_3$	Bisphenol A	10 mg L^{-1}	Natural sunlight, 500 W/m^2	Catalyst dose: 30 mg/50 ml BFO/STO weight ratios: 1.5 Irradiation time: 2 h	95 %	[265]
Ag_3PO_4/ $Bi_{25}FeO_{40}$ /GO	Rhodamine B	10 mg L^{-1}	Xenon lamp, 35 W, 67 mW cm^{-2}	Catalyst dose: 0.1 g/50 mL Irradiation time: 75 min	96.9%	[277]
$Bi_{25}FeO_{40}$ / peroxy-monosulfate	Levofloxacin	5 mg L^{-1}	Visible light	Catalyst dose: 1 g L^{-1} [PMS/PS/H_2O_2] = 0.6750 mM pH of the solution: 9 Irradiation time: 60 min	86.5%	[310]
$Bi_{25}FeO_{40}$ /g-C3N4 /biochar	Tetracycline	20 mg L^{-1}	Xenon lamp, 300 W	Catalyst dose: 1 g L^{-1} pH of the solution: 3 Irradiation time: 60 min	92.2%	[284]
Gd and Cr Co-doping $Bi_{25}FeO_{40}$	Rhodamine B	12 mg L^{-1}	Hg Xe lamp, 500 W, 100 mW cm^{-2}	Catalyst dose: 40 mg/50 mL pH of the solution: 3 Irradiation time: 120 min	99%	[170]
$Bi_{25}FeO_{40}$ /gC_3N_4 /carbon nanotubes	Tetracycline	5 mg L^{-1}	Xenon lamp, 500 W λ > 420 nm 50 mW cm^{-2}	Catalyst dose: 10 mg/50 ml CN/BFO weight ratio: 1 Weight of CNT: 0.05 g pH of the solution: 5.5 Irradiation time: 120 min	87.9%	[285]

As indicated in **Table 2**, several sillenite catalysts without any enhancement techniques displayed effective removal of a wide variety of pollutants, including basic red 46, basic blue 41, methylene blue, norfloxacin, cefuroxime, bisphenol A, tetracycline, levofloxacin, and ciprofloxacin. Taking an example, $Bi_{12}TiO_{20}$ showed the ability to eliminate a concentration of 10 mg L^{-1} of the cefixime antibiotic in 4h with an efficiency of 94.93%. However, in another study, combining the same sillenite with polyaniline was found to be more efficient, where this combination totally removed a high concentration of 30 mg L^{-1} of cefixime within 2 h, showing the benefits of combining sillenite with other material types. Numerous research papers revealed that there are additional coupled systems with the sillenite $Bi_{12}TiO_{20}$ besides polyaniline, such as $Bi_{12}TiO_{20}$/g-C_3N_4, $Bi_{12}TiO_{20}$/$Bi_4Ti_3O_{12}$/Bi_2O_3 and Bi deposited $Bi_{12}TiO_{20}$, and those catalysts exhibited an efficient removal for rhodamine B, 17β-estradiol and Tetracycline, respectively. $Bi_{12}SiO_{20}$ has also been employed extensively in the literature for

the removal of Rhodamine B individually, in heterojunction with Bi_2SiO_5, and doped with Ag in heterojunction with Bi_2SiO_5 with removing efficiencies of 80%, 86.0% and 90%, respectively. Creating a heterojunction interface between $Bi_{12}SiO_{20}$ and Bi_2SiO_5, in which $Bi_{12}SiO_{20}$ is excited to form photo-carriers, which then migrate from VB of $Bi_{12}SiO_{20}$ to CB of $Bi_{12}SiO_{20}$ and onward to CB of Bi_2SiO_5, effectively avoids photo-carriers recombination, considerably improving carrier lifetime and photocatalytic performance. Loading Ag on the surface of the heterojunction $Bi_{12}SiO_{20}/Bi_2SiO_5$ enhances the capacity to absorb visible light, as seen in the UV-visible spectra in **Figure 10 (a)**, where the band gap is reduced from 2.57 eV to 2.48 eV, which is advantageous for visible light photocatalysis applications. Further benefits of loading Ag include its ability to operate as an electron trap, which accelerates the migration of photo-generated carriers by preventing photo-generated electron recombination [256]. The loading of Ag also influences the separation efficiency of electron-hole pairs. Moreover, Ag particles may produce excited electrons under the influence of surface plasmon resonance, and the electrons transfer to the adsorbed O_2, which can produce radicals with strong oxidizing ability [256]. The overall mechanism of this complex system is elucidated in **Figure 10 (b)**.

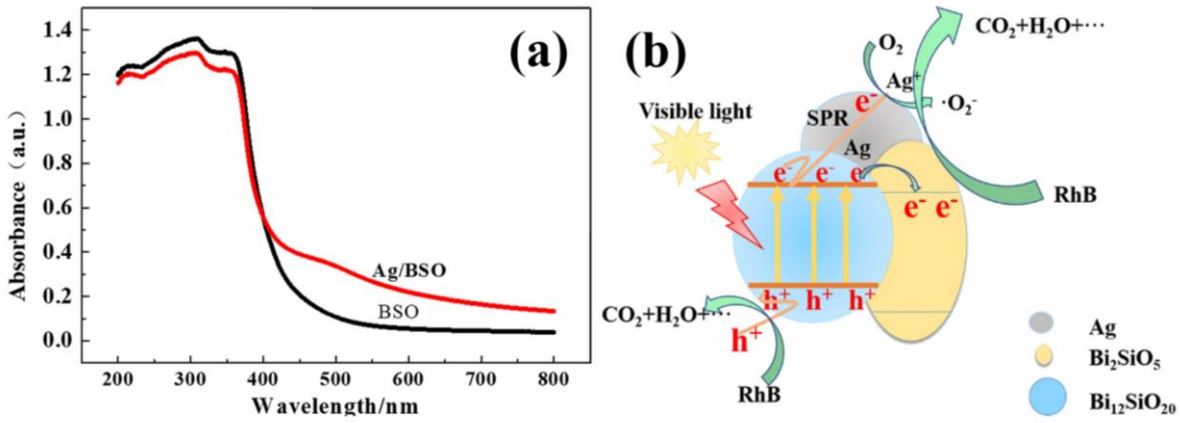

Figure 10. (a) UV–visible absorption spectra of $Bi_{12}SiO_{20}/Bi_2SiO_5$ and Ag–$Bi_{12}SiO_{20}/Bi_2SiO_5$ (b) mechanism of the photocatalytic system Ag–$Bi_{12}SiO_{20}/Bi_2SiO_5$. Reproduced with permission [256]. Copyright 2021, American Chemical Society.

There is also another combination for the sillenite $Bi_{12}SiO_{20}$ with g-C_3N_4, which had a 99.5% efficiency, but the reaction was slow approximately 74 hours. Several other sillenite combinations with increased photocatalytic activity have been reported, including $Bi_{25}VO_{40}$ and heterojunction $Bi_{25}VO_{40}/BiVO_4$, which revealed that the time of reaction for tetracycline degradation using the heterojunction was decreased to half than the sillenite alone. The strength

of these heterogeneous systems compared to sillenite alone is due to the greater efficiency of light absorption and electron-hole separation, as we showed earlier in the previous part.

5.2. Reduction of inorganic ions

For inorganic compounds, most of the work done with sillenite has been on the reduction of hexavalent chromium ions (Cr (VI)), available works in the literature are summarized in **Table 3**. In these applications, the hazardous hexavalent chromium ions Cr (VI) have been reduced to Cr (III), in order to reduce their danger, as these ions are less hazardous than Cr (VI), the mechanism is shown in the section on photocatalytic fundamentals.

Table 3. Sillenite-based systems for inorganic pollutants reduction.

Sillenites-based systems	Pollutant	Potassium dichromate Initial concentration	Light source	Reaction parameters	Reduction efficiency	Ref.
$Bi_{12}CoO_{20}$	Hexavalent chromium	15 mg L^{-1}	Tungsten lamp, 200 W, 8.25 mW cm^{-2}, λ ≥ 630 nm	Catalyst dose: 1 g L^{-1} pH of the solution: 6 Irradiation time: 3 h	67%	[40]
$Bi_{12}ZnO_{20}$	Hexavalent chromium	30 mg L^{-1}	UVA lamp, 24 W, λ ≥ 20 mW cm^{-2}	Catalyst dose: 1 g L^{-1} pH of the solution: 6 Irradiation time: 3 h	77.19%	[67]
$Bi_{12}MnO_{20}$	Hexavalent chromium	10 mg L^{-1}	UV lamp 20 W, 0.75 mW cm^{-2}, λ ≥ 254 nm	Catalyst dose: 2 g L^{-1} pH of the solution: 3 Irradiation time: 2 h	80%	[43]
$Bi_{24}Ga_2O_{39}$	Hexavalent chromium	10 mg L^{-1}	Dy lamp, 300 W, λ ≥ 400 nm	Catalyst dose: 0.5 g/100 mL pH: 2.5 Irradiation time: 120 min	100%	[125]
$Bi_{12}TiO_{20}$	Hexavalent chromium	50 µmol L^{-1}	Xenon lamp; λ ≥ 400 nm	Catalyst dose: 0.15 g/100 mL pH of the solution: 3 Irradiation time: 3h	64.1%	[314]
$Bi_{25}VO_{40}$	Hexavalent chromium	10 mg L^{-1}	Dy lamp, 300 W, λ ≥ 400 nm	Catalyst dose: 0.2 g/100 mL pH of the solution: 2.5 Irradiation time: 3h	91.7%	[302]
$Bi_{12}TiO_{20}$/rGO	Hexavalent chromium	10 mg L^{-1}	Sunlight	Catalyst dose: 0.15 g/100 mL	82.7%	[314]

$Bi_{24}Ga_2O_{39}$ /TiO_2	Hexavalent chromium	10 mg L^{-1}	Sunlight	pH of the solution: 3 Irradiation time : 3h Catalyst dose: 10 mg/10 mL TiO_2 weight: 10% pH: 2.5	95%	[234]
$Bi_{12}GeO_{20}$ /g-C_3N_4	Hexavalent chromium	10 mg L^{-1}	Dy lamp, 300 W, λ ≥ 400 nm	Irradiation time: 3h Catalyst dose: 0.3 g/100 mL g-C_3N_4 weight: 8% pH: 2.5 Irradiation time: 3h	100%	[281]

Various sillenites such as $Bi_{12}CoO_{20}$, $Bi_{12}ZnO_{20}$, $Bi_{12}MnO_{20}$ and $Bi_{12}TiO_{20}$ have shown the potential to reduce hexavalent chromium, but a study about combining $Bi_{12}TiO_{20}$ with reduced graphene oxide rGO showed that the efficiency of those sillenites can be enhanced, where the efficiency of Cr (VI) reduction of $Bi_{12}TiO_{20}$ was enhanced by adding rGO from 64.1% to 82.7%. Other combinations, such as $Bi_{24}Ga_2O_{39}/TiO_2$ and $Bi_{12}GeO_{20}$/g-C_3N_4, have also exhibited very high efficiency for reducing Cr (IV), almost complete removal. In the $Bi_{24}Ga_2O_{39}/TiO_2$ hetero-system, TiO_2 was added to create a heterojunction type I to enhance the photocatalytic efficiency of the sillenite $Bi_{24}Ga_2O_{39}$ where the efficiency has been improved more than double and was faster, as it is demonstrated in **Figure 11 (a)**. The type I heterojunction has improved the overall efficiency by accelerating electron transport and inducing the photoreduction of surface molecular oxygen to superoxide radical anion (O_2 to $O_2^{\bullet-}$). A special addition has been added in this application is the presence of ethanol as a scavenger and electron donor to prevent the formation of $^{\bullet}OH$ radicals, as they have the potential to re-oxidize Cr-(III) to Cr-(VI) again. The mechanism of this application has been illustrated in **Figure 11 (b)**.

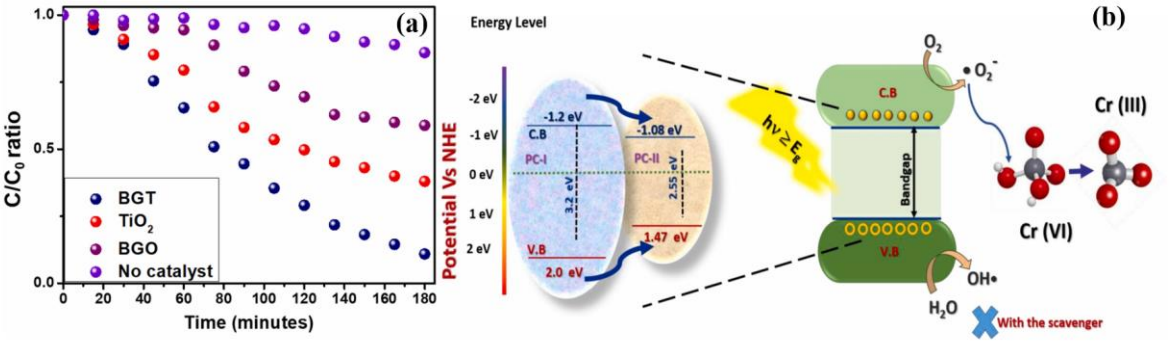

Figure 11. (a) the photoreduction efficiency of Cr (VI) using $Bi_{24}Ga_2O_{39}$, TiO_2, $Bi_{24}Ga_2O_{39}/TiO_2$, and without a photocatalyst, (b) proposed mechanism and band structure of

the system $Bi_{24}Ga_2O_{39}/TiO_2$ for Cr (VI) photoreduction. Reproduced with permission [234]. Copyright 2023, Elsevier.

5.3. Other applications

The use of Sillenite-based materials, unfortunately, in the inactivation of microorganisms was too limited, where only two studies have dealt with this type of material for the inactivation of the bacteria Escherichia coli (E. coli). The first work used $Bi_{12}TiO_{20}/Bi_4Ti_3O_{12}$ thin films, which inactivated E. coli from the concentration of 1.21×10^8 CFU mL^{-1} to less than 1×10^5 CFU mL^{-1}, under the following conditions temperature of 37 °C, UV-A Irradiation and Irradiation time of 48 h [315]. Other work has dealt with the use of Co-doped sillenite $Bi_{25}FeO_{40}$ with the presence of peroxydisulfate, however, exposure to microwaves without light irradiation [316]. This work reported a very high inactivation efficiency where 1-10^7 CFU mL^{-1} of E. coli cell density was totally inactivated in the presence of 1.0 g L^{-1} of the catalyst within only 5 min. As can be seen in **Figure 12 (a)** which shows a comparison of different inactivation systems, doping of this sillenite with cobalt and adding peroxydisulfate (PDS) and assisting with Microwave (MV) have significantly improved the overall efficiency of the system by generating a synergy effect between processes in this hybrid process. **Figure 12 (b)** provides TEM images of *E. coli* before and after treatment by the hybrid system $Bi_{25}FeO_{40}$/MW/PDS to show the morphological changes. As can be seen, before the reaction, E. coli had a complete morphology and a surface resembling a smooth rod. Following a minute, bacteria adsorbed on catalyst particle surfaces, creating physical and oxidative pressure. Due to the decreased lipopolysaccharide molecules in the cell membrane, membrane permeability decreased. The integrity of the cell membrane was destroyed when the response time reached 5 minutes, badly harming then inactivating the bacterial cells [316]. Bacterial death using the hybrid $Bi_{25}FeO_{40}$/MW/PDS system was achieved by inactivation, where the sterilization effect was found too negligible [316]. Adding a light source in this application can effectively increase the efficiency of this process, as sillenites have been already proven to be an efficient photocatalyst rather than their role in this microwave-assisted application. This proves the efficiency of sillenite material type in inactivating microorganisms. Further efforts should be made to this type of material to understand more about their bacterial inactivation performance.

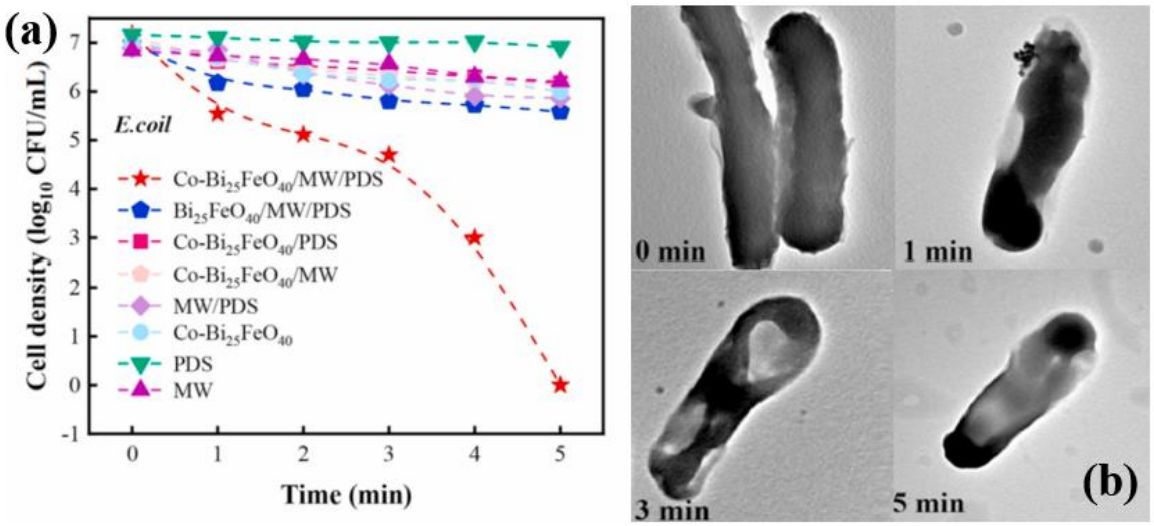

Figure 12. (a) Inactivation of bacteria in different reaction systems, (c) TEM images of *E. coli* before and after treatment by the hybrid system $Bi_{25}FeO_{40}$/MW/PDS. Reproduced with permission [316]. Copyright 2022, Elsevier.

There are also limited works on developing sillenite-based photocatalysts for H_2 generation and CO_2 reduction. M.A. Basith et al. investigated the H_2 production on the sillenite hybrid system $Bi_{25}FeO_{40}$/rGO, and this catalyst exhibited high H_2 generation with H_2 amount reaching 35 ml/g (ml H_2/g catalyst) under 4h visible light irradiation with a catalyst dose of 20 mg/30 mL [278]. As already discussed in the previous sections, H_2 production depends on the potential energy of CB, where it must be higher than the potential of H_2 formation (0 V vs. NHE). Because $Bi_{25}FeO_{40}$ has a potential CB less than 0 V vs. NHE, authors in this work combined $Bi_{25}FeO_{40}$ with rGO, in which a band-shift occurred to the overall system because the Fermi energy of pristine graphene is higher than that of $Bi_{25}FeO_{40}$, making the CB as well as VB of the resulting system more suitable for water splitting and H_2 production. The energy diagram in **Figure 13** summarizes the bands of the system $Bi_{25}FeO_{40}$/rGO compared to other systems as well as its relation to water splitting and H_2 production. Another work has exposed a more efficient sillenite hybrid system with higher efficiency which is Bi/$Bi_{25}FeO_{40}$-C [317], where this study has found that this catalyst can generate a high hydrogen amount of around 190 ml/g in 5h of visible light irradiation and with a catalyst dose 5 mg/10 mL.

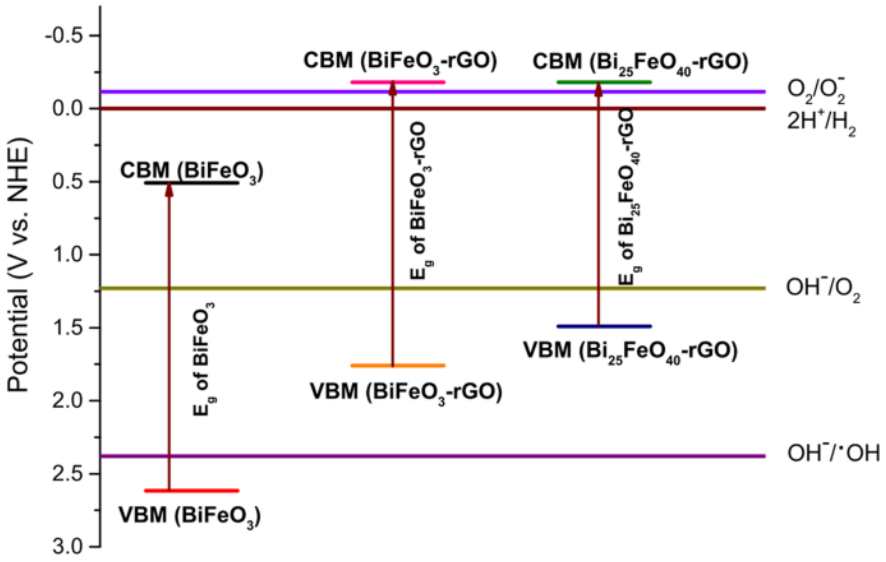

Figure 13. Energy band diagram of the system $Bi_{25}FeO_{40}$/rGO compared to other systems and the relation to water splitting. Reproduced under terms of the CC-BY license [278]. Copyright 2018, M. A. Basith et al, published by Springer Nature.

For CO_2 photoreduction, only a few sillenite-based systems have been used as films, which are $Bi_{12}SiO_{20}$ films [211], $Bi_{12}SiO_{20}$/BiOBr films [212] and Pd-Supported $Bi_{12}TiO_{20}$ films [318]. $Bi_{12}SiO_{20}$ films showed efficient CO_2 reduction, which was demonstrated by measuring the quantity of CO after irradiation, with the amount of CO determined to be 50.64 mol/m^2 after 4 hours of sunlight simulator irradiation. A special synthesis method was presented in this work to generate $Bi_{12}SiO_{20}$ films, where a Bi plate's surface was used to create the precursor film, which was subsequently used to create the $Bi_{12}SiO_{20}$ film using an ion-exchange technique. **Figure 14 (a)** provides a schematic representation of the synthesis process. The films produced by this process have a special morphology, consisting of 12 nm thick 2D nano-sheets resembling hydrangea finch coral, as shown in **Figure 14 (b)**. Besides the special morphology and synthesis method, the potential of the CB and VB of the $Bi_{12}SiO_{20}$ films are located at 1.14 and 1.32 V, respectively, which are more positive than the potential of H_2O/O_2 couple and more negative than the potential CO_2/CO, giving this sillenite an advantage in the CO_2 photoreduction applications. **Figure 14 (c)** depicts the mechanism of CO_2 photoreduction into $Bi_{12}SiO_{20}$ sillenite films. These sillenite films were also been used in another study by combining them with BiOBr for enhanced photocatalytic CO_2 reduction [212]. The $Bi_{12}SiO_{20}$/BiOBr films also exhibited efficient CO_2 reduction to CO, where those films yielded around 168.40 mol/m^2 after 9 hours of Xe-lamp irradiation, which is 3 times higher than $Bi_{12}SiO_{20}$ films alone, which demonstrates the advantage of creating heterojunction using

BiOBr. The sillenite films Pd-Supported $Bi_{12}TiO_{20}$ also generated a high efficiency of CO_2 reduction, as measured by the rate of formic acid generation, reaching 110 mol/h/g under solar simulator irradiation. The analytical approach of by-products differed between the applications of $Bi_{12}SiO_{20}$ films and Pd-Supported $Bi_{12}TiO_{20}$ films because their reduction products differed. As previously stated, the difference in reduction products between catalysts is due to the potential of the catalyst's conduction band for each catalyst.

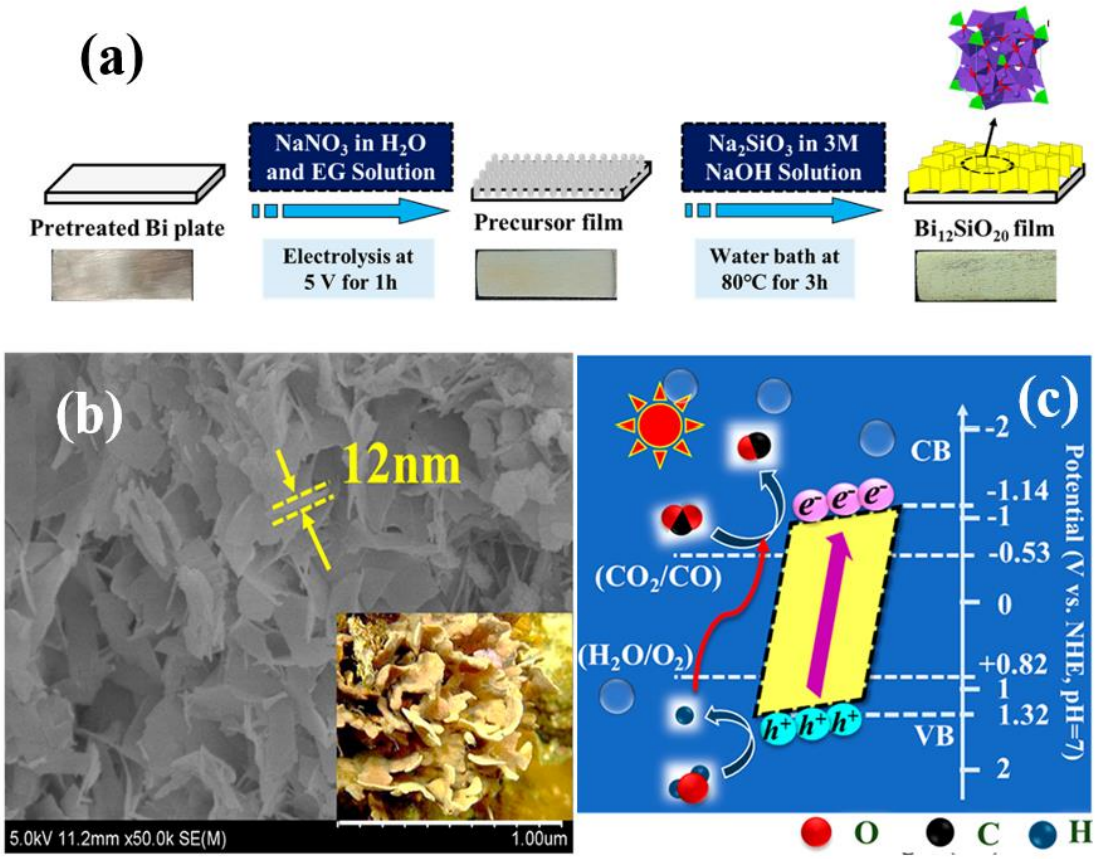

Figure 14. (a) synthesis method (b) SEM image of nano-sheets (c) CO_2 photoreduction mechanism of $Bi_{12}SiO_{20}$ film. Adapted with permission [211]. Copyright 2021 American Chemical Society.

Regrettably, no work has been done in photocatalysis for nitrogen fixation employing those sillenites; however, there is a paper that employed the Sb-modified sillenite $Bi_{25}FeO_{40}$ for nitrogen fixation via electro-catalysis [319]. This hybrid sillenite system demonstrated strong electro-catalytic activity, with an average ammonia (NH_3) production of up to 2.62 $\mu g/h \times cm^{-2}$. This catalyst exhibited high efficiency for N_2 fixation by electro-catalysis, demonstrating the advantages of this material type in this application, since it has oxygen

vacancies in its structure, as previously clarified in the properties section. This shows that these materials can be effective for N_2 fixation as photocatalysts.

6. Perspective and Outlook

According to the research discussed in this review, sillenite crystal catalysts have been demonstrated to be promising materials for photocatalytic applications due to their unique characteristics and high efficiency. As a result, it is critical to understand more about these interesting materials to promote their development. In this section, the perspectives based on each section of the review have been detailed for future advances, including crucial ideas for the design of more efficient and effective photocatalytic systems.

Beginning with sillenite-type material synthesis, improving current synthesis processes, or proposing novel approaches to synthesize sillenite-based materials is an important topic of material research. As previously stated in the synthesis section, the synthesis technique and conditions are crucial in the synthesis of sillenites since they control the morphology and the produced phase. Hydrothermal, sol-gel, solid-state processes and co-precipitation synthesis approaches have shown potential for creating sillenite materials with high efficiency. Nevertheless, advancements in these approaches, such as the use of sonochemical or microwave-assisted synthesis, may result in increased efficiency, higher yields, and better control over the crystal structure and morphology of the resultant materials. Few studies have also demonstrated that the synthesis of sillenite films has several advantages, including the avoidance of powder photocatalyst aggregation and an increase in cycle regeneration, as well as the ease of usage as a fixed catalyst. As a result, additional research into sillenite films is required. Novel methodologies and approaches to the synthesis and design of sillenite-based materials are strongly recommended.

Sillenites have been the subject of recent research due to their distinctive characteristics, with a number of characterization techniques employed for various sillenite crystals. However, despite significant progress in characterizing the structural and optical properties of these materials, some critical properties, such as their electrochemical properties and electronic structure, are still not well understood for the majority of sillenite catalysts. The electrochemical properties of sillenites have been covered in just a few papers [40,266]. The use of these sillenite materials in developing industries like water treatment plants, energy storage and conversion is being constrained by this knowledge gap. To fully realize the potential of these materials for a wide range of applications, more study is thus required to investigate and clarify their electrochemical behavior.

Although the potential of sillenite-type materials as photocatalysts for different water treatments for the degradation of organic molecules and reduction of inorganic ions has been examined, there is a lack of application for these interesting materials in other photocatalytic applications. The use of sillenite-type materials for additional photocatalytic applications is a critical area of research. For example, sillenites have shown potential for use in reducing carbon dioxide to make sustainable fuels or chemicals [211,318], and have also shown potential for use in water splitting and hydrogen generation [278]; However, those studies were not enough to understand and demonstrate the performance of this materials type in these applications. Furthermore, a study proved the ability of sillenite-based materials to nitrogen fixation even without a light source [319]. As is well explained in this review, sillenite catalysts exhibit efficient photocatalytic activity, especially in generating photo-generated carriers, in addition to the presence of oxygen vacancies in their structure. As a result, using these photocatalysts in nitrogen fixation with a light source will result in substantially better efficiency. As can be seen, there is a research gap in these areas, and further research is required. Continued research in CO_2 reduction, hydrogen generation as well as N_2 fixation can lead to new applications for sillenite materials and aid in the development of sustainable water treatment and energy systems.

Proposing novel concepts to improve the design of sillenite-based materials to increase their efficiency is also a crucial approach for advancement in the photocatalytic area. Morphology engineering, doping, heterostructure engineering, and hybrid processes, have all been shown to be efficient strategies for improving sillenite photocatalytic activity. Among these, S-scheme hetero-junction has been shown to improve the optical and electrical properties of the material, leading to higher efficiency in photocatalytic processes, and it has been proven that this type of heterojunction has higher photocatalytic activity than other hetero-junctions [270]. It has also been demonstrated that S-scheme heterojunction has a synergistic effect between the combined catalysts, boosting the overall catalytic activity of the system [320]. However, there is still a paucity of research on using S-scheme type hetero-junction, since just one study has dealt with this sort of heterojunction. Hybrid processes and materials have also shown efficient enhancement for various sillenite catalysts, however, some combinations, such as combining sillenite with other materials such as fluorine-doped tin oxide (FTO) glass, have not yet been investigated. Combining sillenites with FTO glass will be also an opportunity to apply the in-situ electrochemical-ion exchange synthesis method to generate sillenite films and apply them for fixed catalyst application same as in the previous paper that discussed the CO_2 reduction using sillenite films [211]. As already demonstrated, sillenite films are particularly

effective systems in CO_2 photocatalytic reduction applications [211,212,318]. Adding a co-catalyst or Schottky junction type can also be very beneficial in the case of water splitting, CO_2 reduction, and nitrogen fixation because the position of the conduction band of the catalyst has a significant impact on these applications. Applying these strategies to sillenites can change the potential energy of the conduction band of these photocatalysts, thereby increasing and improving the photocatalytic system's efficiency. Schottky junctions, like S-scheme hetero-junctions, may generate a synergistic effect between the sillenite and the co-catalyst, which assists in enhancing junction efficiency [320]. However, this concept has only been studied in one study, which discovered that by adding Bi as a cocatalyst to $Bi_{12}TiO_{20}$, more hot carriers would be generated, improving the productivity of active species [269]. This research is inadequate to establish the effectiveness of this method. As a result, research into the improvement of sillenite catalysts by co-catalysts for enhanced applications is recommended. Continued research into these approaches might lead to the development of novel and enhanced sillenite-based systems for effective photocatalytic applications.

7. Conclusion

Despite the notable surge in interest in employing sillenite-based materials for photocatalytic applications over the past few decades, there remains a considerable dearth of comprehension regarding these distinctive materials, which necessitates further investigation. This research review has investigated the recent progressions made in the use of sillenite-based semiconductors for diverse photocatalytic applications, while also elucidating their properties and potential as photocatalysts. The fundamental principles of photocatalysis utilizing sillenites have been expounded, with a detailed explication of the mechanisms involved in a variety of photocatalytic applications. The primary objective of this section is to establish a comprehensive comprehension of the relationship between the properties of sillenites and their impact on the efficacy of photocatalytic processes. Sillenite crystals do not share the same formula and structure, their composition and structure vary depending on the transition metal present in the crystal lattice. Thus, an extensive study has been conducted on various types and stoichiometries of sillenite, yielding valuable insights into their distinctive characteristics and enabling the formulation of general formulas to describe sillenite crystals.

This research further scrutinized the significance of developing innovative methods for synthesizing sillenite-type materials that possess efficient photocatalytic characteristics. An overview of the existing synthesis approaches for sillenite-type materials was presented,

emphasizing their respective advantages. Notably, hydrothermal, sol-gel, and co-precipitation techniques were found to be appropriate for synthesizing sillenite photocatalysts in powder form, whereas the Czochralski process, which is utilized to produce large single crystals, was found to have several limitations in photocatalytic applications, such as low surface area. Synthesis methods that generate sillenite films, such as in-situ electrochemical-ion exchange, have also been proven to be promising synthesis methods for generating efficient photocatalysts where sillenite films have demonstrated excellent performance in various photocatalytic applications, such as CO_2 reduction.

The unique properties and features of sillenite-type materials have been thoroughly studied, including unique structure with the space group I23, remarkable optical properties characterized by a relatively narrow band gap ranging from 1.66 eV to 2.9 eV, and suitable electronic structure for photocatalytic application. A summary of the latest research efforts exploring the photocatalytic potential of sillenite-type materials for various applications has been presented. It has revealed that these materials are promising as efficient photocatalysts in various photocatalytic applications, including the removal of hazardous organic and inorganic contaminants, disinfection of microorganisms, water splitting, CO_2 reduction, and N_2 fixation. While significant efforts have been directed towards the removal of organic and inorganic pollutants, limited progress has been made in applying these photocatalysts to the other aforementioned areas of photocatalytic applications.

The review has also incorporated the latest developments in the design of photocatalytic systems based on sillenite materials. Various strategies have been employed to enhance their photocatalytic activity, including hybrid/composite systems, ion doping, hetero-junctions, and morphological modification. Of these strategies, hybrid processes, Schottky junctions, and S-scheme hetero-junctions have proven to be effective approaches for improving photocatalytic applications. These approaches modify the overall electronic structure of the photocatalytic system, rendering it more suitable for specific applications.

In the final part, this review paper offers valuable insights and suggestions for future research directions in the field of sillenite-based photocatalysis, where several efficient combinations for enhancing sillenite catalysts have been proposed, including the combination of sillenite films with fluorine-doped tin oxide glass, which can generate effective and appropriate fixed catalysts for various applications. Considering the insights gathered from this review, it is anticipated that in the future, advanced sillenite photocatalytic systems will be

successfully developed to address the energy deficit and environmental concerns. This thorough review of sillenite materials for photocatalytic applications may serve as a valuable resource for researchers seeking to acquire a deeper understanding of the properties and characteristics of these materials for their intended applications.

Conflict of Interest

The authors declare no conflict of interest.

Acknowledgments

We would like to thank The Natural Sciences and Engineering Research Council of Canada (NSERC) for financial support.

References

[1] Lazar MA, Varghese S, Nair SS. Photocatalytic water treatment by titanium dioxide: Recent updates. Catalysts 2012;2:572–601. https://doi.org/10.3390/catal2040572.

[2] Tee PF, Abdullah MO, Tan IAW, Rashid NKA, Amin MAM, Nolasco-Hipolito C, et al. Review on hybrid energy systems for wastewater treatment and bio-energy production. Renew Sustain Energy Rev 2016;54:235–46. https://doi.org/10.1016/j.rser.2015.10.011.

[3] Tzanakakis VA, Paranychianakis N V., Angelakis AN. Water supply and water scarcity. Water (Switzerland) 2020;12. https://doi.org/10.3390/w12092347.

[4] Selihin NM, Tay MG. A review on future wastewater treatment technologies: micro-nanobubbles, hybrid electro-Fenton processes, photocatalytic fuel cells, and microbial fuel cells. Water Sci Technol 2022;85:319–41. https://doi.org/10.2166/wst.2021.618.

[5] Chauhan A, Rastogi M, Scheier P, Bowen C, Kumar RV, Vaish R. Janus nanostructures for heterogeneous photocatalysis. Appl Phys Rev 2018;5. https://doi.org/10.1063/1.5039926.

[6] Mielczarek K, Bohdziewicz J, Włodarczyk-Makuła M, Smol M. Comparison of post-process coke wastewater treatment effectiveness in integrated and hybrid systems that combine coagulation, ultrafiltration, and reverse osmosis. Desalin Water Treat 2014;52:3879–88. https://doi.org/10.1080/19443994.2014.887500.

[7] Carlos M-C, Yulin H, Chunbao X, Amarjeet B. An overview of microbial fuel cell usage in wastewater treatment, resource recovery and energy production. Sci Total Environ 2021;754.

[8] Saba B, Christy AD, Yu Z, Co AC. Sustainable power generation from bacterio-algal microbial fuel cells (MFCs): An overview. Renew Sustain Energy Rev 2017;73:75–84. https://doi.org/10.1016/j.rser.2017.01.115.

[9] Habisreutinger SN, Schmidt-Mende L, Stolarczyk JK. Photocatalytic reduction of CO2 on TiO2 and other semiconductors. Angew Chemie - Int Ed 2013;52:7372–408. https://doi.org/10.1002/anie.201207199.

[10] Asfaha YG, Tekile AK, Zewge F. Hybrid process of electrocoagulation and electrooxidation system for wastewater treatment: A review. Clean Eng Technol

2021;4:100261. https://doi.org/10.1016/j.clet.2021.100261.

[11] Avtar R, Dubey RK, Esteban J, Gomez-Morales A, Okolo CC, Prasad KA. Digitalization to achieve sustainable development goals: Steps towards a Smart Green Planet. Sci Total Environ 2021;794.

[12] Wang XC, Jiang P, Yang L, Fan Y Van, Klemeš JJ, Wang Y. Extended water-energy nexus contribution to environmentally-related sustainable development goals. Renew Sustain Energy Rev 2021;150. https://doi.org/10.1016/j.rser.2021.111485.

[13] Hamiche AM, Stambouli AB, Flazi S. A review of the water-energy nexus. Renew Sustain Energy Rev 2016;65:319–31. https://doi.org/10.1016/j.rser.2016.07.020.

[14] Ni X, Huang X, Guo R, Wang J, Peng K, Zhang W, et al. Water–energy–carbon synergies and trade-offs: A daily nexus analysis for wastewater treatment plants. Resour Conserv Recycl 2023;188. https://doi.org/10.1016/j.resconrec.2022.106712.

[15] Kougias I, Patsialis T, Zafirakou A, Theodossiou N. Exploring the potential of energy recovery using micro hydropower systems in water supply systems. Water Util J 2014;7:25–33.

[16] Sun X, Gou Z, Lau SSY. Cost-effectiveness of active and passive design strategies for existing building retrofits in tropical climate: Case study of a zero energy building. J Clean Prod 2018;183:35–45. https://doi.org/10.1016/j.jclepro.2018.02.137.

[17] Kumar R, Singh L, Malaysia Pahang Faisal Hai UI, Chan A, Salsali H, McBean E, et al. Challenges in the application of microbial fuel cells to wastewater treatment and energy production: A mini review. Sci Total Environ 2020;505:130–7.

[18] Maktabifard M, Zaborowska E, Makinia J. Achieving energy neutrality in wastewater treatment plants through energy savings and enhancing renewable energy production. Rev Environ Sci Biotechnol 2018;17:655–89. https://doi.org/10.1007/s11157-018-9478-x.

[19] Matthews RW. Solar-electric water purification using photocatalytic oxidation with TiO2 as a stationary phase. Sol Energy 1987;38:405–13. https://doi.org/10.1016/0038-092X(87)90021-1.

[20] Baaloudj O, Assadi I, Nasrallah N, El A, Khezami L. Simultaneous removal of antibiotics and inactivation of antibiotic-resistant bacteria by photocatalysis : A review.

J Water Process Eng 2021;42:102089. https://doi.org/10.1016/j.jwpe.2021.102089.

[21] Koe WS, Lee JW, Chong WC, Pang YL, Sim LC. An overview of photocatalytic degradation: photocatalysts, mechanisms, and development of photocatalytic membrane. Environ Sci Pollut Res 2020;27:2522–65. https://doi.org/10.1007/s11356-019-07193-5.

[22] Porcu S, Secci F, Ricci PC. Advances in Hybrid Composites for Photocatalytic Applications: A Review. Molecules 2022;27. https://doi.org/10.3390/molecules27206828.

[23] Zhang Q, Thrithamarassery Gangadharan D, Liu Y, Xu Z, Chaker M, Ma D. Recent advancements in plasmon-enhanced visible light-driven water splitting. vol. 3. Elsevier Ltd; 2017. https://doi.org/10.1016/j.jmat.2016.11.005.

[24] Pereira JHOS, Reis AC, Queirós D, Nunes OC, Borges MT, Vilar VP, et al. Insights into solar TiO2-assisted photocatalytic oxidation of two antibiotics employed in aquatic animal production, oxolinic acid and oxytetracycline. Sci Total Environ 2013;463–464:274–83. https://doi.org/10.1016/j.scitotenv.2013.05.098.

[25] Sellaoui L, Badawi M, Monari A, Tatarchuk T, Jemli S, Luiz Dotto G, et al. Make it clean, make it safe: A review on virus elimination via adsorption. Chem Eng J 2021;412:128682. https://doi.org/10.1016/j.cej.2021.128682.

[26] Deng H, Xu F, Cheng B, Yu J, Ho W. Photocatalytic CO2 reduction of C/ZnO nanofibers enhanced by an Ni-NiS cocatalyst. Nanoscale 2020;12:7206–13. https://doi.org/10.1039/c9nr10451h.

[27] Gao X, Shang Y, Liu L, Fu F. Chemisorption-enhanced photocatalytic nitrogen fixation via 2D ultrathin p–n heterojunction AgCl/Δ-Bi2O3 nanosheets. J Catal 2019;371:71–80. https://doi.org/10.1016/j.jcat.2019.01.002.

[28] Kenfoud H, Nasrallah N, Baaloudj O, Belabed C, Chaabane T, Trari M. Opto-electrochemical characteristics of synthesized BaFe2O4 nanocomposites: Photocatalytic degradation and hydrogen generation investigation. Int J Hydrogen Energy 2022;47:12039–51. https://doi.org/10.1016/j.ijhydene.2022.01.232.

[29] Noh TH, Hwang SW, Kim JU, Yu HK, Seo H, Ahn B, et al. Optical properties and visible light-induced photocatalytic activity of bismuth sillenites (Bi12XO20, X = Si,

Ge, Ti). Ceram Int 2017;43:12102–8. https://doi.org/10.1016/j.ceramint.2017.06.067.

[30] Hou D, Hu X, Wen Y, Shan B, Hu P, Xiong X, et al. Electrospun sillenite Bi12MO20 (M = Ti, Ge, Si) nanofibers: General synthesis, band structure, and photocatalytic activity. Phys Chem Chem Phys 2013;15:20698–705. https://doi.org/10.1039/c3cp53945h.

[31] Akerdi AG, Bahrami SH. Application of heterogeneous nano-semiconductors for photocatalytic advanced oxidation of organic compounds: A review. J Environ Chem Eng 2019;7. https://doi.org/10.1016/j.jece.2019.103283.

[32] Kenfoud H, Nasrallah N, Baaloudj O, Meziani D, Chaabane T, Trari M. Photocatalytic reduction of Cr(VI) onto the spinel CaFe2O4 nanoparticles. Optik (Stuttg) 2020;223:165610. https://doi.org/10.1016/j.ijleo.2020.165610.

[33] Baaloudj O, Kenfoud H, Badawi AK, Assadi AA, El Jery A, Assadi AA, et al. Bismuth Sillenite Crystals as Recent Photocatalysts for Water Treatment and Energy Generation: A Critical Review. Catalysts 2022;12. https://doi.org/10.3390/catal12050500.

[34] Suhadolnik L, Pohar A, Novak U, Likozar B, Mihelič A, Čeh M. Continuous photocatalytic, electrocatalytic and photo-electrocatalytic degradation of a reactive textile dye for wastewater-treatment processes: Batch, microreactor and scaled-up operation. J Ind Eng Chem 2019;72:178–88. https://doi.org/10.1016/j.jiec.2018.12.017.

[35] Krivec M, Pohar A, Likozar B, Drazic G. Hydrodynamics, Mass Transfer, and Photocatalytic Phenol Selective Oxidation Reaction Kinetics in a Fixed TiO2 Microreactor. AIChE J 2014. https://doi.org/10.1002/aic.14648.

[36] Suhadolnik L, Pohar A, Likozar B, Čeh M. Mechanism and kinetics of phenol photocatalytic, electrocatalytic and photoelectrocatalytic degradation in a TiO2-nanotube fixed-bed microreactor. Chem Eng J 2016;303:292–301. https://doi.org/10.1016/j.cej.2016.06.027.

[37] Bitenc M, Horvat B, Likozar BŽ, DraŽić G, Orel ZC. The impact of ZnO load, stability and morphology on the kinetics of the photocatalytic degradation of caffeine and resazurin. Appl Catal B Environ 2013;136–137:202–9.

https://doi.org/10.1016/j.apcatb.2013.02.016.

[38] Qiao X, Pu Y, Li Y, Huang Y, Cheng H, Seo HJ. Structural characteristics and photocatalytic ability of vanadate-sillenite Bi25VO40 nanoparticles. Powder Technol 2016;287:277–84. https://doi.org/10.1016/j.powtec.2015.10.018.

[39] Tho NTM, Khanh DNN, Thang NQ, Lee YI, Phuong NTK. Novel reduced graphene oxide/ZnBi2O4 hybrid photocatalyst for visible light degradation of 2,4-dichlorophenoxyacetic acid. Environ Sci Pollut Res 2020;27:11127–37. https://doi.org/10.1007/s11356-020-07752-1.

[40] Kenfoud H, Baaloudj O, Nasrallah N, Bagtache R, Assadi AA, Trari M. Structural and electrochemical characterizations of Bi12CoO20 sillenite crystals : degradation and reduction of organic and inorganic pollutants. J Mater Sci Mater Electron 2021. https://doi.org/10.1007/s10854-021-06194-w.

[41] Isik M, Sarigul N, Gasanly NM. Thermoluminescence characteristics of Bi12SiO20 single crystals. J Lumin 2020;224:117280. https://doi.org/10.1016/j.jlumin.2020.117280.

[42] Zhu X, Zhang J, Chen F. Study on visible light photocatalytic activity and mechanism of spherical Bi12TiO20 nanoparticles prepared by low-power hydrothermal method. Appl Catal B Environ 2011;102:316–22. https://doi.org/10.1016/j.apcatb.2010.12.019.

[43] Wu X, Li M, Li J, Zhang G, Yin S. A sillenite-type Bi12MnO20 photocatalyst: UV, visible and infrared lights responsive photocatalytic properties induced by the hybridization of Mn 3d and O 2p orbitals. Appl Catal B Environ 2017;219:132–41. https://doi.org/10.1016/j.apcatb.2017.07.025.

[44] Zhou J, Zou Z, Ray AK, Zhao XS. Preparation and characterization of polycrystalline bismuth titanate Bi12TiO20 and its photocatalytic properties under visible light irradiation. Ind Eng Chem Res 2007;46:745–9. https://doi.org/10.1021/ie0613220.

[45] Guo Y, Guo W, Yang Y, Guo Y, Jia Y, Liu H. Self-assembled hierarchical Bi12TiO20-graphene nanoarchitectures with excellent simulated sunlight photocatalytic activity. Phys Chem Chem Phys 2014;16:2705–14. https://doi.org/10.1039/c3cp53070a.

[46] Kim S, Nam SN, Jang A, Jang M, Park CM, Son A, et al. Review of adsorption–

membrane hybrid systems for water and wastewater treatment. Chemosphere 2022;286:131916. https://doi.org/10.1016/j.chemosphere.2021.131916.

[47] Liu H, Wang C, Wang G. Photocatalytic Advanced Oxidation Processes for Water Treatment: Recent Advances and Perspective. Chem - An Asian J 2020;15:3239–53. https://doi.org/10.1002/asia.202000895.

[48] Tijani JO, Fatoba OO, Madzivire G, Petrik LF. A review of combined advanced oxidation technologies for the removal of organic pollutants from water. Water Air Soil Pollut 2014;225. https://doi.org/10.1007/s11270-014-2102-y.

[49] Oller I, Malato S, Sánchez-Pérez JA. Combination of Advanced Oxidation Processes and biological treatments for wastewater decontamination-A review. Sci Total Environ 2011;409:4141–66. https://doi.org/10.1016/j.scitotenv.2010.08.061.

[50] Cordoba A, Saldias C, Urzúa M, Montalti M, Guernelli M, Focarete ML, et al. On the Versatile Role of Electrospun Polymer Nanofibers as Photocatalytic Hybrid Materials Applied to Contaminated Water Remediation: A Brief Review. Nanomaterials 2022;12. https://doi.org/10.3390/nano12050756.

[51] Kannan K, Radhika D, Sadasivuni KK, Reddy KR, Raghu A V. Nanostructured metal oxides and its hybrids for photocatalytic and biomedical applications. Adv Colloid Interface Sci 2020;281:102178. https://doi.org/10.1016/j.cis.2020.102178.

[52] Ren G, Han H, Wang Y, Liu S, Zhao J, Meng X, et al. Recent advances of photocatalytic application in water treatment: A review. Nanomaterials 2021;11. https://doi.org/10.3390/nano11071804.

[53] Sapkota M, Arora M, Malano H, Moglia M, Sharma A, George B, et al. An overview of hybrid water supply systems in the context of urban water management: Challenges and opportunities. Water (Switzerland) 2015;7:153–74. https://doi.org/10.3390/w7010153.

[54] Gupta SM, Tripathi M. A review of TiO2 nanoparticles. Chinese Sci Bull 2011;56:1639–57. https://doi.org/10.1007/s11434-011-4476-1.

[55] Fan J, Wu H, Liu R, Meng L, Sun Y. Review on the treatment of organic wastewater by discharge plasma combined with oxidants and catalysts. Environ Sci Pollut Res 2021;28:2522–48. https://doi.org/10.1007/s11356-020-11222-z.

[56] Samsudin EM, Goh SN, Wu TY, Ling TT, Hamid SBA, Juan JC. Evaluation on the photocatalytic degradation activity of reactive Blue 4 using pure anatase nano-TiO2. Sains Malaysiana 2015;44:1011–9. https://doi.org/10.17576/jsm-2015-4407-13.

[57] Ibhadon AO, Fitzpatrick P. Heterogeneous photocatalysis: Recent advances and applications. Catalysts 2013;3:189–218. https://doi.org/10.3390/catal3010189.

[58] Ahmed SN, Haider W. Heterogeneous photocatalysis and its potential applications in water and wastewater treatment: A review. Nanotechnology 2018;29. https://doi.org/10.1088/1361-6528/aac6ea.

[59] Dahiya S, Singh A, Mishra BK. Capacitive deionized hybrid systems for wastewater treatment and desalination: A review on synergistic effects, mechanisms and challenges. Chem Eng J 2021;417:128129. https://doi.org/10.1016/j.cej.2020.128129.

[60] Mao N, Jiang JX. MgO/g-C 3 N 4 nanocomposites as efficient water splitting photocatalysts under visible light irradiation. Appl Surf Sci 2019;476:144–50. https://doi.org/10.1016/j.apsusc.2019.01.049.

[61] Pelaez M, Nolan NT, Pillai SC, Seery MK, Falaras P, Kontos AG, et al. A review on the visible light active titanium dioxide photocatalysts for environmental applications. Appl Catal B Environ 2012;125:331–49. https://doi.org/10.1016/j.apcatb.2012.05.036.

[62] Tian D, Zhou H, Zhang H, Zhou P, You J, Yao G, et al. Heterogeneous photocatalyst-driven persulfate activation process under visible light irradiation: From basic catalyst design principles to novel enhancement strategies. Chem Eng J 2022;428. https://doi.org/10.1016/j.cej.2021.131166.

[63] Jabri H Al, Feroz S. Studies on the Effect of TiO2 Nano Photocatalysis in the Pretreatment of Seawater Reverse Osmosis Desalination. Int J Environ Sci Dev 2015;6:543–6. https://doi.org/10.7763/ijesd.2015.v6.653.

[64] Hitam CNC, Jalil AA. A review on exploration of Fe2O3 photocatalyst towards degradation of dyes and organic contaminants. J Environ Manage 2020;258:110050. https://doi.org/10.1016/j.jenvman.2019.110050.

[65] Kovačič Ž, Likozar B, Huš M. Photocatalytic CO2Reduction: A Review of Ab Initio Mechanism, Kinetics, and Multiscale Modeling Simulations. ACS Catal 2020:14984–5007. https://doi.org/10.1021/acscatal.0c02557.

[66] Li J, Li H, Zhan G, Zhang L. Solar water splitting and nitrogen fixation with layered bismuth oxyhalides. Acc Chem Res 2017;50:112–21. https://doi.org/10.1021/acs.accounts.6b00523.

[67] Baaloudj O, Nasrallah N, Kenfoud H, Algethami F, Modwi A, Guesmi A, et al. Application of Bi12ZnO20 sillenite as an efficient photocatalyst for wastewater treatment: Removal of both organic and inorganic compounds. Materials (Basel) 2021;14:1–17. https://doi.org/10.3390/ma14185409.

[68] Baaloudj O, Nasrallah N, Assadi AA. Facile synthesis, structural and optical characterizations of Bi12ZnO20 sillenite crystals: Application for Cefuroxime removal from wastewater. Mater Lett 2021;304:130658. https://doi.org/10.1016/j.matlet.2021.130658.

[69] Doufar N, Benamira M, Lahmar H, Trari M, Avramova I, Caldes MT. Structural and photochemical properties of Fe-doped ZrO2 and their application as photocatalysts with TiO2 for chromate reduction. J Photochem Photobiol A Chem 2020;386:112105. https://doi.org/10.1016/j.jphotochem.2019.112105.

[70] Zhang T, Wang X, Zhang X. Recent progress in TiO2-mediated solar photocatalysis for industrial wastewater treatment. Int J Photoenergy 2014;2014. https://doi.org/10.1155/2014/607954.

[71] Li L, Wang M. Advanced Nanomatericals for Solar Photocatalysis. Adv Catal Mater - Photocatal Other Curr Trends 2016. https://doi.org/10.5772/62206.

[72] Byrne C, Subramanian G, Pillai SC. Recent advances in photocatalysis for environmental applications. J Environ Chem Eng 2018;6:3531–55. https://doi.org/10.1016/j.jece.2017.07.080.

[73] Chen Y, Wang K, Lou L. Photodegradation of dye pollutants on silica gel supported TiO2 particles under visible light irradiation. J Photochem Photobiol A Chem 2004;163:281–7. https://doi.org/10.1016/j.jphotochem.2003.12.012.

[74] Chiron S, Fernandez-Alba A, Rodriguez A, Garcia-Calvo E. Pesticide chemical oxidation: State-of-the-art. Water Res 2000;34:366–77. https://doi.org/10.1016/S0043-1354(99)00173-6.

[75] Muniandy L, Adam F, Mohamed AR, Ng EP, Rahman NRA. Carbon modified anatase

TiO2 for the rapid photo degradation of methylene blue: A comparative study. Surfaces and Interfaces 2016;5:19–29. https://doi.org/10.1016/j.surfin.2016.08.006.

[76] Baaloudj O, Nasrallah N, Kebir M, Khezami L, Amrane A, Assadi AA. A comparative study of ceramic nanoparticles synthesized for antibiotic removal: catalysis characterization and photocatalytic performance modeling. Environ Sci Pollut Res 2020;28:13900–13912. https://doi.org/10.1007/s11356-020-11616-z.

[77] Baaloudj O, Nasrallah N, Kebir M, Guedioura B, Amrane A, Nguyen-Tri P, et al. Artificial neural network modeling of cefixime photodegradation by synthesized CoBi2O4 nanoparticles. Environ Sci Pollut Res 2020;28:15436–15452. https://doi.org/10.1007/s11356-020-11716-w.

[78] Baaloudj O, Assadi AA, Azizi M, Kenfoud H, Trari M, Amrane A, et al. Synthesis and Characterization of ZnBi2O4 Nanoparticles : Photocatalytic Performance for Antibiotic Removal under Different Light Sources. Appl Sci 2021;11:3975. https://doi.org/10.3390/app 11093975.

[79] Zuo S, Chen Y, Liu W, Yao C, Li X, Li Z, et al. A facile and novel construction of attapulgite/Cu2O/Cu/g-C3N4 with enhanced photocatalytic activity for antibiotic degradation. Ceram Int 2017;43:3324–9. https://doi.org/10.1016/j.ceramint.2016.11.173.

[80] Ren H, Koshy P, Chen WF, Qi S, Sorrell CC. Photocatalytic materials and technologies for air purification. J Hazard Mater 2017;325:340–66. https://doi.org/10.1016/j.jhazmat.2016.08.072.

[81] Regmi C, Joshi B, Ray SK, Gyawali G, Pandey RP. Understanding Mechanism of Photocatalytic Microbial Decontamination of Environmental Wastewater. Front Chem 2018;6. https://doi.org/10.3389/fchem.2018.00033.

[82] An T, Zhao HJ, Wong PK. Advances in Photocatalytic Disinfection. 2017.

[83] Ray SK, Dhakal D, Regmi C, Yamaguchui T, Lee SW. Inactivation of Staphylococcus aureus in visible light by morphology tuned α-NiMoO4. J Photochem Photobiol A Chem 2018;350:59–68. https://doi.org/10.1016/j.jphotochem.2017.09.042.

[84] Thandu M, Comuzzi C, Goi D. Phototreatment of water by organic photosensitizers and comparison with inorganic semiconductors. Int J Photoenergy 2015;2015:10–2.

https://doi.org/10.1155/2015/521367.

[85] Zhang C, Li Y, Shuai D, Shen Y, Wang D. Progress and challenges in photocatalytic disinfection of waterborne Viruses: A review to fill current knowledge gaps. Chem Eng J 2019;355:399–415. https://doi.org/10.1016/j.cej.2018.08.158.

[86] Deng Y, Li Z, Tang R, Ouyang K, Liao C, Fang Y, et al. What will happen when microorganisms "meet" photocatalysts and photocatalysis? Environ Sci Nano 2020;7:702–23. https://doi.org/10.1039/c9en01318k.

[87] Wang L, Li X, Teng W, Zhao Q, Shi Y, Yue R, et al. Efficient photocatalytic reduction of aqueous Cr(VI) over flower-like SnIn4S8 microspheres under visible light illumination. J Hazard Mater 2013;244–245:681–8. https://doi.org/10.1016/j.jhazmat.2012.10.062.

[88] Chowdhury P, Athapaththu S, Elkamel A, Ray AK. Visible-solar-light-driven photo-reduction and removal of cadmium ion with Eosin Y-sensitized TiO2 in aqueous solution of triethanolamine. Sep Purif Technol 2017;174:109–15. https://doi.org/10.1016/j.seppur.2016.10.011.

[89] Tebani S, Nasrallah N, Bellal B, Chergui A, Trari M, Maachi R. The Co 2 + Reduction on the Hetero-System CuFe 2O 4/ SnO 2 Under Solar Light. Arab J Sci Eng 2017;42:2397–402. https://doi.org/10.1007/s13369-016-2396-8.

[90] Douafer S, Lahmar H, Benamira M, Messaadia L, Mazouzi D, Trari M. Chromate reduction on the novel hetero-system LiMn2O4/SnO2 catalyst under solar light irradiation. Surfaces and Interfaces 2019;17:100372. https://doi.org/10.1016/j.surfin.2019.100372.

[91] Kenfoud H, Nasrallah N, Baaloudj O, Derridj F, Trari M. Enhanced photocatalytic reduction of Cr(VI) by the novel hetero-system BaFe2O4/SnO2. J Phys Chem Solids 2022;160:110315. https://doi.org/10.1016/j.jpcs.2021.110315.

[92] Rosli SA, Alias N, Bashirom N, Ismail S, Tan WK, Kawamura G, et al. Hexavalent chromium removal via photoreduction by sunlight on titanium–dioxide nanotubes formed by anodization with a fluorinated glycerol–water electrolyte. Catalysts 2021;11:1–19. https://doi.org/10.3390/catal11030376.

[93] Kumaravel V, Mathew S, Bartlett J, Pillai SC. Photocatalytic hydrogen production

using metal doped TiO2: A review of recent advances. Appl Catal B Environ 2019;244:1021–64. https://doi.org/10.1016/j.apcatb.2018.11.080.

[94] Morales-Guio CG, Stern LA, Hu X. Nanostructured hydrotreating catalysts for electrochemical hydrogen evolution. Chem Soc Rev 2014;43:6555–69. https://doi.org/10.1039/c3cs60468c.

[95] Rekhila G, Trari M. The photo-electrochemical properties of nano-sized ZnO. Application for the oxidation of dyes under sunlight. React Kinet Mech Catal 2021;133:501–16. https://doi.org/10.1007/s11144-021-01985-y.

[96] Yan J, Hu L, Cui L, Shen Q, Liu X, Jia H, et al. Synthesis of disorder–order TaON homojunction for photocatalytic hydrogen generation under visible light. J Mater Sci 2021;56:9791–806. https://doi.org/10.1007/s10853-021-05896-0.

[97] Liang X, Domen K. Particulate photocatalysts for overall water splitting. Ref Modul Chem Mol Sci Chem Eng 2023. https://doi.org/10.1016/b978-0-323-85669-0.00007-6.

[98] Hagiwara H, Nozawa I, Hayakawa K, Ishihara T. Hydrogen production by photocatalytic water splitting of aqueous hydrogen iodide over Pt/alkali metal tantalates. Sustain Energy Fuels 2019;3:3021–8. https://doi.org/10.1039/c9se00355j.

[99] Shen H, Peppel T, Strunk J, Sun Z. Photocatalytic Reduction of CO2 by Metal-Free-Based Materials: Recent Advances and Future Perspective. Sol RRL 2020;4. https://doi.org/10.1002/solr.201900546.

[100] Vu NN, Kaliaguine S, Do TO. Critical Aspects and Recent Advances in Structural Engineering of Photocatalysts for Sunlight-Driven Photocatalytic Reduction of CO2 into Fuels. Adv Funct Mater 2019;29. https://doi.org/10.1002/adfm.201901825.

[101] Vu NN, Kaliaguine S, Do TO. Plasmonic Photocatalysts for Sunlight-Driven Reduction of CO2: Details, Developments, and Perspectives. ChemSusChem 2020;13:3967–91. https://doi.org/10.1002/cssc.202000905.

[102] Patil SB, Basavarajappa PS, Ganganagappa N, Jyothi MS, Raghu A V., Reddy KR. Recent advances in non-metals-doped TiO2 nanostructured photocatalysts for visible-light driven hydrogen production, CO2 reduction and air purification. Int J Hydrogen Energy 2019;44:13022–39. https://doi.org/10.1016/j.ijhydene.2019.03.164.

[103] Ran J, Jaroniec M, Qiao SZ. Cocatalysts in Semiconductor-based Photocatalytic CO2

Reduction: Achievements, Challenges, and Opportunities. Adv Mater 2018;30. https://doi.org/10.1002/adma.201704649.

[104] Chen S, Liu D, Peng T. Fundamentals and Recent Progress of Photocatalytic Nitrogen-Fixation Reaction over Semiconductors. Sol RRL 2021;5. https://doi.org/10.1002/solr.202000487.

[105] Vu MH, Sakar M, Do TO. Insights into the recent progress and advanced materials for photocatalytic nitrogen fixation for ammonia (NH3) production. Catalysts 2018;8. https://doi.org/10.3390/catal8120621.

[106] Huang R, Li X, Gao W, Zhang X, Liang S, Luo M. Recent advances in photocatalytic nitrogen fixation: From active sites to ammonia quantification methods. RSC Adv 2021;11:14844–61. https://doi.org/10.1039/d0ra10439f.

[107] Chen X, Li N, Kong Z, Ong WJ, Zhao X. Photocatalytic fixation of nitrogen to ammonia: State-of-the-art advancements and future prospects. Mater Horizons 2018;5:9–27. https://doi.org/10.1039/c7mh00557a.

[108] Ali H, Masar M, Guler AC, Urbanek M, Machovsky M, Kuritka I. Heterojunction-based photocatalytic nitrogen fixation: principles and current progress. Nanoscale Adv 2021;3:6358–72. https://doi.org/10.1039/d1na00565k.

[109] Capelletti R, Beneventi P, Kovács L, Fowler WB. Multimode transitions of the tetrahedral MO4 units (M = Si,Ge,Ti) in sillenite single crystals. Phys Rev B - Condens Matter Mater Phys 2002;66:1743071–17430712.

[110] Shamonina E, Kamenov VP, Ringhofer KH, Cedilnik G, Kiessling A, Kowarschik R. Optimum orientation of volume phase gratings in sillenite crystals: is it always [111]? J Opt Soc Am B 1998;15:2552. https://doi.org/10.1364/josab.15.002552.

[111] Sillen LG, Sundvall S. Arkiv Kemi. Miner Geol 1937;12:1.

[112] Schumb WC, Rittner ES. Polymorphism of Bismuth Trioxide. J Am Chem Soc 1943;65:1055–60. https://doi.org/10.1021/ja01246a013.

[113] Levin EM, Roth RS. Polymorphism of bismuth sesquioxide. II. Effect of oxide additions on the polymorphism of Bi2O3. J Res Natl Bur Stand Sect A Phys Chem 1964;68A:197. https://doi.org/10.6028/jres.068a.020.

[114] Aurivillius B, Sillen LG. Polymorphy of bismuth trioxide. Nature 1945;155:305–6. https://doi.org/10.1038/155305a0.

[115] Elkhouni T, Amami M, Ben Salah A. Structural, spectroscopic studies and magnetic properties of doped sillenites-type oxide Bi12[M]O20 M=Fe, Co. J Supercond Nov Magn 2013;26:2997–3004. https://doi.org/10.1007/s10948-013-2271-8.

[116] Hu Y, Derek Sinclair, Anthony West. Structure-composition-property relationships of stoichiometric and non-stoichiometric" Bi12MO20" sillenites. Chem Mater 2013;12:48–54.

[117] Arenas DJ, Middleton C, Kemper AF. First-principles study of the phonon modes in bismuth sillenites. Phys Rev B - Condens Matter Mater Phys 2015;91. https://doi.org/10.1103/PhysRevB.91.144103.

[118] Shamonina E, Cedilnik G, Mann M, Kiessling A, Webb DJ, Kowarschik R, et al. Investigation of two-wave mixing in arbitrary oriented sillenite crystals. Appl Phys B Lasers Opt 1996;64:49–56. https://doi.org/10.1007/s003400050144.

[119] Burkov VI, Egorysheva A V., Kargin YF, Egoryshev A V., Kargin YF. Optical and chiro-optical properties of crystals with sillenite structure. Kristallografiya 2001;46:356–80. https://doi.org/10.1134/1.1358415.

[120] Arenas DJ, Jegorel T, Knab C, Gasparov L V., Martin C, Pajerowski DM, et al. Raman spectroscopy evidence of inhomogeneous disorder in the bismuth-oxygen framework of Bi 25InO 39 and other sillenites. Phys Rev B - Condens Matter Mater Phys 2012;86. https://doi.org/10.1103/PhysRevB.86.144116.

[121] Valant M, Suvorov D. A stoichiometric model for sillenites. Chem Mater 2002;14:3471–6. https://doi.org/10.1021/cm021173l.

[122] Sakoske GE, Sarver JE. Bismuth-containing laser markable compositions and methods of making and using same 2004.

[123] Wang Y, He R, Yang M, Wen T, Zhang H, Liang J, et al. Hydrothermal growths, optical features and first-principles calculations of sillenite-type crystals comprising discrete MO4 tetrahedra. CrystEngComm 2012;14:1063–8. https://doi.org/10.1039/c1ce06220d.

[124] Kim BH, Lim TH, Roh JW, Lee SG, Ju CS, Park SS, et al. Effect of Cr doping on the

properties and photocatalytic activity of Bi12TiO20. React Kinet Mech Catal 2010;99:217–24. https://doi.org/10.1007/s11144-009-0122-1.

[125] Meng X, Zhang G, Li N. Bi24Ga2O39 for visible light photocatalytic reduction of Cr(VI): Controlled synthesis, facet-dependent activity and DFT study. Chem Eng J 2017;314:249–56. https://doi.org/10.1016/j.cej.2016.12.090.

[126] Yao WF, Xu XH, Zhou JT, Yang XN, Zhang Y, Shang SX, et al. Photocatalytic property of sillenite Bi24AlO39 crystals. J Mol Catal A Chem 2004;212:323–8. https://doi.org/10.1016/j.molcata.2003.11.012.

[127] Oliveira TM, Santos C, Lima AF, Lalic M V. Antisite defect as rule for photorefractive, photochromic and photocatalytic properties of Bi12MO20 (M = Ge, Si, Ti) sillenite crystals. J Alloys Compd 2017;720:187–95. https://doi.org/10.1016/j.jallcom.2017.05.247.

[128] Nogueira AE, Longo E, Leite ER, Camargo ER. Visible-light photocatalysis with bismuth titanate (Bi12TiO20) particles synthesized by the oxidant peroxide method (OPM). Ceram Int 2015;41:12073–80. https://doi.org/10.1016/j.ceramint.2015.06.024.

[129] Delice S, Isik M, Gasanly NM, Darvishov NH, Bagiev VE. Structural and temperature-tuned optical characteristics of Bi12GeO20 sillenite crystals. Chinese J Phys 2020;66:422–9. https://doi.org/10.1016/j.cjph.2020.04.005.

[130] Wu Y, Lu J, Li M, Yuan J, Wu P, Chang X, et al. Bismuth silicate photocatalysts with enhanced light harvesting efficiency by photonic crystal. J Alloys Compd 2019;810:151839. https://doi.org/10.1016/j.jallcom.2019.151839.

[131] Zhang X, Zhang L, Hu JS, Pan CL, Hou CM. Facile hydrothermal synthesis of novel Bi12TiO20 -Bi2WO6 heterostructure photocatalyst with enhanced photocatalytic activity. Appl Surf Sci 2015;346:33–40. https://doi.org/10.1016/j.apsusc.2015.03.104.

[132] Zhang H, Lü M, Liu S, Xiu Z, Zhou G, Zhou Y, et al. Preparation and photocatalytic properties of sillenite Bi12TiO20 films. Surf Coatings Technol 2008;202:4930–4. https://doi.org/10.1016/j.surfcoat.2008.04.081.

[133] Scurti CA, Auvray N, Lufaso MW, Takeda S, Kohno H, Arenas DJ. Electron diffraction study of the sillenites Bi12SiO 20, Bi25FeO39 and Bi25InO 39: Evidence of short-range ordering of oxygen-vacancies in the trivalent sillenites. AIP Adv

2014;4. https://doi.org/10.1063/1.4893341.

[134] Kuz'micheva GM, Mel'nikova TI, Kaurova IA, Bolotina NB. Structure peculiarities and point defects in new sillenite-type (Bi,Sm)24V2O40 crystals. Mater Lett 2017;199:75–8. https://doi.org/10.1016/j.matlet.2017.04.040.

[135] Marrakchi A, Johnson R V., Tanguay AR. Polarization properties of enhanced self-diffraction in sillenite crystals. IEEE J Quantum Electron 1987;23:2142–51. https://doi.org/10.1109/JQE.1987.1073287.

[136] Reyher HJ, Hellwig U, Thiemann O. Optically detected magnetic resonance of the bismuth-on-metal-site intrinsic defect in photorefractive sillenite crystals. Phys Rev B 1993;47:5638–45. https://doi.org/10.1103/PhysRevB.47.5638.

[137] Ahmad I, Marinova V, Goovaerts E. High-frequency electron paramagnetic resonance of the hole-trapped antisite bismuth center in photorefractive bismuth sillenite crystals. Phys Rev B - Condens Matter Mater Phys 2009;79:2–5. https://doi.org/10.1103/PhysRevB.79.033107.

[138] Lin X, Huang F, Wang W, Xia Y, Wang Y, Liu M, et al. Photocatalytic activity of a sillenite-type material Bi25GaO39. Catal Commun 2008;9:572–6. https://doi.org/10.1016/j.catcom.2007.02.004.

[139] Deng C, Wei X, Liu R, Du Y, Pan L, Zhong X, et al. Synthesis of sillenite-type Bi36Fe2O57 and elemental bismuth with visible-light photocatalytic activity for water treatment. Front Mater Sci 2018;12:415–25. https://doi.org/10.1007/s11706-018-0442-z.

[140] Skorikov VM, Kargin YF, Egorysheva A V., Volkov V V., Gospodinov M. Growth of sillenite-structure single crystals. Inorg Mater 2005;41. https://doi.org/10.1007/s10789-005-0317-4.

[141] Yao WF, Wang H, Xu XH, Zhou JT, Yang XN, Zhang Y, et al. Sillenites materials as novel photocatalysts for methyl orange decomposition. Chem Phys Lett 2003;377:501–6. https://doi.org/10.1016/S0009-2614(03)01209-0.

[142] Abrams BL, Wilcoxon JP. Nanosize semiconductors for photooxidation. vol. 30. 2005. https://doi.org/10.1080/10408430500200981.

[143] Baaloudj O, Nasrallah N, Bouallouche R, Kenfoud H, Khezami L, Assadi AA. High

efficient Cefixime removal from water by the sillenite Bi12TiO20: Photocatalytic mechanism and degradation pathway. J Clean Prod 2022;330:129934. https://doi.org/10.1016/j.jclepro.2021.129934.

[144] Brahimi B, Kenfoud H, Benrighi Y, Baaloudj O. Structural and Optical Properties of Bi12NiO19 Sillenite Crystals: Application for the Removal of Basic Blue 41 from Wastewater. Photochem 2021;1:319–29. https://doi.org/10.3390/photochem1030020.

[145] Wu Y, Chang X, Li M, Hei XP, Liu C, Zhang X. Studying the preparation of pure Bi12SiO20 by Pechini method with high photocatalytic performance. J Sol-Gel Sci Technol 2021;97:311–9. https://doi.org/10.1007/s10971-020-05447-0.

[146] Han JT, Huang YH, Wu XJ, Wu CL, Wei W, Peng B, et al. Tunable synthesis of bismuth ferrites with various morphologies. Adv Mater 2006;18:2145–8. https://doi.org/10.1002/adma.200600072.

[147] Prokofiev V V., Kamshilin AA, Jaeaeskelaeinen T. Progress in the synthesis of photorefractive sillenite structure materials. Solid State Cryst Growth Charact 1997;3178:14–21. https://doi.org/10.1117/12.280714.

[148] Khan FA. Synthesis of nanomaterials: Methods & technology. Appl Nanomater Hum Heal 2020:15–21. https://doi.org/10.1007/978-981-15-4802-4_2.

[149] Ganachari S V., Banapurmath NR, Salimath B, Yaradoddi JS, Shettar AS, Hunashyal AM, et al. Synthesis techniques for preparation of nanomaterials. Handb Ecomater 2019;1:83–103. https://doi.org/10.1007/978-3-319-68255-6_149.

[150] Ben Smida Y, Marzouki R, Kaya S, Erkan S, Faouzi Zid M, Hichem Hamzaoui A. Synthesis Methods in Solid-State Chemistry. Synth Methods Cryst 2020. https://doi.org/10.5772/intechopen.93337.

[151] Rane AV, Kanny K, Abitha VK, Thomas S. Chapter 5 - Methods for Synthesis of Nanoparticles and Fabrication of Nanocomposites _ Elsevier Enhanced Reader.pdf. Synth Inorg Nanomater 2018:121–39.

[152] Burianek M, Haussühl S, Kugler M, Wirth V, Mühlberg M. Some physical properties of boron sillenite: Bi24.5BO 38.25. Cryst Res Technol 2006;41:375–8. https://doi.org/10.1002/crat.200510590.

[153] Kityk I V., Majchrowski A, Sahraoui B. IR-induced nonlinear optics in Ge-doped

Bi12TiO20 large-sized nanocrystallites. Opt Lasers Eng 2005;43:75–83. https://doi.org/10.1016/j.optlaseng.2004.06.011.

[154] Kowalczyk M, Kaczkan M, Majchrowski A, Malinowski M. A Comparative Study of Eu3+-Doped Sillenites: Bi12SiO20 (BSO) and Bi12GeO20 (BGO). Materials (Basel) 2023;16:1621. https://doi.org/10.3390/ma16041621.

[155] Martinez-Lopez J, Caballero MA, Santos MT, Arizmendi L, Dieguez E. Solid-liquid interface in the growth of sillenite-type crystals. J Cryst Growth 1993;128:852–8. https://doi.org/10.1016/S0022-0248(07)80057-1.

[156] Shen C, Zhang H, Zhang Y, Xu H, Yu H, Wang J, et al. Orientation and temperature dependence of piezoelectric properties for sillenite-type Bi12TiO20 and Bi12SiO20 single crystals. Crystals 2014;4:141–51. https://doi.org/10.3390/cryst4020141.

[157] Burianek M, Mühlberg M. Crystal growth of boron sillenite Bi24B2O39. Cryst Res Technol 1997;32:1023–7. https://doi.org/10.1002/crat.2170320803.

[158] Romcevic N, Lekic M, Kovacevic A, Paunovic N, Vasic B, Romcevic M. Structural properties of femtosecond laser irradiation induced bismuth oxide based nano-objects in Bi12SiO20 (BSO) single crystal. Phys E Low-Dimensional Syst Nanostructures 2023;148. https://doi.org/10.1016/j.physe.2023.115653.

[159] Budenkova ON, Vasiliev MG, Yuferev VS, Bystrova EN, Kalaev V V., Bermúdez V, et al. Simulation of global heat transfer in the Czochralski process for BGO sillenite crystals. J Cryst Growth 2004;266:103–8. https://doi.org/10.1016/j.jcrysgro.2004.02.035.

[160] Rojo JC, Marín C, Derby JJ, Diéguez E. Heat transfer and the external morphology of Czochralski-grown sillenite compounds. J Cryst Growth 1998;183:604–13. https://doi.org/10.1016/S0022-0248(97)00496-X.

[161] Pepe Y, Isik M, Karatay A, Gasanly N, Elmali A. Wavelength dependence of the nonlinear absorption performance and optical limiting in Bi12TiO20 single crystal. J Lumin 2023;253. https://doi.org/10.1016/j.jlumin.2022.119494.

[162] Isik M, Delice S, Gasanly NM, Darvishov NH, Bagiev VE. Investigation of optical properties of Bi12GeO20 sillenite crystals by spectroscopic ellipsometry and Raman spectroscopy. Ceram Int 2020;46:12905–10.

https://doi.org/10.1016/j.ceramint.2020.02.056.

[163] Isik M, Delice S, Gasanly NM, Darvishov NH, Bagiev VE. Trapping centers in Bi12TiO20 single crystals by thermally stimulated current. Opt Mater (Amst) 2021;122. https://doi.org/10.1016/j.optmat.2021.111797.

[164] Isik M, Gasanly NM. Linear and nonlinear optical characteristics of Bi12SiO20 single crystals. Opt Mater (Amst) 2022;131. https://doi.org/10.1016/j.optmat.2022.112692.

[165] Surucu G, Isik M, Gencer A, Gasanly N. Experimental and theoretical investigation of the mechanical characteristics of sillenite compound: Bi12GeO20. J Alloys Compd 2021;882. https://doi.org/10.1016/j.jallcom.2021.160686.

[166] Isik M, Gasanly NM. Linear and nonlinear optical properties of Bi12GeO20 single crystal for optoelectronic applications. Mater Sci Semicond Process 2023;153. https://doi.org/10.1016/j.mssp.2022.107170.

[167] Isik M, Gasanly NM, Darvishov NH, Bagiev VE. Spectroscopic ellipsometry study of Bi12TiO20 single crystals. J Mater Sci Mater Electron 2021;32:7019–25. https://doi.org/10.1007/s10854-021-05411-w.

[168] Isik M, Gasanly NM, Rustamov FA. Determination of mechanical properties of Bi12TiO20 crystals by nanoindentation. Mater Sci Semicond Process 2022;140. https://doi.org/10.1016/j.mssp.2021.106389.

[169] Isik M, Delice S, Gasanly NM, Darvishov NH, Bagiev VE. Temperature-tuned bandgap characteristics of Bi12TiO20 sillenite single crystals. J Mater Sci Mater Electron 2021;32:1316–22. https://doi.org/10.1007/s10854-020-04904-4.

[170] Sharmin F, Basith MA. Simple Low Temperature Technique to Synthesize Sillenite Bismuth Ferrite with Promising Photocatalytic Performance. ACS Omega 2022;7:34901–11. https://doi.org/10.1021/acsomega.2c03457.

[171] Sobhani A, Salavati-Niasari M. Sodium dodecyl benzene sulfonate-assisted synthesis through a hydrothermal reaction. Mater Res Bull 2012;47:1905–11. https://doi.org/10.1016/j.materresbull.2012.04.020.

[172] Sobhani A, Salavati-Niasari M. Optimized synthesis of ZnSe nanocrystals by hydrothermal method. J Mater Sci Mater Electron 2016;27:293–303. https://doi.org/10.1007/s10854-015-3753-1.

[173] Sun Y, Xiong X, Xia Z, Liu H, Zhou Y, Luo M, et al. Study on visible light response and magnetism of bismuth ferrites synthesized by a low temperature hydrothermal method. Ceram Int 2013;39:4651–6. https://doi.org/10.1016/j.ceramint.2012.10.212.

[174] Sobhani A, Salavati-Niasari M. CdSe nanoparticles: facile hydrothermal synthesis, characterization and optical properties. J Mater Sci Mater Electron 2015;26:6831–6. https://doi.org/10.1007/s10854-015-3297-4.

[175] Zhang CY, Sun HJ, Chen W, Zhou J, Li B, Wang YB. Hydrothermal synthesis and photo-catalytic property of Bi 25FeO40 powders. IEEE Int Symp Appl Ferroelectr 2009. https://doi.org/10.1109/ISAF.2009.5307531.

[176] Zhang L, Zhang X, Zou Y, Xu YH, Pan CL, Hu JS, et al. Hydrothermal synthesis, influencing factors and excellent photocatalytic performance of novel nanoparticle-assembled Bi25FeO40 tetrahedrons. CrystEngComm 2015;17:6527–37. https://doi.org/10.1039/c5ce00743g.

[177] Vavilapalli DS, Melvin AA, Bellarmine F, Mannam R, Velaga S, Poswal HK, et al. Growth of sillenite Bi12FeO20 single crystals: structural, thermal, optical, photocatalytic features and first principle calculations. Sci Rep 2020;10:1–10. https://doi.org/10.1038/s41598-020-78598-3.

[178] Shi H, Feng G, Li S, Liu J, Yang X, Li Y, et al. Weak Pb-O of confined [Pb-O4] in pyramidal sillenite-type Bi12PbO20 for enhanced electrochemical ozone production. J Mater Chem A 2022;10:5430–41. https://doi.org/10.1039/d1ta10701a.

[179] Guo H, Chen J, Weng W, Wang Q, Li S. Facile template-free one-pot fabrication of ZnCo2O4 microspheres with enhanced photocatalytic activities under visible-light illumination. Chem Eng J 2014;239:192–9. https://doi.org/10.1016/j.cej.2013.11.021.

[180] Banoth P, Sohan A, Kandula C, Kanaka RK, Kollu P. Microwave-Assisted Solvothermal Route for One-Step Synthesis of Pure Phase Bismuth Ferrite Microflowers with Improved Magnetic and Dielectric Properties. ACS Omega 2022;7:12910–21. https://doi.org/10.1021/acsomega.2c00219.

[181] Zhu X, Hang Q, Xing Z, Yang Y, Zhu J, Liu Z, et al. Microwave hydrothermal synthesis, structural characterization, and visible-light photocatalytic activities of single-crystalline bismuth ferric nanocrystals. J Am Ceram Soc 2011;94:2688–93.

https://doi.org/10.1111/j.1551-2916.2011.04430.x.

[182] Zhang Q, Ravindra, Xia H, Zhang L, Zeng K, Xu Y, et al. Microwave hydrothermal synthesis of a Bi2SiO5/Bi12SiO20 heterojunction with oxygen vacancies and multiple charge transfer for enhanced photocatalytic activity. Appl Surf Sci 2022;581. https://doi.org/10.1016/j.apsusc.2021.152337.

[183] Zarycka A, Lisińska-Czekaj A, Czuber J, Orkisz T, Ilczuk J, Czekaj D. The sol-gel synthesis of bismuth titanate electroceramic thin films. Mater Sci Pol 2005;23:167–75.

[184] Sharmin F, Ara F, Basith MA. Comparison of the structure-property relationships between sillenite and perovskite phases of Bi 0.9 Dy 0.1 FeO 3 nanostructures . New J Chem 2023. https://doi.org/10.1039/d2nj05600c.

[185] Mahdiani M, Sobhani A, Salavati-Niasari M. The first synthesis of CdFe12O19 nanostructures and nanocomposites and considering of magnetic, optical, electrochemical and photocatalytic properties. J Hazard Mater 2019;367:607–19. https://doi.org/10.1016/j.jhazmat.2019.01.007.

[186] Lopes Matias JA, Silva IBT, da Silva AO, Oliveira JBL, Ribeiro da Silva D, Morales MA. (Bi13Co11)Co2O40–Co3O4 nanocomposites: Approach to different fuels in sol-gel combustion synthesis using the Box-Behnken design. Ceram Int 2022;48:481–94. https://doi.org/10.1016/j.ceramint.2021.09.124.

[187] Yoleva A, Djambazov S, Ivanova Y, Kashchieva E. Sol-gel synthesis of titanate phases from aurivillius and sillenite type (Bi4Ti3O12 and Bi12TiO20). J Univ Chem Technol Metall 2011;46:255–60.

[188] Cherkashina NI, Pavlenko A V. Synthesis of Polymer Composite Based on Polyimide and Bi12SiO20 Sillenite. Polym - Plast Technol Eng 2018;57:1923–31. https://doi.org/10.1080/03602559.2018.1447129.

[189] Li X, Xiang X, Chen J, Jin D, Cheng J. Synthesis of Highly Active Photocatalyst Mesoporous Bi24Fe2O39 Nanoparticles Via a P123-Assisted Sol–Gel Method. Jom 2022;74:2783–90. https://doi.org/10.1007/s11837-022-05214-2.

[190] Mohassel R, Sobhani A, Salavati-Niasari M, Goudarzi M. Pechini synthesis and characteristics of Gd2CoMnO6 nanostructures and its structural, optical and photocatalytic properties. Spectrochim Acta - Part A Mol Biomol Spectrosc

2018;204:232–40. https://doi.org/10.1016/j.saa.2018.06.050.

[191] Jebari H, Tahiri N, Boujnah M, Bounagui O El, Boudad L, Taibi M, et al. Structural, optical, dielectric, and magnetic properties of iron-sillenite Bi25FeO40. Appl Phys A Mater Sci Process 2022;128. https://doi.org/10.1007/s00339-022-05973-4.

[192] Navarro-Rojero MG, Romero JJ, Rubio-Marcos F, Fernandez JF. Intermediate phases formation during the synthesis of Bi4Ti3O12 by solid state reaction. Ceram Int 2010;36:1319–25. https://doi.org/10.1016/j.ceramint.2009.12.023.

[193] Lee SL, Lee CK, Sinclair DC. Synthesis and characterisation of bismuth phosphate-based sillenites. Solid State Ionics 2005;176:393–400. https://doi.org/10.1016/j.ssi.2004.08.015.

[194] Valant M, Suvorov D. Synthesis and characterization of a new sillenite compound - Bi12(B0.5P0.5)O20. J Am Ceram Soc 2002;85:355–8. https://doi.org/10.1111/j.1151-2916.2002.tb00096.x.

[195] Carrasco MF, Mendiratta SK, Marques L. Formation of an intermediate phase in the ball milling synthesis of the sillenite phase of BSO and BTO. Appl Phys A Mater Sci Process 2005;80:361–7. https://doi.org/10.1007/s00339-003-2231-4.

[196] Bäcker M, Baumann A, Brunkahl O, Erbe M, Schneller T. Chemical Solution Deposition (CSD). Digit Encycl Appl Phys 2019:1–34. https://doi.org/10.1002/3527600434.eap807.

[197] Yao WF, Wang H, Xu XH, Cheng XF, Huang J, Shang SX, et al. Photocatalytic property of bismuth titanate Bi 12 TiO 20 crystals. Appl Catal 2011;243:185–90.

[198] He C, Gu M. Photocatalytic activity of bismuth germanate Bi12GeO20 powders. Scr Mater 2006;54:1221–5. https://doi.org/10.1016/j.scriptamat.2005.12.028.

[199] Kartavtseva MS, Gorbenko OY, Kaul AR, Murzina T V., Savinov SA, Barthélémy A. BiFeO3 thin films prepared using metalorganic chemical vapor deposition. Thin Solid Films 2007;515:6416–21. https://doi.org/10.1016/j.tsf.2006.11.133.

[200] Nagao Y, Mimura Y. Growth and characterization of Bi12SiO20 films by metalorganic chemical vapor deposition. IEEE J Quantum Electron 1987;23:2152–8. https://doi.org/10.1109/JQE.1987.1073299.

[201] Thanabodeekij N, Gulari E, Wongkasemjit S. Bi12TiO20 synthesized directly from bismuth (III) nitrate pentahydrate and titanium glycolate and its activity. Powder Technol 2005;160:203–8. https://doi.org/10.1016/j.powtec.2005.08.015.

[202] Rayan DA, Abdel-Mawla EA, Mohamed SK, Mohamed AA, Rashad MM. An investigation on structural and optical properties of nanocrystalline bismuth ferrite and manganese sillenite powders. Key Eng Mater 2020;835 KEM:317–23. https://doi.org/10.4028/www.scientific.net/KEM.835.317.

[203] Kalikeri S, Shetty Kodialbail V. Solar light-driven photocatalysis using mixed-phase bismuth ferrite (BiFeO3/Bi25FeO40) nanoparticles for remediation of dye-contaminated water: kinetics and comparison with artificial UV and visible light-mediated photocatalysis. Environ Sci Pollut Res 2018;25:13881–93. https://doi.org/10.1007/s11356-018-1291-0.

[204] Lu J, Wang X, Jiang H. Synthesis of pure Bi12SiO20 powder by molten salt method. Appl Mech Mater 2012;182–183:52–6. https://doi.org/10.4028/www.scientific.net/AMM.182-183.52.

[205] Ren L, Lu SY, Fang JZ, Wu Y, Chen DZ, Huang LY, et al. Enhanced degradation of organic pollutants using Bi25FeO40 microcrystals as an efficient reusable heterogeneous photo-Fenton like catalyst. Catal Today 2017;281:656–61. https://doi.org/10.1016/j.cattod.2016.06.028.

[206] Flores Morales SS, León Flores JA, Pérez Mazariego JL, Marquina Fábrega V, Gómez González RW. Synthesis of Bi25FeO39 by molten salts method and its mössbauer spectrum. Phys B Condens Matter 2017;504:109–11. https://doi.org/10.1016/j.physb.2016.10.019.

[207] Ivleva LI, Kuz'minov YS, Osiko V V., Polozkov NM. The growth of multicomponent oxide single crystals by stepanov's technique. J Cryst Growth 1987;82:168–76. https://doi.org/10.1016/0022-0248(87)90182-5.

[208] Antonov PI, Nikanorov SP. Physical problems in crystal growth by the Stepanov method. J Cryst Growth 1980;50:3–7. https://doi.org/10.1016/0022-0248(80)90225-0.

[209] Nogueira AE, Lima ARF, Longo E, Leite ER, Camargo ER. Structure and photocatalytic properties of Nb-doped Bi12TiO20 prepared by the oxidant peroxide

method (OPM). J Nanoparticle Res 2014;16. https://doi.org/10.1007/s11051-014-2653-2.

[210] Busuioc C, Olaret E, Stancu IC, Nicoara AI, Jinga SI. Electrospun fibre webs templated synthesis of mineral scaffolds based on calcium phosphates and barium titanate. Nanomaterials 2020;10. https://doi.org/10.3390/nano10040772.

[211] Zhang X, Xue T, Zhang C, Wang J, Xue J, Li R, et al. In Situ Synthesis of Hydrangea Finch Coral-like Bi12SiO20Film with Highly Effective Photocatalytic CO2 Reduction Performance. ACS Appl Energy Mater 2021;4:15–9. https://doi.org/10.1021/acsaem.0c02663.

[212] Xue T, Zhang X, Zhang C, Li R, Liu J, Wang Y, et al. In-situ electrochemical-ion-exchange synthesis of novel Bi12SiO20/BiOBr composite film from Bi plate for enhanced photocatalytic CO2 reduction activity. Mater Lett 2020;274. https://doi.org/10.1016/j.matlet.2020.127990.

[213] Burianek M, Held P, Mühlberg M. Improved single crystal growth of the boron sillenite "Bi24B2O39" and investigation of the crystal structure. Cryst Res Technol 2002;37:785–96. https://doi.org/10.1002/1521-4079(200208)37:8<785::AID-CRAT785>3.0.CO;2-R.

[214] Valant M, Suvorov D. Processing and Dielectric Properties of Sillenite Compounds Bi12MO20-δ (M: Si, Ge, Ti, Pb, Mn, B1/2P1/2). ChemInform 2010;33:no-no. https://doi.org/10.1002/chin.200210013.

[215] Lima AF, Farias SAS, Lalic M V. Structural, electronic, optical, and magneto-optical properties of Bi 12MO20 (M Ti, Ge, Si) sillenite crystals from first principles calculations. J Appl Phys 2011;110. https://doi.org/10.1063/1.3652751.

[216] Rangavittal N, Row T, Rao C. A study of cubic bismuth oxides of the type bi(26-X)m(X)O(40-delta) (m=ti, mn, fe, co, ni or pb) related to gamma-bi2O3. Eur J Inorg Chem 1994;31:409–22.

[217] Abrahams SC, Jamieson PB, Bernstein JL. Crystal structure of piezoelectric bismuth germanium oxide Bi 12GeO20. J Chem Phys 1967;47:4034–41. https://doi.org/10.1063/1.1701572.

[218] Deng H, Hao W, Xu H. First-principles calculations of novel sillenite compounds Bi

24M 2O 40 (M=Se or Te). Rare Met 2011;30:135–9. https://doi.org/10.1007/s12598-011-0255-z.

[219] Zhoua P, Xiaoa F, Jia L. Bi12NiO19 micro-sheets grown on graphene oxide: Temperature-dependent facile synthesis and excellent electrochemical behavior for supercapacitor electrode. J Electroanal Chem 2021;884. https://doi.org/10.1016/j.jelechem.2021.115075.

[220] Pei LZ, Wei T, Lin N, Zhang H. Synthesis of bismuth nickelate nanorods and electrochemical detection of tartaric acid using nanorods modified electrode. J Alloys Compd 2016;663:677–85. https://doi.org/10.1016/j.jallcom.2015.12.177.

[221] Rajamoorthy M, Geetha D, Sathiya Priya A. Synthesis of Cobalt-Doped Bi12NiO19: Structural, Morphological, Dielectric and Magnetic Properties. Arab J Sci Eng 2021;46:737–44. https://doi.org/10.1007/s13369-020-04889-6.

[222] Gayo GX, Lavat AE. Green ceramic pigment based on chromium recovered from a plating waste. Ceram Int 2018;44:22181–8. https://doi.org/10.1016/j.ceramint.2018.08.336.

[223] Medina E, Pathirana VH, Li J, Ramirez AP, Subramanian MA. Tetrahedral Mn4+ as chromophore in sillenite-type compounds. J Solid State Chem 2020;289. https://doi.org/10.1016/j.jssc.2020.121463.

[224] Zhang H, Ke H, Ying P, Luo H, Zhang L, Wang W, et al. Crystallisation process of Bi5Ti3FeO15 multiferroic nanoparticles synthesised by a sol–gel method. J Sol-Gel Sci Technol 2018;85:132–9. https://doi.org/10.1007/s10971-017-4530-9.

[225] Lima AF, Lalic M V. Ab initio study of structural, electronic and optical properties of the Bi12TiO20 sillenite crystal. Comput Mater Sci 2010;49:321–5. https://doi.org/10.1016/j.commatsci.2010.05.017.

[226] Petrov MP, Bryksin V V., Petrov VM, Wevering S, Krätzig E. Dispersion law of photorefractive waves in sillenites. Phys Rev A - At Mol Opt Phys 1999;60:2413–9. https://doi.org/10.1103/PhysRevA.60.2413.

[227] Deliolanis NC, Kourmoulis IM, Apostolidis AG, Vanidhis ED, Papazoglou DG. Diffractive properties of volume phase gratings in photorefractive sillenite crystals of arbitrary cut under the influence of an external electric field. Phys Rev E - Stat

Physics, Plasmas, Fluids, Relat Interdiscip Top 2003;68:1–17. https://doi.org/10.1103/PhysRevE.68.056602.

[228] Tian T, Yan X, Kong Y, Liu H, Zheng D, Liu S, et al. Improvement in the photorefractive response speed and mechanism of pure congruent lithium niobate crystals by increasing the polarization current. Crystals 2017;7. https://doi.org/10.3390/cryst7120368.

[229] Papazoglou DG, Apostolidis AG, Vanidhis ED. Measurement of the electro-optic coefficient of Bi12GeO20 (BGO), Bi12TiO20 (BTO) crystals. Synth Met 1996;83:281–5. https://doi.org/10.1016/S0379-6779(97)80086-0.

[230] Hernández-Alonso MD, Fresno F, Suárez S, Coronado JM. Development of alternative photocatalysts to TiO2: Challenges and opportunities. Energy Environ Sci 2009;2:1231–57. https://doi.org/10.1039/b907933e.

[231] Abdullah EA. Band edge positions as a key parameter to a systematic design of heterogeneous photocatalyst. Eur J Chem 2019;10:82–94. https://doi.org/10.5155/eurjchem.10.1.82-94.1809.

[232] Ahmad R, Ahmad Z, Khan AU, Mastoi NR, Aslam M, Kim J. Photocatalytic systems as an advanced environmental remediation: Recent developments, limitations and new avenues for applications. J Environ Chem Eng 2016;4:4143–64. https://doi.org/10.1016/j.jece.2016.09.009.

[233] Ji W, Li M, Zhang G, Wang P. Controlled synthesis of Bi25FeO40 with different morphologies: Growth mechanism and enhanced photo-Fenton catalytic properties. Dalt Trans 2017;46:10586–93. https://doi.org/10.1039/c6dt04864a.

[234] Preethi R, Singh S. Ga based Sillenite-TiO2 composite for efficient sunlight induced photo reduction of Cr (VI) and photo degradation of ampicillin. J Environ Manage 2023;326. https://doi.org/10.1016/j.jenvman.2022.116831.

[235] Xue J, Zhang H, Han J, Ling Y. Thermal, magnetic and photoelectrical behaviors of sillenite Bi25FeO39 microcrystals. Ceram Int 2021;47:9941–7. https://doi.org/10.1016/j.ceramint.2020.12.138.

[236] Hou J, Qu Y, Krsmanovic D, Ducati C, Eder D, Kumar R V. Solution-phase synthesis of single-crystalline Bi12TiO 20 nanowires with photocatalytic properties. Chem

Commun 2009:3937–9. https://doi.org/10.1039/b906290d.

[237] Wang Z, Wang Y, Zhang Y, Sun X, Lou Y, Zhang Y, et al. Efficient photothermal degradation on Bi12CoO20 sillenite with a strong internal electric field induced by the thermal effect. Appl Catal B Environ 2022;313. https://doi.org/10.1016/j.apcatb.2022.121452.

[238] Sobhani A, Salavati-Niasari M. Cobalt selenide nanostructures: Hydrothermal synthesis, considering the magnetic property and effect of the different synthesis conditions. J Mol Liq 2016;219:1089–94. https://doi.org/10.1016/j.molliq.2016.03.062.

[239] Murugesan S, Smith YR, Subramanian V. Hydrothermal synthesis of Bi12TiO20 nanostrucutures using anodized TiO2 nanotubes and its application in photovoltaics. J Phys Chem Lett 2010;1:1631–6. https://doi.org/10.1021/jz100404v.

[240] Wang XL, Xiao Y, Lv ZJ, Yu H, Yang Y, Dong XT. A novel 2D nanosheets self-assembly camellia-like ordered mesoporous Bi12ZnO20 catalyst with excellent photocatalytic property. J Alloys Compd 2020;835:155409. https://doi.org/10.1016/j.jallcom.2020.155409.

[241] Raja Preethi V, Radha R, Vinod RK, Balakumar S, Gupta B, Singh S. Controlled synthesis of photoactive gallium based sillenite single crystal and its application in environmental remediation. Sol Energy 2021;220:890–900. https://doi.org/10.1016/j.solener.2021.03.060.

[242] Gao T, Li X, Wu G, Wang C, Wu X, Hu X, et al. Growth and Magneto-optical Properties of Bi25FeO40 Crystals with heavy Co/Fe co-doping. J Alloys Compd 2023. https://doi.org/10.1016/j.jallcom.2023.169502.

[243] Nizhankovskiy VI. Comparison of optical properties of Cr-doped Bi12TiO20 and Fe-doped Bi12SiO20. J Alloys Compd 2019;771:1036–9. https://doi.org/10.1016/j.jallcom.2018.09.011.

[244] Tassev V, Diankov G, Gospodinov M. Doped sillenite crystals applicable for fiber-optic magnetic sensors. Opt Mater (Amst) 1996;6:347–51. https://doi.org/10.1016/S0925-3467(96)00058-4.

[245] Carvalho JF, Franco RWA, Magon CJ, Nunes LAO, Hernandes AC. Optical and

magnetic characterization of pure and vanadium-doped Bi12TiO20 sillenite crystals. Opt Mater (Amst) 1999;13:333–8. https://doi.org/10.1016/S0925-3467(99)00077-4.

[246] Carvalho JF, Hernandes AC. Growth and optical characterization of cerium and lead-doped Bi 12TiO20 sillenite single crystals. Cryst Res Technol 2005;40:847–51. https://doi.org/10.1002/crat.200410444.

[247] Marinova V. Optical properties of Bi12TiO20 doped with Al, P, Ag, Cu, Co and co-doped with Al + P single crystals. Opt Mater (Amst) 2000;15:149–58. https://doi.org/10.1016/S0925-3467(00)00029-X.

[248] Egorysheva A V., Burkov VI, Kargin YF, Vasil'ev AY, Volkov V V., Skorikov VM. Spectroscopic properties of Bi12SiO20 and Bi12TiO20 crystals doped with Mn, Mn + P, Cr + P, Cr + Ga, and Cr + Cu. Inorg Mater 2001;37:817–24. https://doi.org/10.1023/A:1017991500219.

[249] Nechitailov AA, Krasin'kova M V., Mokrushina E V., Petrov AA, Kartenko NF, Prokof'ev V V. Impurity defects in Cr-doped Bi12SiO20 and Bi12TiO20 crystals. Inorg Mater 2000;36:820–5. https://doi.org/10.1007/BF02758604.

[250] Marquet H, Tapiero M, Merle JC, Zielinger JP, Launay JC. Determination of the factors controlling the optical background absorption in nominally undoped and doped sillenites. Opt Mater (Amst) 1998;11:53–65. https://doi.org/10.1016/S0925-3467(98)00018-4.

[251] Tassev V, Diankov G, Gospodinov M. Optical activity of doped sillenite crystals. Mater Res Bull 1995;30:1263–7. https://doi.org/10.1016/0025-5408(95)00112-3.

[252] Chmyrev VI, Skorikov VM, Larina E V. Doping effect on the optical, electro-optic, and photoconductive properties of Bi12MO20 (M = Ge, Si, Ti). Inorg Mater 2006;42:381–92. https://doi.org/10.1134/S0020168506040091.

[253] Geim AK, Grigorieva I V. Van der Waals heterostructures. Nat Rev Methods Prim 2022;2. https://doi.org/10.1038/s43586-022-00151-5.

[254] Yamamoto K, Yoshikawa K, Uzu H, Adachi D. High-efficiency heterojunction crystalline Si solar cells. Jpn J Appl Phys 2018;57. https://doi.org/10.7567/JJAP.57.08RB20.

[255] Ruan X, Hu H, Che H, Che G, Li C, Liu C, et al. Facile fabrication of

Ag2O/Bi12GeO20 heterostructure with enhanced visible-light photocatalytic activity for the degradation of various antibiotics. J Alloys Compd 2019;773:1089–98. https://doi.org/10.1016/j.jallcom.2018.09.312.

[256] Wu Y, Han L, Lu J, Ning Q. Preparation of Ag–Bi12SiO20/Bi2SiO5 with high visible light photocatalytic property: the synergistic effect of the heterojunction and the heterogeneous interface. J Mater Sci Mater Electron 2021;32:6976–83. https://doi.org/10.1007/s10854-021-05404-9.

[257] Yao J, Huang L, Li Y, Liu J, Liu J, Shu S, et al. Facile synthesizing Z-scheme Bi12O15Cl6/InVO4 heterojunction to effectively degrade pollutants and antibacterial under light-emitting diode light. J Colloid Interface Sci 2022;627:224–37. https://doi.org/10.1016/j.jcis.2022.07.026.

[258] Rasi UPM, Shihab NK, Angappane S, Gangineni RB. Coexistence of ferromagnetic and spin glass-like magnetic order in Bi10Co16O38 – Bi25FeO40 powder composite. Ceram Int 2019;45:15171–7. https://doi.org/10.1016/j.ceramint.2019.05.001.

[259] Zhang L, Zou Y, Song J, Pan CL, Sheng SD, Hou CM. Enhanced photocatalytic activity of Bi25FeO40-Bi2WO6 heterostructures based on the rational design of the heterojunction interface. RSC Adv 2016;6:26038–44. https://doi.org/10.1039/c6ra00334f.

[260] Wang L, Li H, Zhang S, Long Y, Li L, Zheng Z, et al. One-step synthesis of Bi4Ti3O12/Bi2O3/Bi12TiO20 spherical ternary heterojunctions with enhanced photocatalytic properties via sol-gel method. Solid State Sci 2020;100. https://doi.org/10.1016/j.solidstatesciences.2019.106098.

[261] Chang F, Yang C, Wang X, Zhao S, Wang J, Yang W, et al. Mechanical ball-milling preparation and superior photocatalytic NO elimination of Z-scheme Bi12SiO20-based heterojunctions with surface oxygen vacancies. J Clean Prod 2022;380. https://doi.org/10.1016/j.jclepro.2022.135167.

[262] Liu H, Mei H, Li S, Pan L, Jin Z, Zhu G, et al. Rational design of n-Bi12TiO20@p-BiOI core–shell heterojunction for boosting photocatalytic NO removal. J Colloid Interface Sci 2022;607:242–52. https://doi.org/10.1016/j.jcis.2021.08.126.

[263] Lv CN, Zhang L, Hu JS, Huang XH, Hou CM. Band engineering of Ag-Bi12GeO20-

Bi2WO6 composite photocatalyst: Interface regulation and enhanced photocatalytic performance. Ceram Int 2019;45:5249–58. https://doi.org/10.1016/j.ceramint.2018.11.222.

[264] Liu X, Liu Y, Liu T, Jia Y, Deng H, Wang W, et al. Alkali-mediated dissolution-recrystallization strategy for in situ construction of a BiVO4/Bi25VO40 heterojunction with promoted interfacial charge transfer: Formation mechanism and photocatalytic tetracycline degradation studies. Chem Eng J 2022;431. https://doi.org/10.1016/j.cej.2021.134181.

[265] Rani A, Saravanan P. Heterojunction built sillenite/ perovskite (Bi25Fe2O39-SrTiO3) composite of distinct light sensitive nature for an interactive solar photocatalysis performance. J Environ Chem Eng 2023;11. https://doi.org/10.1016/j.jece.2023.109550.

[266] Zhang L, Zhang X, Huang YQ, Pan CL, Hu JS, Hou CM. Novel Bi12ZnO20-Bi2WO6 heterostructures: Facile synthesis and excellent visible-light-driven photocatalytic activities. RSC Adv 2015;5:30239–47. https://doi.org/10.1039/c5ra01327e.

[267] Wu Y, Li M, Yuan J, Lu J, Wu P, Liu C, et al. A facile Pechini method to synthesize novel Bi12SiO20–Bi2SiO5 heterostructure photocatalysts with enhanced visible light photocatalytic activity. J Mater Sci Mater Electron 2018;29:4503–8. https://doi.org/10.1007/s10854-017-8398-9.

[268] Liu H, Pan L, Nie J, Mei H, Zhu G, Jin Z, et al. Bi12TiO20-TiO2 S-scheme heterojunction for improved photocatalytic NO removal: Experimental and DFT insights. Sep Purif Technol 2023:123575. https://doi.org/10.1016/j.seppur.2023.123575.

[269] Wang T, Liu X, Zhan H, Liao R, Wang Y. In-situ metallic Bi deposited Bi12TiO20 with improved photocatalytic activity. Opt Mater (Amst) 2023;135. https://doi.org/10.1016/j.optmat.2022.113374.

[270] Zhong Y, Peng C, He Z, Chen D, Jia H, Zhang J, et al. Interface engineering of heterojunction photocatalysts based on 1D nanomaterials. Catal Sci Technol 2021;11:27–42. https://doi.org/10.1039/d0cy01847c.

[271] Chang F, Wang X, Yang C, Li S, Wang J, Yang W, et al. Enhanced photocatalytic NO

removal with the superior selectivity for NO2−/NO3− species of Bi12GeO20-based composites via a ball-milling treatment: Synergetic effect of surface oxygen vacancies and n-p heterojunctions. Compos Part B Eng 2022;231. https://doi.org/10.1016/j.compositesb.2021.109600.

[272] Mathew M, Shinde P V., Samal R, Rout CS. A review on mechanisms and recent developments in p-n heterojunctions of 2D materials for gas sensing applications. J Mater Sci 2021;56:9575–604. https://doi.org/10.1007/s10853-021-05884-4.

[273] Das K, Bariki R, Majhi D, Mishra A, Das KK, Dhiman R, et al. Facile synthesis and application of CdS/Bi20TiO32/Bi4Ti3O12 ternary heterostructure: A synergistic multi-heterojunction photocatalyst for enhanced endosulfan degradation and hydrogen evolution reaction. Appl Catal B Environ 2022;303. https://doi.org/10.1016/j.apcatb.2021.120902.

[274] Li X, Shen R, Ma S, Chen X, Xie J. Graphene-based heterojunction photocatalysts. Appl Surf Sci 2018;430:53–107. https://doi.org/10.1016/j.apsusc.2017.08.194.

[275] Fu J, Yu J, Jiang C, Cheng B. g-C3N4-Based Heterostructured Photocatalysts. Adv Energy Mater 2018;8. https://doi.org/10.1002/aenm.201701503.

[276] Aydin C, Taskin M, Aydin H. The effect of graphene oxide on structural, opto-electrical and thermal properties of manganese sillenite (Bi12MnO20) nano-powders. J Therm Anal Calorim 2020;139:3821–32. https://doi.org/10.1007/s10973-019-09203-7.

[277] Huang Y, Zhang X, Zhu G, Gao Y, Cheng Q, Cheng X. Synthesis of silver phosphate/sillenite bismuth ferrite/graphene oxide nanocomposite and its enhanced visible light photocatalytic mechanism. Sep Purif Technol 2019;215:490–9. https://doi.org/10.1016/j.seppur.2019.01.024.

[278] Basith MA, Ahsan R, Zarin I, Jalil MA. Enhanced photocatalytic dye degradation and hydrogen production ability of Bi25FeO40-rGO nanocomposite and mechanism insight. Sci Rep 2018;8:33–5. https://doi.org/10.1038/s41598-018-29402-w.

[279] Sun A, Chen H, Song C, Jiang F, Wang X, Fu Y. Magnetic Bi25FeO40-graphene catalyst and its high visible-light photocatalytic performance. RSC Adv 2013;3:4332–40. https://doi.org/10.1039/c3ra22626c.

[280] Muthukrishnaraj A, Arun A, Kalaivani SS, Maiyalagan T, Manikandan A,

Balasubramanian N. Solvothermal synthesis and characterizations of graphene-ZnBi12O20 nanocomposites for visible-light driven photocatalytic applications. Ceram Int 2020;46:18534–43. https://doi.org/10.1016/j.ceramint.2020.04.159.

[281] Wan Z, Zhang G, Wu X, Yin S. Novel visible-light-driven Z-scheme Bi12GeO20/g-C3N4 photocatalyst: Oxygen-induced pathway of organic pollutants degradation and proton assisted electron transfer mechanism of Cr(VI) reduction. Appl Catal B Environ 2017;207:17–26. https://doi.org/10.1016/j.apcatb.2017.02.014.

[282] Zhang Z, Ren L, Li H, Jiang D, Fang Y, Du H, et al. π-Conjugated In-Plane Heterostructure Enables Long-Lived Shallow Trapping in Graphitic Carbon Nitride for Increased Photocatalytic Hydrogen Generation. Small 2023. https://doi.org/10.1002/smll.202207173.

[283] Sun H, Li J, Zhang G, Li N. Microtetrahedronal Bi12TiO20/g-C3N4 composite with enhanced visible light photocatalytic activity toward gaseous formaldehyde degradation: Facet coupling effect and mechanism study. J Mol Catal A Chem 2016;424:311–22. https://doi.org/10.1016/j.molcata.2016.09.012.

[284] Ma ZP, Zhang L, Ma X, Zhang YH, Shi FN. Design of Z-scheme g-C3N4/BC/Bi25FeO40 photocatalyst with unique electron transfer channels for efficient degradation of tetracycline hydrochloride waste. Chemosphere 2022;289. https://doi.org/10.1016/j.chemosphere.2021.133262.

[285] Li X, Qiu Y, Zhu Z, Zhang H, Yin D. Novel recyclable Z-scheme g-C3N4/carbon nanotubes/Bi25FeO40 heterostructure with enhanced visible-light photocatalytic performance towards tetracycline degradation. Chem Eng J 2022;429. https://doi.org/10.1016/j.cej.2021.132130.

[286] Nan Y, Yang D, Tong Z, Sun Y, Jiang Z. Fabrication of nanoplate-like g-C3N4/Bi12TiO20 heterojunction with enhanced visible-light photocatalytic activity. Mater Res Bull 2017;93:91–101. https://doi.org/10.1016/j.materresbull.2017.04.024.

[287] Cao L, Li YF, Tong Y, Yang R, Sun L, Cao Q, et al. A novel Bi12TiO20/g-C3N4 hybrid catalyst with a bionic granum configuration for enhanced photocatalytic degradation of organic pollutants. J Hazard Mater 2019;379. https://doi.org/10.1016/j.jhazmat.2019.120808.

[288] Yu W, Zou L, Wang H, Wang X. Novel Bi12TiO20/g-C3N4 composite with enhanced photocatalytic performance through Z-scheme mechanism. J Mater Sci 2018;53:10039–48. https://doi.org/10.1007/s10853-018-2311-7.

[289] Chen CC, Chen TT, Shaya J, Wu CL, Lu CS. Bi12SiO20/g-C3N4 heterojunctions: Synthesis, characterization, photocatalytic activity for organic pollutant degradation, and mechanism. J Taiwan Inst Chem Eng 2021;123:228–44. https://doi.org/10.1016/j.jtice.2021.05.042.

[290] Berardinelli A, Hamrouni A, Dirè S, Ceccato R, Camera-Roda G, Ragni L, et al. Features and application of coupled cold plasma and photocatalysis processes for decontamination of water. Chemosphere 2021;262. https://doi.org/10.1016/j.chemosphere.2020.128336.

[291] Taranto J, Frochot D, Pichat P. Combining cold plasma and TiO2 photocatalysis to purify gaseous effluents: A preliminary study using methanol-contaminated air. Ind Eng Chem Res 2007;46:7611–4. https://doi.org/10.1021/ie0700967.

[292] Bagal M V., Gogate PR. Wastewater treatment using hybrid treatment schemes based on cavitation and Fenton chemistry: A review. Ultrason Sonochem 2014;21:1–14. https://doi.org/10.1016/j.ultsonch.2013.07.009.

[293] Zularisam AW, Ismail AF, Salim MR, Sakinah M, Matsuura T. Application of coagulation-ultrafiltration hybrid process for drinking water treatment: Optimization of operating conditions using experimental design. Sep Purif Technol 2009;65:193–210. https://doi.org/10.1016/j.seppur.2008.10.018.

[294] Ren Y, Yu J, Li X, Lv L, Zhang W. Different combined systems with Fenton-like oxidation and ultrafiltration for industrial wastewater treatment. J Memb Sci 2021;638. https://doi.org/10.1016/j.memsci.2021.119688.

[295] Baaloudj O, Nasrallah N, Kenfoud H, Bourkeb KW, Badawi AK. Polyaniline/Bi12TiO20 Hybrid System for Cefixime Removal by Combining Adsorption and Photocatalytic Degradation. ChemEngineering 2023;7:4. https://doi.org/10.3390/chemengineering7010004.

[296] Grandclement C, Seyssiecq I, Piram A, Wong-Wah-Chung P, Vanot G, Tiliacos N, et al. From the conventional biological wastewater treatment to hybrid processes, the

evaluation of organic micropollutant removal: A review. Water Res 2017;111:317. https://doi.org/10.1016/j.watres.2017.01.005.

[297] Kickelbick G. Hybrid Materials: Synthesis, Characterization, and Applications. Hybrid Mater Synth Charact Appl 2007:1–498. https://doi.org/10.1002/9783527610495.

[298] Drisko GL, Sanchez C. Hybridization in materials science - Evolution, current state, and future aspirations. Eur J Inorg Chem 2012:5097–105. https://doi.org/10.1002/ejic.201201216.

[299] Rurack K, Martã-nez-Mãñez R. The Supramolecular Chemistry of Organic-Inorganic Hybrid Materials. Supramol Chem Org Hybrid Mater 2010. https://doi.org/10.1002/9780470552704.

[300] Juwita E, Sulistiani FA, Darmawan MY, Oshima D, Kato T, Suharyadi E. Microstructures, Magnetic Properties and Specific Absorption Rate of Polymer-Modified Bismuth Ferrite Nanoparticles. Key Eng Mater 2023;940:21–9. https://doi.org/10.4028/p-sc9eqe.

[301] Balakumar V, Ramalingam M, Sekar K, Chuaicham C, Sasaki K. Fabrication and characterization of carbon quantum dots decorated hollow porous graphitic carbon nitride through polyaniline for photocatalysis. Chem Eng J 2021;426:131739. https://doi.org/10.1016/j.cej.2021.131739.

[302] Wang P, Ji W, Li M, Zhang G, Wang J. Bi25VO40 microcube with step surface for visible light photocatalytic reduction of Cr(VI): Enhanced activity and ultrasound assisted regeneration. Ultrason Sonochem 2017;38:289–97. https://doi.org/10.1016/j.ultsonch.2017.03.016.

[303] Salavati-Niasari M, Esmaeili-Zare M, Sobhani A. Synthesis and characterisation of cadmium selenide nanostructures by simple sonochemical method. Micro Nano Lett 2012;7:831–4. https://doi.org/10.1049/mnl.2012.0443.

[304] Wu H, Tan HL, Toe CY, Scott J, Wang L, Amal R, et al. Photocatalytic and Photoelectrochemical Systems: Similarities and Differences. Adv Mater 2020;32. https://doi.org/10.1002/adma.201904717.

[305] Ropero-Vega JL, Meléndez AM, Pedraza-Avella JA, Candal RJ, Niño-Gómez ME. Mixed oxide semiconductors based on bismuth for photoelectrochemical applications.

J Solid State Electrochem 2014;18:1963–71. https://doi.org/10.1007/s10008-014-2420-4.

[306] Kane A, Assadi AA, Jery A El, Badawi AK, Kenfoud H, Baaloudj O, et al. Advanced Photocatalytic Treatment of Wastewater Using Immobilized Titanium Dioxide as a Photocatalyst in a Pilot-Scale Reactor : Process Intensification. Materials (Basel) 2022. https://doi.org/10.3390/ ma15134547.

[307] Naghmash MA, Saif M, Mahmoud HR. Transition metal ions doped Bi12SiO20 as novel catalysts for the decomposition of hydrogen peroxide (H2O2). J Taiwan Inst Chem Eng 2021;121:268–75. https://doi.org/10.1016/j.jtice.2021.03.037.

[308] Bu S, Cai D, Li J, Yu S, Jin D, Cheng J. Structure and photocatalytic properties of Bi 25FeO 40 crystallites derived from the PEG assisted sol-gel methods. Mater Res Soc Symp Proc 2012;1324:149–55. https://doi.org/10.1557/opl.2011.843.

[309] Wen Y, Feng M, Zhang P, Zhou H-C, Sharma VK, Ma X. Metal Organic Frameworks (MOFs) as Photocatalysts for the Degradation of Agricultural Pollutants in Water. ACS ES&T Eng 2021;1:804–26. https://doi.org/10.1021/acsestengg.1c00051.

[310] Liu Y, Guo H, Zhang Y, Tang W, Cheng X, Li W. Heterogeneous activation of peroxymonosulfate by sillenite Bi25FeO40: Singlet oxygen generation and degradation for aquatic levofloxacin. Chem Eng J 2018;343:128–37. https://doi.org/10.1016/j.cej.2018.02.125.

[311] Li W, Zhang Y, Liu Y, Cheng X, Tang W, Zhao C, et al. Kinetic performance of peroxymonosulfate activated by Co/Bi 25 FeO 40 : radical and non-radical mechanism. J Taiwan Inst Chem Eng 2019;100:56–64. https://doi.org/10.1016/j.jtice.2019.02.033.

[312] Duan X, Niu X, Gao J, Wacławek S, Tang L, Dionysiou DD. Comparison of sulfate radical with other reactive species. Curr Opin Chem Eng 2022;38. https://doi.org/10.1016/j.coche.2022.100867.

[313] Du C, Li D, He Q, Liu J, Li W, He G, et al. Design and simple synthesis of composite Bi12TiO20/Bi4Ti3O12 with a good photocatalytic quantum efficiency and high production of photo-generated hydroxyl radicals. Phys Chem Chem Phys 2016;18:26530–8. https://doi.org/10.1039/c6cp05223a.

[314] Gan H, Pan S, Liu X, Huang Y. Enhanced Photocatalytic Removal of Hexavalent

Chromium over Bi12 TiO20/RGO Polyhedral Microstructure Photocatalysts. Nanomaterials 2022;12. https://doi.org/10.3390/nano12132138.

[315] Grao M, Redfern J, Kelly PJ, Ratova M. Magnetron co-sputtered Bi12TiO20/Bi4Ti3O12 composite – An efficient photocatalytic material with photoinduced oxygen vacancies for water treatment application. Appl Surf Sci 2021;552. https://doi.org/10.1016/j.apsusc.2021.149486.

[316] Li S, Wu Y, Zheng H, Zheng Y, Jing T, Tian J, et al. High microwave responsivity Co–Bi25FeO40 in synergistic activation of peroxydisulfate for high efficiency pollutants degradation and disinfection: Mechanism of enhanced electron transfer. Chemosphere 2022;288. https://doi.org/10.1016/j.chemosphere.2021.132558.

[317] Li F, Zhou J, Gao C, Qiu H, Gong Y, Gao J, et al. A green method to prepare magnetically recyclable Bi/Bi25FeO40-C nanocomposites for photocatalytic hydrogen generation. Appl Surf Sci 2020;521. https://doi.org/10.1016/j.apsusc.2020.146342.

[318] Raja KS, Smith YR, Kondamudi N, Manivannan A, Misra M, Subramanian V. CO2 photoreduction in the liquid phase over Pd-supported on TiO2 nanotube and bismuth titanate photocatalysts. Electrochem Solid-State Lett 2011;14. https://doi.org/10.1149/1.3543567.

[319] Zhang Y, Cao S, Liang C, Shen J, Chen Y, Feng Y, et al. Electrocatalytic performance of Sb-modified Bi25FeO40 for nitrogen fixation. J Colloid Interface Sci 2021;593:335–44. https://doi.org/10.1016/j.jcis.2021.02.106.

[320] Wang S, Du X, Yao C, Cai Y, Ma H, Jiang B, et al. S-scheme heterojunction/Schottky junction tandem synergistic effect promotes visible-light-driven catalytic activity. Nano Res 2023;16:2152–62. https://doi.org/10.1007/s12274-022-4960-8.

Declaration of interests

☐The authors declare that they have no known competing financial interests or personal relationships that could have appeared to influence the work reported in this paper.

☒The authors declare the following financial interests/personal relationships which may be considered as potential competing interests:

Phuong Nguyen-Tri reports financial support was provided by Université du québec à trois rivieres. Phuong Nguyen-Tri reports a relationship with University of Québec in Trois-Rivières that includes: employment.

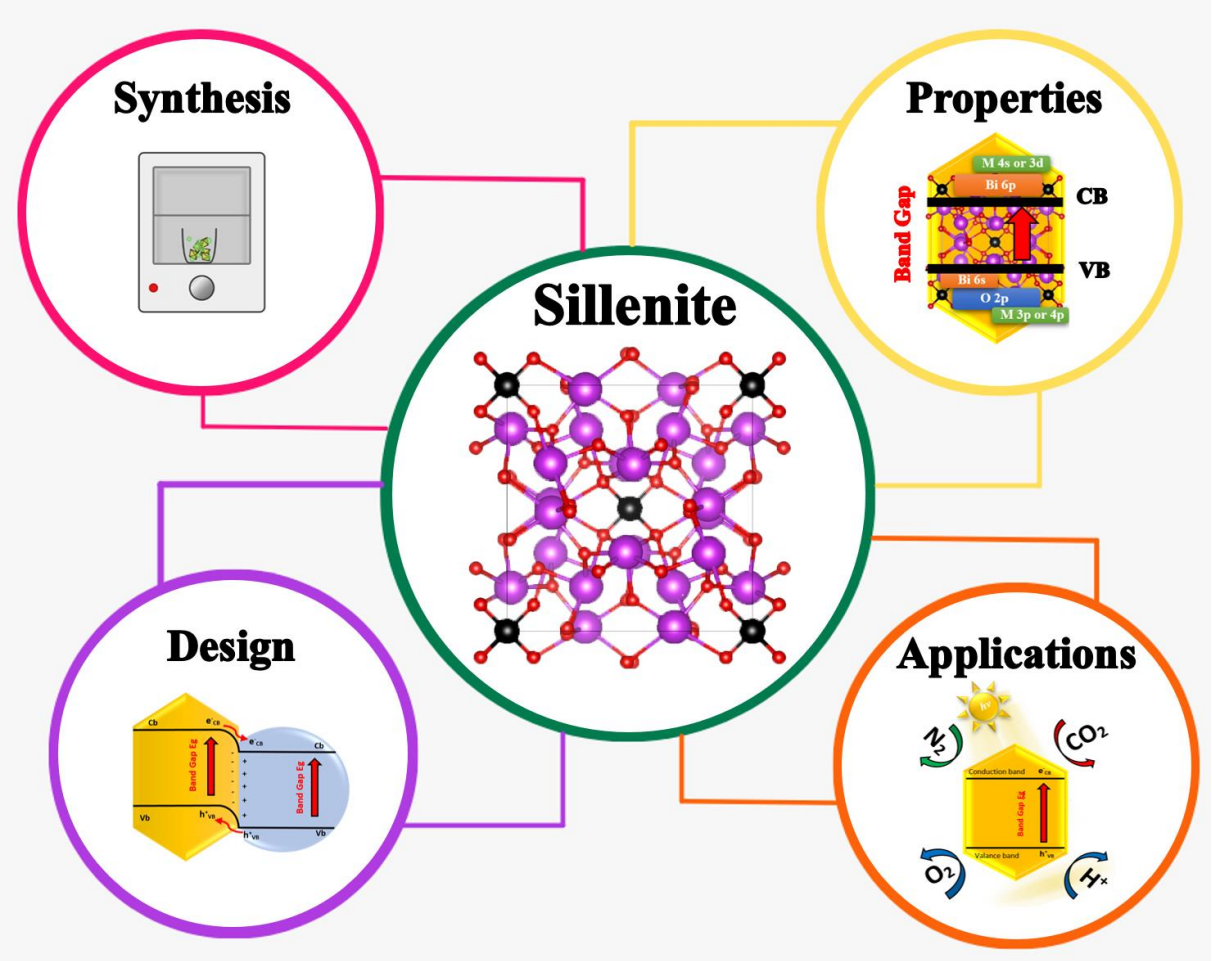
Synthesis
Properties
M 4s or 3d
Bi 6p
Band Gap
CB
VB
Bi 6s
O 2p
M 3p or 4p
Sillenite
Design
Cb
Band Gap Eg
Vb
Applications
Conduction band
Valance band
CO2
N2
O2
Hx

Highlights

- Recent concepts on various photocatalytic applications have been discussed.
- Available synthesis techniques for sillenite materials have been covered.
- Properties of sillenite-type materials have been highlighted.
- The potential of sillenite crystals as photocatalysts has been explained.
- Recent findings on using sillenite-based photocatalysts have been summarized.
- Current approaches for enhancing the efficiency sillenites have been provided.